A STUDY ON STRUCTURAL, VISCOELASTIC PROPERTY AND OSTEOBLAST CHANGES IN OSTEOLYTIC METASTASES

CHEN, XIULI

(B.Eng (Hons.), National University of Singapore)

A THESIS SUBMITTED

FOR THE DEGREE OF DOCTOR OF PHILOSOPHY

DEPARTMENT OF BIOENGINEERING

NATIONAL UNIVERSITY OF SINGAPORE

2012

DECLARATION

I hereby declare that the thesis is my original work and it has been written by me in its entirety. I have duly acknowledged all the sources of information which have been used in the thesis. This thesis has also not been submitted for any degree in any university previously.

Chen Xiuli

8 August 2012

ACKNOWLEDGMENTS

The work completed in this thesis was supported by the research funding NMRC/1087/2006 (R-397-000-059-213) from the National Medical Research Council (NMRC), Singapore.

The author will like express her gratitude to her supervisor, Assistant Professor Dr Lee Taeyong, her examination panel members Professor Goh James and Dr Kim Sang-Ho who provided advice for the development of the project.

The author will also like to take the opportunity to extend her gratitude to Professor Lim Chwee Teck, Professor Teoh Swee-Hin and Professor Zhang Yong for kindly granting the use of their facilities and for providing guidance and assistance wherever possible. On this note, the author will also like to thank the following people: Mr. Yuan Jian, Dr Zhang Shaoping and Dr Niagara Muhammad Idris for their technical assistance towards this project.

The author wishes to express her gratitude towards Mr. Park Sung Yun, a fellow graduate student for his full time role as surgeon and partner for induction of tumour model. The author will also like to take the opportunity to warmly thank Mr. Chan Yong Hoow for his assistance as a fellow team-mate and for his micro-CT help towards this project. Special thanks also go to Dr Kim Young Jick, our previous post-doctorate, for his mentorship and guidance on the surgery and cell culturing techniques during the initial periods of adjustments to the candidature.

Last but not least, it is a pleasure to thank the following people for their teachings and guidance: fellow graduate students, Ms Yang Xiao, Ms. Padmalosini Muthukumaran, Mr. Chen Wenming as well as all friends (Ms Adeline Sham and Ms Priscilla Peh) and colleagues who have helped throughout this period.

TABLE OF CONTENTS

Summary vii

List of Tables ix

List of Figures x

List of Symbols xiv

Chapter 1: Introduction **1**

1.1 Project Significance 2

1.2 Use of an immunocompetent model of bone metastasis 8

1.2.1 Examining bone densitometric and micro-structural properties 11

1.2.2 Examining bone viscoelastic properties 13

1.3 Osteoblast changes due to metastatic cancer 17

1.3.1 A biomechanical approach to study bone cells 19

1.4 Overview of thesis and hypotheses 22

Chapter 2: Immunocompetent model of osteolytic metastases **24**

2.1 Summary of Chapter 25

2.2 Development of model 26

2.3 Methodology 29

2.4 Discussions of the model 36

Chapter 3: Sclerotic response of bone tissue in immunocompetent model of osteolytic metastases **44**

3.1 Summary of Chapter 45

3.2 Introduction 46

3.3 Methodology 48
3.4 Results 55
3.5 Discussions 65
3.6 Conclusions 73

Chapter 4: Mechanical property changes of tumor affected bone cells 74

4.1 Summary of Chapter 75
4.2 Introduction 76
4.3 Methodology 78
4.4 Results 85
4.5 Discussions 91
4.6 Conclusions 96

Chapter 5: Mechanosensing of tumor conditioned bone cells to vibration 97

5.1 Summary of Chapter 98
5.2 Introduction 99
5.3 Methodology 101
5.4 Results 108
5.5 Discussions 115
5.6 Conclusions 120

Chapter 6: Conclusions 122

6.1 Conclusions 123
6.2 Original Contributions 127
6.3 Future Work 128

Bibliography **130**

Appendix: Vita **145**

SUMMARY

Breast cancer has a strong tendency to develop bone metastases, which effectively reduce mobility and survival rate of patients. Osteolytic bone metastasis, which is the more destructive form of metastasis, presents characteristics of enhanced osteoclast-mediated bone resorption and impaired bone formation. Clinically, sclerotic (tissue hardening) development in osteolytic lesions is common but little is known regarding the underlying mechanism and intrinsic mechanical property changes. It was also observed that there was a lack of compensatory bone formation in osteolytic bone metastases. The effect of tumour cells on bone cell mechanosensing and therefore tissue level adaptation remains unknown. Investigating the changes in bone cell mechanical and mechanosensing properties could illuminate some of the possible pathological changes in bone cells in osteolytic metastasis.

In this thesis, a modified method of immunocompetent model of osteolytic metastases was established. A novel characterization of sclerotic bone responses using densitometric, microstructural and viscoelastic parameters was carried out. Sclerotic response was shown to constitute reactive bone formation accompanied by absence of tumor cells. Densitometric and microstructural changes showed increased bone formation and enhanced microarchitecture in the trabecular region. Significantly reduced creep effect was observed in both trabeculae and cortical bone, whereas nanolevel elastic properties did not show a significant difference, despite the active modeling. Thus, it was concluded that viscoelastic nanomechanical property would serve as a more sensitive indicator of modeling in bone than elastic properties.

Through the use of a tumor explants (T) culture, a stronger sustained inhibition of bone cells viability, differentiation and mineralization was demonstrated. Tumor explants cells were revealed to have metastatic potential and similar phenotypic signature as the original cell line, but with higher levels of TGF-β1 released. Here, significant decrease in cell stiffness and increase in hysteresis for T-conditioned bone cells were first shown. It was positively associated with cytoskeletal changes and possibly with inhibited bone cell differentiation. Defective bone matrix deposition was also observed in T-conditioned bone cells, which could further affect bone cell attachment and mechanosensing.

Mechanosensitivity to low magnitude, high frequency (LMHF) vibration was demonstrated to be significantly decreased in T-condtioned bone cells and not improved with subsequent vibration. By inhibiting PI3K pathway through which TGF-β mediate its effect, the inhibition on mechanosensing properties of tumor conditioned bone cells was alleviated, possibly through the maintainence of cytoskeletal organization. Thus, growth factors like TGF-β1 could be good pharmocological targets for osteoblast treatment in osteolytic metastasis.

In conclusion, sclerotic development in this immunocompetent model was shown to be reactive bone formation with reduced local creep properties. Nano-level viscoelastic property was shown to be a sensitive indicator of modelling changes in bone. In addition, the tumor cells inhibition of bone cells viability, functionality, mechanical property and mechanosensitivity could contribute to the defunct bone formation activity. It therefore reinforces the need to expand on osteoblast-targeted therapy for comprehensive treatment of bone metastasis.

LIST OF TABLES

Table	Description	Page
1	Densitometric, microstructural parameters and weight at 50th day post-surgery.	40
2	Nanomechanical property changes of LYTIC and SHAM as measured by nanoindentation. Group averages are represented as mean ± SD.	42
3	Nanomechanical properties changes and mean linear attenuation coefficients. Group averages are represented as mean ± SD.	60
4	Summary of effects on various parameters of bone quality at 50th day post surgery.	66

LIST OF FIGURES

Figure	Description	Page
1	Osteolytic metastases development, via RANKL mediated osteoclastogenesis.	3
2	Chemical Structure of bisphosphonates.	5
3	(A) Distinct drill hole made (black arrow) using 18G needle through intercondylar notch at 42 days' time-point and (B) Surgical drilling using a 22G needle (black arrowhead).	27
4	W256 cells in gel sandwich, with 0.6% agarose and 10% tryphase phosphate broth as bottom layer as well as 0.6% agarose top layer.	28
5	(A) Epoxy embedding of femur sample and (B) sample sectioned at 2.5mm from distal end.	32
6	Experimental fitting of bone creep response to Voigt model.	35
7	Radiographical examination of different bone responses induced in this model: (A) SHAM with no reactive bone response, (B) Osteolytic (Score 3) with soft tissue tumor burden, (C) Osteolytic (Score 1) with minimal but detectable lesion and (D) SCL with tissue hardening (white arrowheads).	37
8	Tumor cells infiltration into soft tissue (*) and fragmented distal metaphyseal growth plate (black arrow).	38
9	(A) Dynamic mechanical analyzer single cantilever set up, showing fixation of the cortical bone section (black arrow) and (B) Sinusoidal stress applied on linear viscoelastic material and showing phase lag δ.	53
10	(A) Healing cascade (black arrows) at 10^{th} day at 20x magnification, (B) Immature bone formation and osteoblasts activity (black arrows) at 50^{th} day, 10x magnification for sclerotic bone and (C) Collagen staining (white arrows) of sclerotic bone at 50^{th} day, at 10x magnification with Masson's Trichrome stain.	56

11	(A) pQCT sequential sections at metaphyseal region showed infiltration of new bone into the medullary for SCL bone in sections closer towards diaphyseal region, (B) Bone Mineral Density (BMD), (C) Bone Mineral Content (BMC) and (D) mean Trabecular Density. * indicated $p<0.05$, one way ANOVA with bonferroni corrections.	57
12	Micro-CT images of SHAM and SCL, with isotropic voxel at 9 μm. SCL showed enhanced trabecular microarchitecture (arrows) compared to SHAM.	58
13	Micro-CT indices of SHAM and SCL: Bone volume fraction (BV/TV), Bone surface density (BS/TV), Trabecular number (Tb.N), Trabecular thickness (Tb.Th), Trabecular separation (Tb.Sp) and Structural model index (SMI). * indicated $p<0.05$.	59
14	(A) Cortical and (B)Trabecular viscosity of SHAM and SCL with * indicating significant difference between groups, (C) Correlation between η and E and (D) Correlation between η and H.	61
15	Tan delta of SHAM and SCL groups across different frequencies (1-20 Hz).	62
16	Storage moduli of SHAM and SCL groups across different frequencies (1-20 Hz).	63
17	Loss moduli for SHAM and SCL across different frequencies (1-20 Hz).	64
18	Confluent bone cell culture at 4x magnification under bright-field imaging.	79
19	AFM fluid cell set-up where cells can remain hydrated in phosphate buffered saline under experiment loading conditions.	82
20	Force-displacement curves obtained from AFM elastic tests.	84
21	Spherical AFM tip on adhered cell.	84
22	(A) Immunocompetent SD rat injected with W256 carcinoma cells, (B)	86

	aggressive malignant lesion (white arrow) induced with elevated periosteal reaction and a soft tissue mass with aneurysmal features, (C) Histological image of sham operated bone and (D) of tumor (T) burdened bone at same magnification.	
23	(A) Growth inhibition of bone cells and (B) Alkaline phosphatase activity inhibition of bone cells by W and T conditioned medium for 3, 5 and 7 days of exposure. * indicated $p < 0.05$ and ** indicated $p < 0.001$ for one way ANOVA analysis, with Tukey's HSD post hoc test	87
24	(A) Von Kossa staining of Control well, (B) W conditioned well (C) T conditioned well at 4x magnification; corresponding F-actin staining of (D) control well, (E) W-conditioned well and (F) T-conditioned well at 40x magnification, scale bar: 50μm. Cell nucleus was counterstained with DAPI.	89
25	(A) Graph of indentation force versus depth, (B) Bar plot of elastic moduli and (C) Bar plot of hysteresis values for control, W- and T-conditioned groups. **-indicated $p<0.001$, * -indicated $p < 0.05$.	91
26	Experimental outline of cell preparation and analysis.	105
27	Vimentin and cytokeratin expression by (T) tumor explants and (W) W256 cells, at 60x magnification, scale bar: 30 μm	108
28	Soft agar assay of W256 cells, (A) with one large colony and (B) smaller colonies; (C, D) Tumor cells with smaller colonies at 10x magnification after 13 days.	109
29	(A) Collagen I staining of control cells with distinct collagen fiber organization, (B) W conditioned cells with less distinct collagen fiber organization, (C) T conditioned cells with amorphous collagen formation at 20x magnification at 3 weeks and (D) Bar plot of collagen fiber length, *-indicated $p < 0.05$ and **- indicated $p < 0.001$	110
30	(A, B) Von Kossa staining of control cells with larger size of bone nodules formed and darker staining of mineralization; (C, D) W conditioned cells with smaller area of bone nodules and less intense staining and (E, F) T conditioned cells, less intense staining of mineralization. All pictures taken at 4x magnification at 2 weeks, with n=3 sets of experiments.	111

31	Normalized nitric oxide levels across 3 groups (control, W conditioned and T conditioned cells) in vibrated plates at 0.3g, 30 Hz. Results are presented in mean ± SEM, n=6 sets of experiment. * indicated $p<0.05$ for one way ANOVA, with Bonferroni corrections.	112
32	Normalized ALP and MTT levels across 3 groups (control, W- and T-conditioned cells) in vibrated plates. Results are presented in mean ± SD, n=3 sets of experiment.	113
33	Bar chart of normalized NO levels in Control, W- and T-conditioned groups, with or without LY294002 treatment (PI3K/Akt inhibitor). F-actin staining at 60x magnification, for control (C), W256(W)- and T-conditioned groups (T) with or without treatment of LY294002, with vibration.	114

LIST OF SYMBOLS

Z_0	Amplitude of displacement oscillation
F_0	Amplitude of force oscillation
ϕ	Phase angle between applied load and resulting displacement in CSM mode of nanoindentation
P	Load applied to sample surface
A	Projected area of indentation
β	Term related to geometry of the nanoindentation tip; $\beta = 1.034$ for Berkovich tip
E	Elastic component of Voigt model
η	Viscosity, a parameter reflecting viscous-like deformation in a solid under loading
$h(t)$	Creep displacement under maximum load as a function of time
α	An equivalent cone semi-angle (70.3 °) to the face angle of the Berkovich indenter (65.27 °)
P_o	Maximum load
E_c	Cortical elastic modulus
E_t	Trabecular elastic modulus
H_c	Cortical hardness
H_t	Trabecular hardness
η_c	Cortical viscosity
η_t	Trabecular viscosity
σ	Oscillating stress
ε	Strain
ω	Angular frequency

δ	phase angle between stress σ and strain ε in response to a sinusoidal stress σ (t) in DMA
E^*	Complex modulus
E'	Storage modulus
E''	Loss modulus
Tan δ	Loss tangent, a ratio of E'' to E'
E_{cell}	Cell elastic modulus
h	Indentation depth into cell
v	Poisson's ratio, assumed to be 0.5 for cellular samples and 0.3 for bone samples
R	Radius of the spherical bead
F	Indentation force
Z	Displacement
d	Deflection
k	Spring constant

Chapter 1: Introduction

1.1 Project Significance

In 2009, there were 192, 370 diagnosed cases of invasive breast cancer in United States and it is considered the second deadliest type of cancer after lung and bronchi cancers (Bussard & Mastro 2009). Breast cancer has a strong tendency to develop bone metastases, where metastasis is defined as the migration of cancer cells from primary neoplasm to secondary sites. Bone is one of most preferred sites for metastasis, with 60-70% prevalence for patients with advanced stages of breast cancer (Clines & Guise 2008).

Bone metastases, which lead to bone pain and fracture, nerve compression as well as hypercalcemia (with extensive bone lesions), effectively reduce the mobility and life expectancy of patients. For instance, breast cancer patients with bone metastases have a median survival span of 2 years and 60% will suffer from bone fractures (Kozlow & Guise 2005).

Most cancers tend to fall within a spectrum between two forms of metastases i.e. osteoblastic and osteolytic metastases. Of the two, osteolytic metastasis represents a more common and more destructive form of metastasis, where there is enhanced bone resorption but bone formation is seemingly impaired. In the case of osteoblastic metastasis, there is increased bone formation without previous bone resorption (Kozlow & Guise 2005). In the both forms of bone metastasis, the normal tight coupling of bone resorption (mediated by osteoclast) and bone formation processes (mediated by osteoblast) in bone remodeling is observed to be uncoupled e.g. only bone resorption in osteolytic metastases.

Pathological development of osteolytic metastases with breast cancer has been associated with the enhanced activation of osteoclasts promoted by osteoblasts, which have been affected by tumour cells. Increased levels of parathyroid hormone-related protein (PTHrP) released by tumour cells increased receptor activator of nuclear factor-κB ligand (RANKL) expression and reduced expression of osteoprotegrin (OPG), a RANKL inhibitory protein by osteoblasts (Fig. 1). Enhanced levels of RANKL protein, together with reduced levels of RANKL inhibitor, activated osteoclast precursors, thus increasing bone resorption activity.

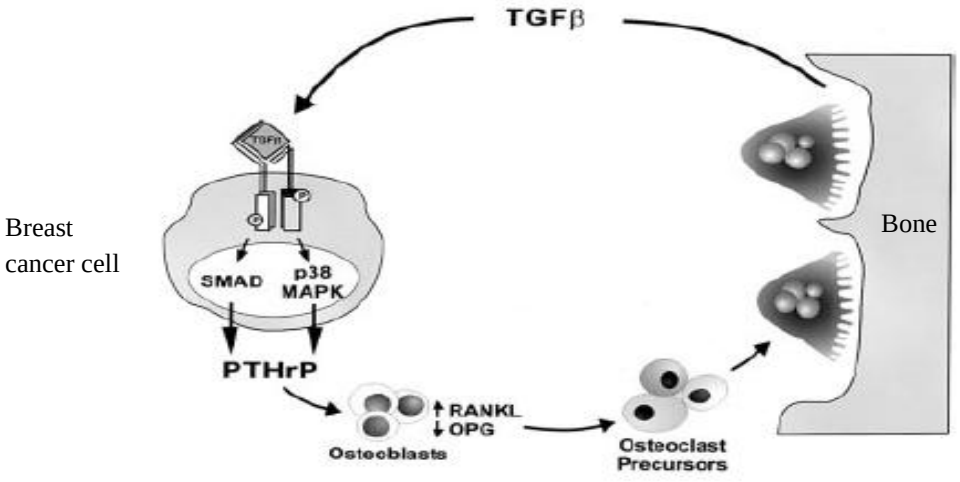

Figure 1: Osteolytic metastases development, via RANKL mediated osteoclastogenesis (Kakonen & Mundy 2003).

Transforming growth factor-β (TGFβ), which is subsequently released from the bone matrix due to resorption, provided further feedback for tumour cells to produce more PTHrP, giving rise to a vicious cycle of destruction (Kakonen & Mundy 2003, Kozlow & Guise 2005, Clines & Guise 2008).

For slow growing or benign lytic lesions, sclerosis (tissue hardening) development is a frequent occurrence (Priolo & Cerase 1998) . In a study of 274 patients over 10 years, regression indicators in osteolytic bone metastasis were found to be recalcification of lesion (11.6%), foci of sclerosis around the lesion (13.5%) which are apparent as low calcified spots and lack of deterioration of lesion (10.5%) over a period of at least 12 months (Huber et al 2002).

Although sclerosis development in bone is seemingly favorable, little is known regarding the intrinsic material and mechanical property changes. It is postulated that the immune system might have an important role in sclerotic development for slow-growing lesions, which could serve to limit the growth of the lesion. A study of sclerotic development in osteolytic lesions in an immunocompetent model of breast cancer metastasis could help in understanding some of the underlying mechanisms and in examining bone mechanical property changes.

There is an important need to cover other existing gaps of knowledge in the pathophysiology of bone metastasis which will help pave way for new therapeutic options. One existing gap in knowledge is the effect of tumour cells on bone cell mechanosensing and restorative bone formation process, of which little information is known (Mastro et al 2004).

Histological evidence based on nude rat model induced with human breast cancer cells demonstrated that there was a decrease in the ratio of osteoid surface to bone surface (97%), which hinted at defunct bone formation activity as a contributor towards the decrease in calcified bone volume (Phadke et al 2006).

However, less effort has been expanded on osteoblast-targeted therapy for a comprehensive treatment (Casimiro et al 2009). Standard therapeutic options for osteolytic bone metastasis mainly comprised of chemotherapeutic drugs and bisphosphonates (Coleman et al 2008). Other modes of treatment have included radiotherapy or surgery to bone which often occur in patients with bone metastasis (Clines & Guise 2008).

Bisphosphonates (a class of anti-resorptive drug) have been found to be able to successfully reduce skeletal related events in bone such as pathological fractures and hypercalcemia (Costa & Major 2009). These drugs preferentially bind to hydroxyapatite surfaces of bone and inhibit osteoclast resorption as well as induce osteoclast apoptosis. Bisphosphonates have a P-C-P structure, with two R side chains that provide the basis for their two main functions and potency, as shown in Figure 2.

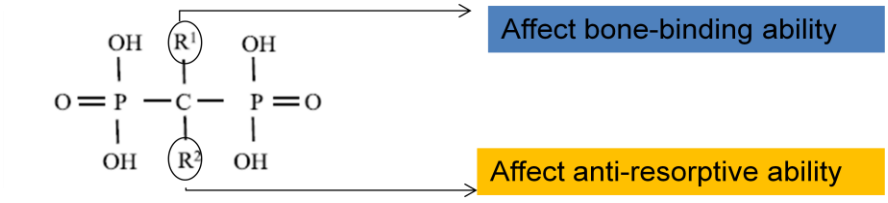

Figure 2: Chemical Structure of bisphosphonates

Nonetheless, there was a lack of bone healing reported after bisphosphonate treatment (Sasaki et al 1995), which suggested a need to look into restoration of bone formation. As such, it would be pertinent to investigate the effects of tumor cells on bone cells (osteoblast lineage), which could provide foundation for the development of osteoblast-targeted therapy.

With the increasingly different combination therapies that could arise, there is also the need for improved methods to evaluate possible differential responses in bone in order to optimize therapeutic performance. For instance, there were synergistic effects of doxorubicin (anticancer drug) with zoledronic acid (bisphosphonate) in inhibiting the development of bone metastasis (Ottewell et al 2008). In contrast, some chemotherapeutic drugs such as 17AAG were also found to have an adverse effect on bone remodeling and therefore treatment efficacy in preventing fractures (Coleman et al 2008). Thus, there is a need for improved methods to assess varying bone properties under different drug therapies.

As a hierarchical composite material of mineral hydroxyapatite and collagen, bone exhibits viscoelastic behavior at different scales. Viscoelastic behavior is defined as behavior that is a combination of elastic (solid) and viscous (liquid) properties (Jones 1999). Viscoelastic mechanical properties have been of recent interest as a plausible indicator of bone strength changes (Fortis et al 2004, Les et al 2004, Yeni et al 2004, Les et al 2005). Other traditional indicators of bone strength changes have involved bone density (Kurth et al 2001), micro-architecture (Kurth et al 2001, Fritz et al 2007) and geometry (Siu et al 2003, Jiang et al 2008). Since bone metastasis represents a degradation of bone integrity and increased fracture risk, the combination of densitometric, microstructural and viscoelastic parameters to assess bone property changes would be of interest in this thesis.

These highlighted concerns are in line with recommendations from the second Cambridge conference for advancing metastatic bone cancer treatment (Coleman et al 2008). These recommendations include: (1) oncogenic bone metastasis models maintained in immunocompetent model, (2) new tests to evaluate treatment responses and (3) restorative bone formation.

Therefore, in this thesis, a modified immunocompetent model of osteolytic bone metastasis was established and a combination of densitometric, microstructural and viscoelastic parameters were used to assess osteolytic and in particular, sclerotic healing responses in bone. The effects of tumour on bone cells mechanical and mechanosensing property in response to vibration were also examined. The subsequent sections would entail prior literature to the work covered in this thesis.

1.2 Use of an immunocompetent model of bone metastasis

Many studies conducted to understand the mechanism of bone metastasis and to compare drug treatment effects have adopted the use of xenograft tumour in immuno-compromized animals (Neudert et al 2003, Cowey et al 2007, Arrington et al 2008, Chanda et al 2008, Ottewell et al 2008). However, it has been suggested that the presence of immune system has a major impact on the tumor promotion and suppression (Song et al 2008) and there is a significant cross-talk between tumour cells, immune cells and host microenvironment (Bussard & Mastro 2009). Thus, it has been argued that an immunocompetent model of bone metastasis will be more appropriate in simulating disease progression (Coleman et al 2008).

The establishment of a successful immunocompetent model of bone metastasis plays a vital role in the overall project, since the results of the study are dependent on tumour growth in bone microenvironment and varying bone responses. There have been a number of studies (Bassani et al 1990, Kurth et al 2001, Medhurst et al 2002, Alvarez et al 2003) which used immunocompetent models for stimulating osteolytic bone lesions and they could be categorized into four types.

The first method involved injection of malignant ascites into the bone or artery. Ascites is defined to be an accumulation of fluid in the peritoneal cavity and malignant cells in ascitic fluid could be used to induce bone metastases (Badraoui et al 2009). For instance, Wistar rats were injected intra-peritoneally with Walker 256 (W256) breast carcinosarcoma cells and malignant ascites was

extracted and re-injected into other Wistar rats intra-arterially (Jung et al 1984) or in an intra-osseous manner (Mao-Ying et al 2006). In another instance, W256/B cells (variant cells of W256) were serially passaged intra-peritoneally in Sprague Dawley rats before being re-injected into medullary cavity of healthy rats (Badraoui et al 2009).

The advantage of this method is that it is highly reproducible in establishing osteolytic metastases across different studies (Jung et al 1984, Krempien et al 2003, Mao-Ying et al 2006, Badraoui et al 2009). However, significant osteolytic destruction of femur and tibia could be found within a short period of time i.e. 7 days (Jung et al 1984) that might not depict clinical cases of tumor induced osteolysis which tended to grow more slowly (Body 1993).

The second method involved intra-osseous injection of tumour cells directly into the medullary cavity. In one example, W256 cells were injected into the medullary cavity of Fischer 344 rats. On the other hand, Kurth et al directly implanted Walker 256 cells in 0.6% agarose gel enriched with medium into the medullary cavity of Sprague Dawley rats (Kurth et al 2000, Kurth et al 2001, Kurth et al 2007). There are some limitations to the protocol, which involved the direct inoculation of osteolytic W256 rat breast cancer cells into rat bone. It could be pointed out that it does not represent the selective process of cancer metastasis i.e. detachment, invasion across vascular walls and into circulation, where only 0.01% of cancer cells survive to induce metastasis (Fidler 2003).

Nonetheless, there are obvious advantages of tumour localization, which could facilitate for longer host survival and ease of monitoring of tumour growth.

Moreover, the use of rat mammary carcinosarcoma (W256 cells) provides some clinical relevance as they have characteristics similar to human breast cancer: poor immunogenicity and high metastatic ability(Badraoui et al 2009) as well as differential response to hormonal treatment(Blouin et al 2005). In addition, Kurth's methodology appeared to be repeatable over the years of 2000- 2001 and 2007.

The third method comprised of injecting syngeneic tumour cells into the bone i.e. tumour cells were derived from rats of the same species and injected into healthy rats. For instance, MRMT-1 cells were injected into bone of Sprague Dawley rats. MRMT-1 are rat mammary gland carcinoma cells that were pre-developed in immune-impaired rats of the same species, which were fed with 3-methylcholanthrene (Medhurst et al 2002). Another example will be that of 13762 rat mammary carcinoma cells in Fischer rats, where 13762 cells were derived from Fischer rats fed with 7, 12 dimethylbenzanthracene (Alvarez et al 2003). While a syngeneic model of tumor metastasis is preferrable, the tumor cells derived in this manner would be spontaneously metastatic (Medhurst et al 2002 , Alvarez et al 2003), with dissemination to other sites (Alvarez et al 2003). As such, there could be lowered host survival and little possibility of sclerosis development which only appears in the case of benign and slow growing lesions.

The fourth type was to induce localized cancer invasion into the bone e.g. injection of Walker 256(A) carcinoma cells into the muscle adjacent to tibia and allowing for the cancer cells to invade into the bone (Guaitani et al 1985, Bassani et al 1990). However, it was observed that bone errosion occurred closest to the

edge of the tumor and was more representative of an external invasion of bone than tumor induced osteolysis.

After due considerations, a rodent model of bone metastasis modified after Kurth's protocol (Kurth et al 2000, Kurth et al 2001, Kurth et al 2007) was adopted and modification of technique is elaborated under Chapter 2.

1.2.1 Examining bone densitometric and micro-structural changes

Non-invasive densitometric assessments using peripheral quantitative computed tomography (pQCT) and dual-energy X-ray absorptiometry (DXA) have been used in monitoring osteolytic effects (Kurth et al 2001, Mann et al 2008) and corresponding drug efficacies in the treatment of bone metastasis (Kurth et al 2002, Kurth et al 2007).

pQCT measures the attenuation of the X-ray radiation passing through bone at a pixel resolution of 0.1mm. By using a hydroxyapatite standard, pQCT is able to provide corresponding volumetric bone mineral content (vBMC) and density (vBMD). It could also provide site specific (cortical or trabecular) and geometric information such as cross sectional area (CSA), cortical thickness and cross-sectional moment of inertia (CSMI).

Since osteolytic metastasis gives rise to deterioration in bone integrity resulting in increased fracture risk, bone densitometry and geometric parameters could provide useful indicators in assessing bone mass and strength changes. For instance, BMD which indicates amount of mineralized bone mass, was found to have a wide range of correlations to fracture load ($r = 0.387$-0.813) (Ferretti et al

1996, Siu et al 2003, Jiang et al 2008) and failure torque ($r^2 = 0.28$) (Kurth et al 2001). The wide range of correlations implied that BMD is not sufficient to reflect bone strength changes and that bone mechanical behavior is also influenced by bone organic components and other factors. Bone geometrical properties such cortical CSA and CSMI also yielded moderate correlations i.e. r = 0.64-0.83 (Jiang et al 2008, Kokoroghiannis et al 2009) and r = 0.42-0.86 (Jamsa et al 1998, Siu et al 2003, Jiang et al 2008) respectively, to fracture load.

BMD and geometrical indexes from pQCT are not sufficient as the only parameters to assess bone integrity and strength changes as a result of bone metastasis. Bone microstructural changes, which cannot be analyzed using pQCT because of its limited resolution, is another important parameter associated with bone strength and relative fracture fragility (Krempien et al 2003).

The technique of micro-computed tomography is capable of providing non-destructive, three-dimensional, high-resolution imaging and assessment of bone microstructural properties. It is capable of identifying bone metastasis 71%-100% of the time (Slavo et al 2009). For instance, it was reported by Fritz et al that imaging of osteolysis using micro-CT has allowed for early detection of osteolytic lesions before radiological observance (Fritz et al 2007). However, for micrometastases which have not produced enough bone changes, there could be failures to detect metastases (Chappard et al 2010). Nevertheless, micro-CT could provide an improved diagnosis within a short period of time.

Quantitative microstructural parameters such as bone volume fraction (BV/TV), bone surface density (BS/TV), trabecular thickness (Tb.Th), trabecular

separation (Tb.Sp), trabecular number (Tb.N) and structure model index (SMI) have already been adopted in number of studies to monitoring relative microarchitectural changes in disease models such as osteoporosis (OVX) (Jiang et al 2000 , Sheng et al 2008, Lespessailles et al 2009) and bone metastasis (Fritz et al 2007, Kurth et al 2007, Halvorson et al 2008, Ottewell et al 2008). SMI quantifies the three-dimensional structure of trabecular bone in terms of plates and rods. It is 0 for ideal plate and 3 for rod-like structure, independent of dimension (Lespessailles et al 2006).

Strong correlations for BV/TV (R^2 = 0.83-0.877) (Teo et al 2006, Nazarian et al 2008) and moderate correlations to ultimate strength of cancellous bone were found for Tb.N (R^2 = 0.67), Tb.Sp (R^2 = 0.54) and SMI (R^2 = 0.56) (Teo et al 2006). Nonetheless, changes in bone mass, geometric and microstructural properties assessed by pQCT and micro-CT techniques are still not adequate in providing information on tissue property changes that could affect bone integrity and strength.

1.2.2 Examining bone viscoelastic changes

Bone is a heterogeneous two phase composite material comprising of mineral hydroxyapatite crystals and organic components (mainly collagen type I). Organic component of bone and water content play important roles towards bone viscoelastic behavior, in which mechanical property changes over the loading duration (Kim et al 2010). The strain rate dependence of bone is reported to have contributed to a fifth of the human femoral bone strength during high-speed

loading in vitro (Les et al 2004). Moreover, remodeling which affects degree of mineralization was found to affect damping efficiency at low frequency (6 Hz or less) in osteoporotic samples (Les et al 2004). Therefore, viscoelastic tissue property changes could constitute another possible indicator that could be assessed in development of bone metastasis.

Bone viscoelastic behavior could be assessed at the nano-level using nanoindentation (Agilent G200 nanoindentor) and at the tissue level using dynamic mechanical analysis (DMA 8000 dynamic mechanical analyzer). One of the rationales for examining bone viscoelastic behavior at the nano-level is that it can reflect local material property changes of bone that undergoes substantial bone remodeling (Tai et al 2007). Thus, it could be indicative of local remodeling changes occurring in bone metastasis.

Nanoindentation technique using Berkovich tip provides the following advantages: probing surface with spatial resolution less than 1 μm (Rho et al 1997), provides quantification of intrinsic microstructural bone properties and new aspects to inter-specimen biological variation (Isaksson et al 2010a).

It could be used to study local viscoelasticity changes, by analyzing the creep effect of the bone under constant load using rheological models such as Burger (Isaksson et al 2010a , Isaksson et al 2010b) and Voigt model (Kim et al 2010). While Burger and Voigt models were shown to be able to provide adequate fitting to experimental results of creep in bone (Isaksson et al 2010a , Isaksson et al 2010b, Kim et al 2010), there are simplified assumptions involved e.g. Voigt model assumes reversible elastic indentation, whereas irreversible

plastic deformation was observed in bone with Berkovich tip indentation. A visco-elastic-plastic approach that takes into account plastic deformation (Olesiak et al 2010) could constitute a more appropriate model examining creep behavior in bone. However, in order to establish a trend and better relate to other literature derived values of diseased bone (Kim et al 2013, Yang et al 2013), we have adopted Voigt model for creep component in this thesis.

A variety of approaches have also been utilized to assess the nano-level elastic properties by using quasi-static (Ishimoto et al 2011), modified (Li et al 2012b), semi-dynamic (Isaksson et al 2010a, Isaksson et al 2010b) and dynamic loading methods (Yang et al 2013, Pathak et al 2011).

Nanoindentation has been useful in monitoring localized nanomechanical property changes in ovariectomized bones with or without drug administration (Bala et al 2011, Chang et al 2011 , Li et al 2012b, Kim et al 2013, Yang et al 2013), osteolytic bones (Nazarian et al 2008), regenerating (Ishimoto et al 2011) and normal bone tissues (Isaksson et al 2010a, Isaksson et al 2010b, Kim et al 2010). As such, nanoindentation could aid in establishing a trend in intrinsic material property changes with disease progression.

On the other hand, dynamic mechanical analysis could be used to measure tissue viscoelastic properties. Viscoelastic properties of material, including ability to dissipate energy (damping) and ability to recover from deformation, can be measured by dynamic mechanical analyzer (DMA) which applies an oscillating force on sample and obtains the resultant deformation. Depending on the material, the phase lag (δ) in resultant deformation could range from 0^0 to 90^0 (0 degrees

for purely elastic material, 90 degrees for purely viscous material). Tan δ could be derived, which reflects damping response of material and is a ratio of energy dissipated to energy stored in elastic component. Tissue property dependence on strain rate can be estimated using a range of frequency scans over which oscillating force is applied (Dong et al 2004). By scanning in a range of frequencies, it can also provide information on active energy dissipation mechanisms in composite material since different energy dissipation mechanisms may be activated in a predictable range of frequencies (Yeni et al 2007). One advantage is that DMA facilitates for the testing of small samples, e.g. advantageous when using human cadavers and laboratory animals.

Although not many studies have used dynamic mechanical analysis on viscoelastic assessment of diseased bone, it was found that damping response (tan δ) in ovariectomized sheep bone was greatly decreased (80%) and storage modulus was lowered (5.2%) (Les et al 2005). While the disease mechanism between osteoporosis and osteolytic metastasis are not identical, both diseases presented overall enhanced bone resorption. A similar alteration in viscoelastic property changes might be expected in osteolytic bone metastasis and could be investigated as another useful parameter to assess bone strength and quality changes.

1.3 Osteoblast changes due to metastatic cancer

Emerging evidence from recent studies suggests that apart from increased RANKL expression and reduction in OPG expression by osteoblasts, there are more profound effects on osteoblasts due to metastatic cancer cells, which may explain the lack of new bone formation or healing reported in event of osteolytic metastasis even with bisphosphonate treatment (Mastro et al 2004).

Mercer et al found that MC3T3- E1 osteoblasts cultured in MDA-MB231 breast cancer cell- conditioned medium were unable to differentiate normally. The differentiation process typically involved the secretion of bone matrix materials such as alkaline phosphatase, osteopontin and sialoprotein, followed by mineralization in which osteocalcin is expressed and nodules are formed. They observed that there was down-regulation in sialoprotein and osteocalcin expression, no observable alkaline phosphatase activity and an apparent inhibition of *in-vitro* mineralization (Mercer et al 2004). The inhibition on alkaline phosphatase activity and bone nodules was similarly observed for fetal carvarial cells exposed to 50% conditioned medium from MDA-MB-231(Zhu et al 2009).

Morphological changes of the osteoblasts have also been observed in co-culture with metastatic breast cancer cells, from cuboidal shape to a more elongated appearance. The change in morphology could be tied in with the observations of significant cytoskeleton reorganization where actin stress-fibers become clumped and punctuated (instead of forming smooth long fibers) and with reduction in focal adhesion complex formation (Mercer et al 2004, Dhurjati et al 2008).

Studies done by Mastro et al on the other hand, found that exposure of human osteoblast line hFOB1. 19 to conditioned medium of MDA-MB-231 or MDA-MB-435 human metastatic breast cancer cells induced osteoblast apoptosis (programmed cell death); with an increase in terms of the percentage of apoptotic osteoblasts from 2% (normal culture of osteoblasts) to 8-12% by TUNEL assay (Mastro et al 2004).

In view of recent in-vitro studies, it could be seen that another contributing factor of bone loss in bone metastasis may be associated with the loss in normal function of osteoblasts and osteoblast apoptosis, on top of cytokine (biochemical signal) release from osteoblasts that promotes osteoclast activation (Dhurjati et al 2008). There has been much focus on reducing tumour burden and inhibiting osteoclasts activity through the use of anticancer and antiresorptive treatments but fewer on the treatment of osteoblasts affected by metastatic cancer environment.

Since osteoblasts are important for synthesizing bone matrix constituents as well as for bone homeostasis, it would be essential to investigate mechanisms by which osteoblasts are affected by metastatic breast cancer to help in establishing effective treatments.

1.3.1 A biomechanical approach to study bone cells

In this thesis, a biomechanical approach was adopted for the investigation of bone cells under the influence of metastatic breast cancer. This approach is intrinsically relevant as bone cells are mechanosensitive cells sensitized to changes in type, degree and duration of mechanical loading, giving rise to various biochemical responses which may affect tissue structure (Tanaka et al 2005, Li et al 2007, Ponik et al 2007, Kinder et al 2008). For example, it has been reported that cell stretching of human osteoblasts at intermittent loading (3 x 3h, 3 x 6 h, magnitude 1 %) resulted in up-regulation of RANKL, which increased osteoclast activity and subsequently bone resorption (Kreja et al 2008).

Based on the prior observations made of significant cytoskeletal change in osteoblastic cells exposed to the metastatic breast cancer conditioned medium, i.e. less actin stress fiber formation (Dhurjati et al 2008), it could be hypothesized that the cancer-affected bone cells would have changes in stiffness which could be quantified using the atomic force microscopic technique (AFM).

AFM is a scanning probe based technique that is dependent on the interaction forces between the probe (AFM tip attached on cantilever spring) and the sample surface. It provides advantages of studying cells in its native biological environment in real time (Sokolov 2007), force sensitivity to the scale of piconewton (Lim et al 2006), nanoscale scanning resolution (Kuznetsova et al 2007, Sokolov 2007) and provides information about cell elastic and viscoelastic properties.

Stiffness of cancer-affected bone cells could be calculated using the Hertz-Sneddon formula for spherical probe of radius R which has been adopted in many studies involving cells (Lekka et al 1999, Charras et al 2001, Jaasma et al 2006, Lim et al 2006, Kuznetsova et al 2007, Sokolov 2007, Bacabac et al 2008). The quantification of cell stiffness changes could be potentially used as an indicator of disease progression.

On further note, the ability of osteoblasts to detect mechanical signals and respond with appropriate biochemical signals is dependent on the cytoskeleton, as suggested by key findings of prior research (Li et al 2007, Myers et al 2007). For instance through microfilament disruption, osteoblasts subjected to cyclical compression loading were found to be inhibited in terms of c-Fos mRNA and protein expression which are important for bone growth and mineralization (Li et al 2007). It can therefore be further postulated that changes in osteoblast cell cytoskeleton could result in significant reduction in cell mechanosensing, mechanotransduction and bone remodeling events.

Mechanotransduction is a process involving the conversion of mechanical stimulus to biochemical or electrical signals through mechanosensing, signal transduction and effector cell (osteoblast and osteoclast) response (Papachroni et al 2009). In bone, which functionally adapts its mass and structure according to mechanical loading, the osteocyte network and lacuno-canalicular porosity are believed to be main constituents facilitating mechanosensing (Burger 2001). Although the exact mechanisms are not known for certain, it has been demonstrated in an increasing number of studies that fluid flow (Chen et al 2000,

Myers et al 2007, Ponik et al 2007, Willems et al 2011), possibly through bone lacunar-canalicular porosity could mediate bone cells mechanosensing. High frequency, low magnitude vibration i.e. using vibration table, has also been employed in both in-vivo and in-vitro studies for stimulating bone (Rubin et al 2002, Rubin et al 2004 , Ozcivici et al 2007, Wenger et al 2010), pre-osteoblast and stem cell differentiation (into osteoblasts) (Patel et al 2009, Ozcivici et al 2010, Pre et al 2011) as well as bone cell osteogenic responses (Bacabac et al 2006, Dumas et al 2010, Hou et al 2011).

It has been reported that the earliest response of osteoblasts to mechanical loading or fluid stress is the rapid increase in calcium concentration within the cell, which triggers signals involved in mechanotransduction (Casimiro et al 2009). Changes in nitric oxide (NO) levels were also monitored to assess the degree of bone cell activation, as NO is released by osteoblastic and osteocyte-like cells with load stimulation (Vatsa et al 2006, McGarry et al 2008).

Biochemical indicators in response to mechanical loading may thus be monitored to assess the differences in mechanosensitivity of the cells from tumour conditioned and non-conditioned groups. The changes in degree of mechanosensitivity of bone cells may also contribute towards the reduction in bone formation activity observed in-vivo.

1.4 Overview of thesis and hypotheses

In this thesis, a modified method of immunocompetent model of osteolytic metastases would be established. It is hypothesized that there would be changes in microstructural and intrinsic mechanical properties for sclerotic bone (disease regression), as arising from increased osteoblast activities. Characterization of bone responses using densitometric, microstructural and viscoelastic parameters would be carried out in the course of this work. Viscoelastic properties were assessed using nanoindentation and dynamic mechanical analysis, with the former technique providing information on local material property changes arising due to changes in local cellular (bone formation) activity.

It is also hypothesized that there would be changes in mechanical and mechanosensing properties of tumor-affected osteoblast cells. To investigate the changes of bone cell mechanical property due to conditioning by primary tumour cells, atomic force microscopy indentation was utilized. The mechanosensing changes in tumor affected bone cells were also examined by assessing nitric oxide level changes to low magnitude, high frequency vibration. By probing the changes in cell stiffness and in degree of mechanosensitivity of bone cells *in vitro*, it could serve to understand one mechanism by which the cellular level bone formation is affected in bone metastasis. This could be important in developing biomechanical strategies for treatment e.g. whole body vibration.

Research Hypotheses

1) There would be changes in microstructural and intrinsic mechanical properties in sclerotic bone compared to normal bone.
2) Variation in cell stiffness would occur due to tumor-conditioning, which also induced cell structural changes.
3) Mechanosensing properties of bone cells to low magnitude, high frequency vibration would be altered by tumor conditioning.

Research Contributions

The current study which involved combination of *in-vivo* rodent model and *in-vitro* bone cellular studies would help to answer: 1) A clinical question: Partly to answer how sclerosis development could have arisen and how it would affect bone microstructural and intrinsic mechanical properties; 2) A scientific question: An important start to understanding the influence of tumor on the mechanical and mechanosensing properties of bone cells and examining the potential of biomechanical strategies e.g. vibration on stimulation of osteogenic response.

Chapter 2: Immunocompetent model of osteolytic metastases

2.1 Summary of Chapter

Establishing an immunocompetent model of osteolytic metastasis is important as the presence of immune system has an impact on the tumor promotion and suppression (Jaganjac 2008, Song et al 2008) and there is a significant cross-talk between tumour cells, immune cells and bone microenvironment (Bussard & Mastro 2009). Thus, it has been argued that an immunocompetent model of bone metastasis will be more appropriate in simulating disease progression (Coleman et al 2008).

While there has not been unequivocal evidence demonstrating immunocompromized models to be less realistic in simulating osteolytic metastases, it has also not been shown that sclerotic development could arise in immunocompromized models (Neudert et al 2003, Cowey et al 2007, Arrington et al 2008, Chanda et al 2008, Ottewell et al 2008). On the other hand, it has been shown that there was spontaneous regression of tumor growth with presence of immune system *in-vivo* (Jaganjac 2008). Since it is our interest to examine sclerotic development which is a clinical sign of disease regression, it would be pertinent to adopt an immunocompetent model which could simulate both disease progression and regression phases. This chapter outlines the development, methodology and discussion of the immunocompetent model of osteolytic metastases adopted in this work.

2.2 Development of model

The surgical induction of osteolytic bone metastasis in an immune-competent Sprague Dawley rodent model was modified after the method adopted by Kurth et al (Kurth & Muller 2001, Kurth et al 2001, Kurth et al 2007). It is selected for the advantages of tumour localization, which could facilitate for longer host survival and monitoring of tumour growth. Moreover, the use of rat mammary carcinosarcoma (W256 cells) provides some clinical relevance as they have characteristics similar to human breast cancer: poor immunogenicity and high metastatic ability (Badraoui et al 2009) as well as differential response to hormonal treatment (Blouin et al 2005). In addition, Kurth's methodology appeared to be repeatable over the years of 2000- 2001 and 2007.

In his method, 2 x 10^6 Walker 256 rat breast carcinosarcoma cells were cultured in 0.6% agarose gel solution and the tumour cells in gel were surgically implanted into the medullary canal through a drill hole made in the intercondylar notch using an 18 gage needle. Kurth's method of drilling through the intercondylar notch was found to have destructive effects on the metaphyseal region, as a distinct drill hole (black arrow) was observed even at the time point of 42 days post surgery (Figure 3A).

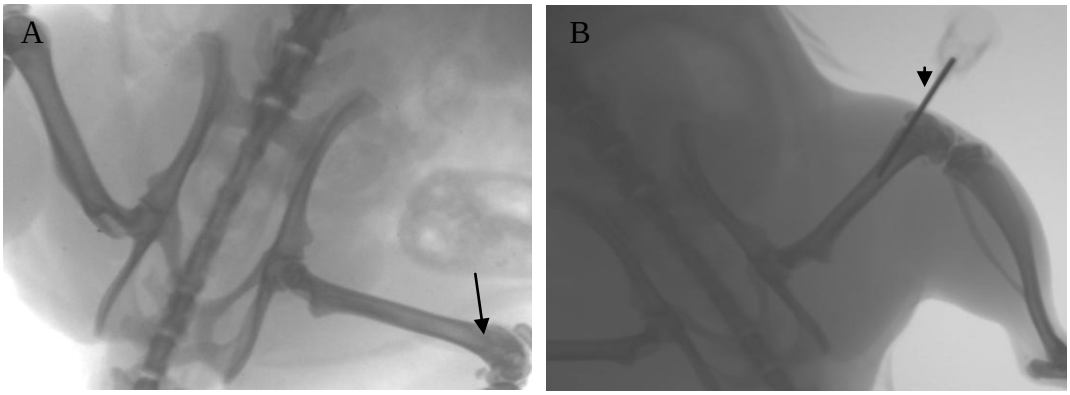

Figure 3: (A) Distinct drill hole made (black arrow) using 18G needle through intercondylar notch at 42 days time-point and (B) Surgical drilling using a 22G needle (black arrowhead).

A number of modifications were made to the technique: (1) change of the surgical insertion site to avoid drilling through the intercondylar notch (and in particular the distal metaphyseal area), (2) using a smaller needle size to reduce surgical damage, (3) increase in the number of cells used and (4) to inject cells without the use of the agarose gel (which is explained in subsequent paragraphs). In our modified technique, 8-10 weeks old female Sprague Dawley rats were subjected to anaesthesia and 10^7 Walker 256 rat breast carcinoma cells (CCL-38, ATCC, USA) were suspended in 0.1 ml of medium and injected into the medullary cavity from an insertion site at least 5 mm away from the distal condyle (Figure 3B).

The modification of surgical insertion site to avoid drilling through the metaphyseal area has grounds based on literature. A study on the kinetics of metastatic human breast cancer cells migration in mice bone have found that the cancer cells were arrested mainly in the metaphyseal area within an hour of intra-

arterial injection and with preliminary evidences of cytokines favouring metaphyseal regions (Phadke et al 2006). Moreover, it was found that W256 cells have a higher growth rate adjacent to trabecular surfaces than when it is more than 50 μm from bone (Kostenuik et al 1993). Thus, reducing the destructive effects of surgical drilling on the metaphyseal area, together with the increased cell density inoculated, is postulated to increase success of tumour adhesion and growth.

Preliminary testing with agarose gel mixed with cells at the stipulated concentration according to Kurth's protocol has yielded less satisfactory results. Trials to optimize agarose gel concentration (0.06%, 0.15%, 0.3%, 0.45%, 0.6%) with addition of tryptose phosphate broth (Li et al 1989) at 10%, 25%, 50%, 75%, 100% v/v with culture medium have not been successful. W256 cells did not grow well in those conditions as shown in Figure 4. While 0.6% agarose with 10% tryphase phosphate broth gel sandwich layer demonstrated the best gelling property and cell compatibility among the different combinations, the cell morphology and growth (clumps of dead cells seen) were affected in those conditions.

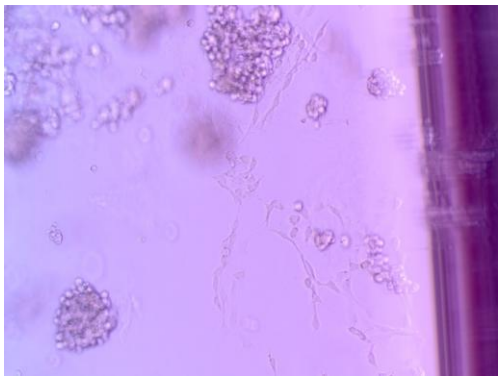

Figure 4: W256 cells in gel sandwich, with 0.6% agarose and 10% tryphase phosphate broth as bottom layer as well as 0.6% agarose top layer.

As such, direct inoculation with cells was used without agarose gel, but with a higher cell concentration to increase chances of inoculation that might be reduced by in-vivo conditions e.g. blood flow out of the surgical site.

2.3 Methodology

Immunocompetent rat model of osteolytic metastases

Thirty nine Sprague Dawley (SD) female rats, 8 -10 weeks old (Laboratory Animal Centre, National University of Singapore) were housed at 25^{o}C with a 12:12 hour light-dark cycle and were given standard rodent diet (Harland, Model T.2018S) and water *ad libitum.* All animal experiments were conducted in accordance with an approved protocol from Institutional Animal Care and Use Committee (IACUC) at National University of Singapore. Surgical procedures were carried out after 5 days of acclimatization of the rats at animal housing unit. The rats were randomly divided into 2 groups: one group (EXP, n=30), was subjected to surgical inoculation of 10^7 W256 cells (ATCC, USA) in 0.1 ml M199 culture medium into the medullary cavity of left femur using a 22G needle, while the right femur was kept intact (Chen et al 2013a). The other group (SHAM, n=9) was surgically inoculated with M199 culture medium into the left femur while the right femur was kept intact.

Radiography

At 10 days interval, rats were subjected to in vivo scanning using Kodak X-ray system (Carestream Health Inc, USA), at 35kV tube voltage, 0.3mA current

and 2 mins exposure time. X-ray analysis was performed with radiological scores given as follows; 0 for no radiolucent lesion observed, 1 for minimal but detectable lysis, 2 for moderate lysis limited to medullary cavity, 3 for extensive lesions extending into soft tissues (Mann et al 2008). Sclerotic bone formation is identified by calcified regions within the medullary and labeled as SCL. Two examiners have graded the radiographs on independent occasions without specimen labelings. Based on the radiographic indication of sclerotic development, some of the rats from the EXP group were allotted to the sclerotic response group (SCL, n=15). The remaining 15 rats showed either varying osteolytic (n=7), mixed osteolytic and sclerotic (n=2) or no lesion responses (n=6).

Histological analyses

Histological analyses were performed on paraffin embedded bone using Hematoxylin and Eosin (H&E) staining for signs of tumor proliferation and bone cell response. The remaining rats from osteolytic groups LYTIC (n=6) and SHAM groups (n=9) were sacrificed at 50 days post-surgery and both femurs were harvested. The bones were wrapped in gauze soaked with phosphate buffered saline (PBS), stored at -20^0C until used for experiments. Prior to testing, the bones were thawed to room temperature (25^0C).

pQCT analysis

Geometric and densitometric properties of left-operated femurs and right intact femurs from both SHAM and LYTIC groups were measured using

peripheral quantitative computed tomography (pQCT) (XCT Research SA+; Stratec, Germany). The bone was scanned from 1mm above the distal metaphyseal growth plate as determined from a prior scout scan, using a voxel size of 100 μm. The metaphyseal region is of interest because any modeling and/or repair of osteolysis, typically associated with trabecular bone loss (Mann et al 2008), could be best assessed at the trabecular rich metaphyseal area. All measurements were averaged across 4 cross-sectional slices, each with a thickness of 0.5mm and slice-to-slice distance of 0.75mm. A threshold of 280 mg/cm^3 was used to separate bone from soft tissue and inner threshold of 550 mg/cm^3 was used to separate trabecular bone from sub-cortical and cortical bone during the analysis (Chen et al 2013a, Yang et al 2011). Bone mineral density (BMD), bone mineral content (BMC), cortical and trabecular density and bone area were calculated for both femurs of each animal.

Micro-CT analysis

The distal femoral metaphysis was scanned using the SkyScan micro-CT machine (SkyScan 1172, Konitch, Belgium) with standardized settings of 100KeV peak energy, 18 μm nominal resolution, with a fixed source to object distance of 121 mm and source to detector distance of 161 mm. The region of interest (ROI), containing 200 micro-CT slices, was scanned from 1mm above the distal metaphyseal growth plate, same as pQCT scans. The images were then analyzed using the CT Analyser program (Skyscan, Belgium). A semi-automated contouring method was employed to select trabecular from cortical bone and the

morphological indices, namely bone volume fraction (BV/TV), bone surface density (BS/TV), trabecular number (Tb.N), trabecular separation (Tb.Sp), trabecular thickness (Tb.Th) and structure model index (SMI) were obtained.

Nanoindentation Testing

Thawed femur bones were rehydrated for 16 hours and then embedded in epoxy resin (Struers, USA) overnight, with the femur positioned upright (Fig. 5A). The embedded sample was cut precisely using a diamond blade (Isomet 1000 precision saw, Buehler, USA) at approximately 2.5 mm from the distal end of the femur (Fig 5B) to expose the metaphyseal growth plate and rehydrated overnight.

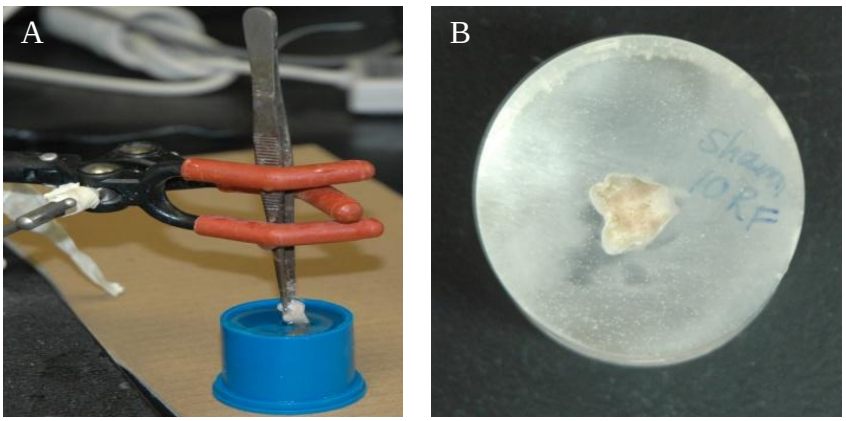

Figure 5: (A) Epoxy embedding of femur sample and (B) sample sectioned at 2.5mm from distal end

The bone was then ground using a series of grinding paper with increasing fineness: 320, 500, 1200 and 4000; then polished using micro-bead suspensions of 3μm followed by 1μm. The sample height was monitored to ensure that indentations were made within the same region of interest (ROI), i.e. 1mm above the distal growth plate, across different samples. Embedded femur specimens

were placed in the testing chamber at room temperature for 2 hours prior to indentation to achieve thermal stabilization (Ishimoto et al 2011). A pyramidal Berkovich tip was used to indent on the bone specimen using dynamic loading i.e. continuous stiffness mode (CSM) (G200 nanoindentor, Agilent, US).

The CSM mode superimposes small oscillation amplitude Z_0, which is a constant of two nanometers, on loading signal at 45Hz. As size of contact increases, force oscillation amplitude, F_0 increases as well to maintain the constant displacement oscillation amplitude. Thus, CSM provides a continuous calculation of indentation modulus (E) and indentation hardness (H) based from amplitude ratio (F_0 / Z_0) (Yang et al 2013). This differed from traditional quasi-static method that yields only one value of E and H at maximum depth (Huja et al 2010).

Specifically, indentation modulus (E) is defined (Herbert et al 2008) as:

$$\frac{E}{(1-\nu^2)} = \frac{F_0}{Z_0} \cos\phi \left(\frac{\sqrt{\pi}}{2}\right)\left(\frac{1}{\beta}\right)\left(\frac{1}{\sqrt{A}}\right) \quad \text{.....Equation (1)}$$

Where ϕ is phase angle between the applied load and resulting displacement, β =1.034 for Berkovich tip (Herbert et al 2008), ν is Poisson's ratio and A is the projected contact area.

On the other hand, hardness (H) is defined as:

$$H = \frac{P}{A} \quad \text{.....Equation (2)}$$

Where P is the load applied to sample surface and A is the projected contact area

A total of 50 indentations of maximum indentation depth of 1200 nm were carried out on the trabecular and cortical regions. Neighboring indents were

spaced more than 60 μm apart and indentations were placed away from the cortical bone/epoxy interface in order to minimize interference due to penetration by epoxy. E and H were determined at a depth of 700-800nm, to avoid interference due to surface roughness.

In this study, bone was assumed to be isotropic (Zysset et al 1999) with Poisson ratio of 0.3 (Kim et al 2013, Huja et al 2010, Zysset et al 1999). An isotropic material is homogenous in all directions for mechanical properties and other physical properties (Lespessailles et al 2006). In contrast, bone is an anisotropic material (Hofmann et al 2006) but indentations on different anatomical locations within transverse section of femoral bone (medial, lateral, anterior, posterior) have indicated that there were no comparative differences between groups. This suggested that bone material could be assumed to be isotropic at nano-level in the longitudinal direction. The assumption made for compressibility is similarly acceptable since sensitivity studies have indicated that the error of E associated with the variation of Poisson ratio (within 0.2-0.4) to be less than 10% (Rho et al 1997, Zysset et al 1999).

A separate creep test was carried out in the cortical and trabecular regions at a maximum load of 6.3mN and hold time of 400s. The indenter tip was then unloaded to 10% of the maximum load and held another 50s for thermal drift measurement. Viscosity (η), which is defined as a parameter reflecting viscous-like deformation in a solid under loading, was evaluated using Equation (3) (Kim et al 2010, Kim et al 2013, Yang et al 2013):

$$h^2(t) = \left(\frac{\pi}{2}\right) P_o \omega t \, \alpha \left[\frac{\left(1 - e^{(-tE/\eta)}\right)}{E}\right] \quad \text{.....Equation (3)}$$

where *h(t)* is the creep displacement under maximum load as a function of time, α is an equivalent cone semi-angle (70.3 °) to the face angle of the Berkovich indenter (65.27 °), *E* is an elastic element of the Voigt model (separately derived from the creep test) and P_o is the maximum load. Figure 6 showed good experimental fitting of bone creep response using Voigt model by non-linear least squares regression (R^2 >0.99 for all indentations).

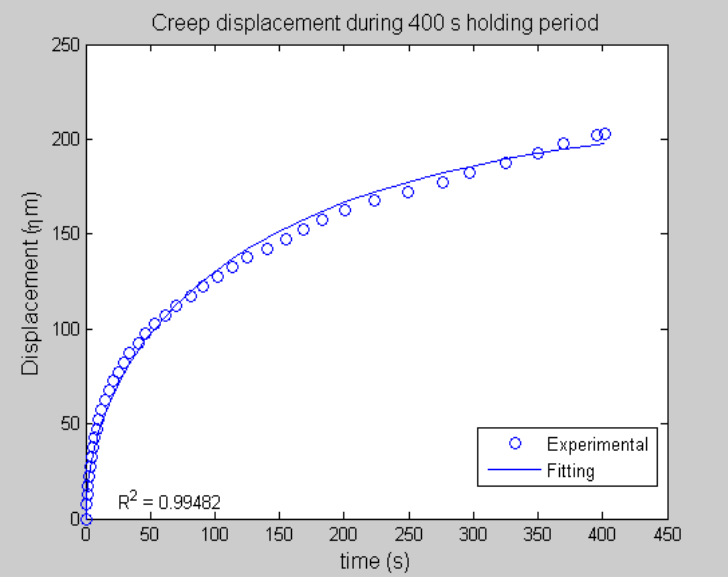

Figure 6: Experimental fitting of bone creep response to Voigt model

2.4 Discussions of the model

One of the primary identifications for bone metastases included bone radiography, which is a standard for differentiating bone lesions (Salvo et al 2009). Osteolytic lesions give a radiolucent appearance due to the destruction of bone and could be associated with or without sclerosis (tissue hardening) formation (Priolo & Cerase 1998). Sclerosis (tissue hardening) development is typical of benign or slow growing lesions, with new and reactive bone formation about the lesion area (Priolo & Cerase 1998).

Through preliminary diagnosis using radiography, it was estimated that out of 30 rodents, 15 had sclerotic response, 7 had highly variable osteolytic effects, 2 presented mixed effect and 6 had no visible bone response. There were no reactive bone changes as a result of the operation, as shown by the sham-operated bone (Fig. 7A). The animal model presented a highly variable osteolytic effect i.e. with 1 rat having extensive radiolucent lesions and fracture (Fig. 7B) and 6 rats with minimal lysis (Fig. 7C). Sclerotic response (Fig. 7D) was the predominant response over other responses (osteolytic, mixed and no response), which was illustrated by highly calcified tissues extending into the medullary cavity.

Since earlier models of both immunocompetent and immunocompromized models of osteolytic metastases have typically presented mainly osteolytic responses (Sasaki et al 1995, Hiraga et al 2001, Kurth et al 2001, Neudert et al 2003, Kurth et al 2007, Zheng et al 2007), there has been no prior report of sclerotic development. As such, even though quantitatively, there was only up to

50% chance of sclerotic response, it was interpreted to be a predominant response over other 3 types of possible responses in this model.

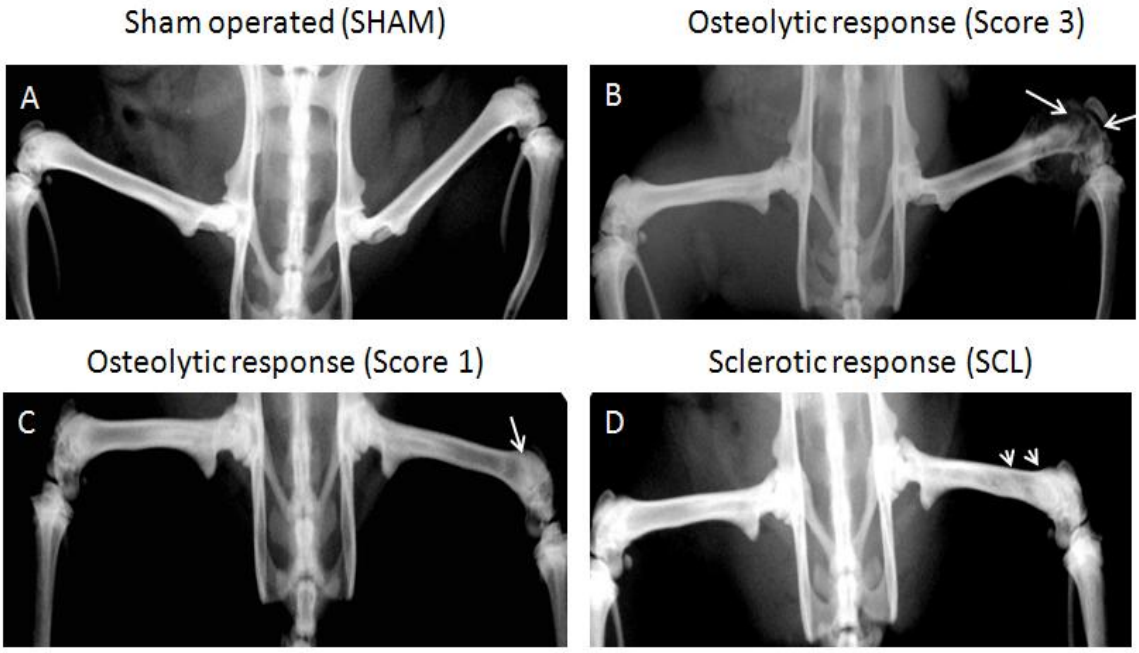

Figure 7: (A) Radiographical examination of different bone responses induced in this model: SHAM with no reactive bone response, (B) Osteolytic (Score 3) with soft tissue tumor burden, (C) Osteolytic (Score 1) with minimal but detectable lesion and (D) SCL with tissue hardening (white arrowheads).

Histological examination has yielded similar results, with 1 rat having aggressive osteolytic tumor burden at the metasphyseal region (Fig. 8), while majority presented stages of tumor regression. Tumor cells were being eliminated as early as 10 days for rats presenting a sclerotic response (Elaboration under Chapter 3). The mechanism for a spontaneous W256 tumor regression was not well understood but has been associated with immune response (Jaganjac et al 2008).

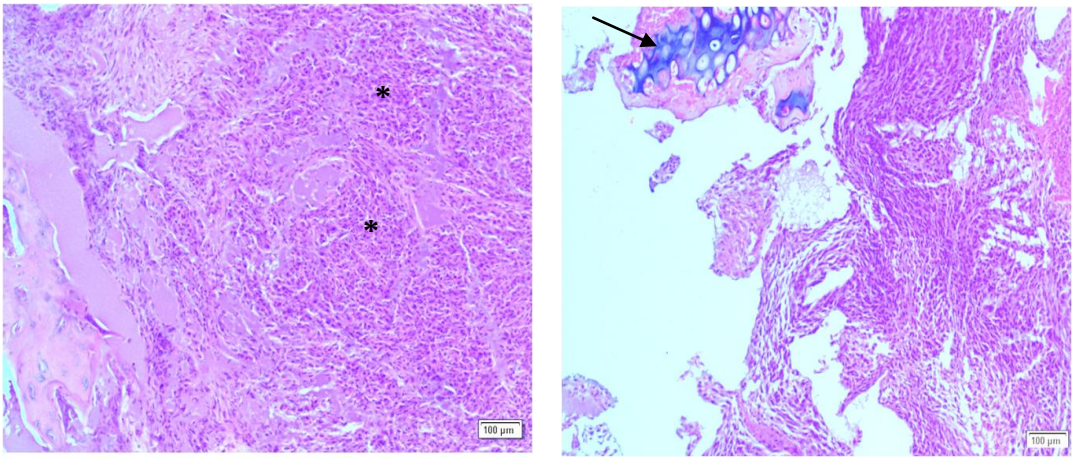

Figure 8: Tumor cells infiltration into soft tissue (*) and fragmented distal metaphyseal growth plate (black arrow).

The variability in tumor growth rates could thus possibly indicate the involvement of the adaptive immune response. Moreover, it was possible that only a small percentage of the heterogeneous tumor cells possess the molecular signature for bone metastasis (Li et al 2008) that could contribute to varying degrees of osteolysis.

Since majority of the osteolytic samples have radiological score of 1 (i.e. 6/7), these rats constituting the LYTIC group (n=6) were used for in-vitro analysis. Rat with soft tumor burden (with soft tumor excised) was used for establishment of primary tumor culture for experiments under Chapter 4 and 5.

pQCT results have indicated that there was significant decrease in trabecular content (-28.7%, p=0.006) for LYTIC group (n=6) compared to SHAM group (n=9) as observed from Table 1. Since osteolysis gives rise to considerable trabecular bone loss before cortical bone integrity is affected (Mann et al 2008), the higher resolution micro-CT is a better tool to assess changes in rat trabecular

bone volume and microstructure. Nevertheless, no significant differences between both groups in terms of trabecular microstructure were found from micro-CT (Table 1). It is plausible that the LYTIC group presented cases of micrometastases, of which micro-CT could have failed to diagnose. Since micro-CT provided a pixel resolution of 18μm which was in the size range of the resorption pits (Chappard et al 2010), a higher resolution micro-CT could assist in providing better diagnosis.

On the other hand, BMD, BMC and weight of LYTIC group were still significantly higher than SHAM group. It has been reported that BMD (Kurth et al 2002, Medhurst et al 2002, Alvarez et al 2003, Fritz et al 2007), BMC (Medhurst et al 2002) and microstructural indices (Kurth & Muller 2001, Fritz et al 2007, Badraoui et al 2009) decreased significantly with increased tumor burden. It was also duly observed that rat with increasing tumor burden appeared to have weight loss and mobility issues. Thus, based on the combined assessment from pQCT, micro-CT and weight changes, the osteolytic effect in the LYTIC group is likely minimal (low tumor burden), which is in accordance with radiological score of 1.

There could be a possibility that some samples constituted a false positive e.g. up to 2% based on X-ray diagnosis (Tudor et al 1997). However, all the bones have been included regardless, since the preliminary diagnoses have indicated positive. As such, it was essential for a number of complementary imaging modalities (pQCT, micro-CT, radiography) to be used for assessment of osteolysis.

Table 1. Densitometric, microstructural parameters and weight at 50th day post surgery.

Variables	Groups			
	LYTIC (Operated LF)	LYTIC (Intact RF)	SHAM (Operated LF)	SHAM (Intact RF)
BMD (mg/cm^3)	795.8 ± 33.0 [a, b]	783.4 ± 40.8	739.4 ± 41.2	725.6 ± 48.4
Trab.BMD (mg/cm^3)	419.1 ± 46.2	432.7 ± 45.0	402.0 ± 45.3	398.7 ± 43.5
Cort.BMD (mg/cm^3)	1051.4 ± 80.1	1045.7 ± 83.1	1056.8 ± 111.1	1068.9 ± 91.3
BMC (mg/cm)	16.2 ± 3.30 [a ,b]	15.8 ± 2.80	14.1 ± 2.88	13.9 ± 2.73
Trab.content (mg/cm)	1.51 ± 0.68 [a, b]	1.58 ± 0.80	2.12 ± 0.64	2.35 ±0.65
Bone Area (cm^2)	20.9 ± 3.83	20.2 ± 3.03	19.1 ± 3.79	19.2 ± 3.70
BV/TV (%)	13.1 ± 1.52	16.0 ± 3.89	11.5 ± 6.22	13.6 ± 5.97
BS/TV (1/mm)	4.24 ± 0.3	5.11 ± 0.94	3.63 ± 1.49	4.31 ± 1.35
Tb.N (1/mm)	0.93 ± 0.11	1.15 ± 0.24	0.77 ± 0.34	0.97 ± 0.34
Tb.Th (mm)	0.14 ± 0.002	0.13 ± 0.006	0.14 ± 0.02	0.13 ± 0.015
Tb.Sp (mm)	0.59 ± 0.10	0.56 ± 0.13	0.73 ± 0.22	0.64 ± 0.16
SMI	2.53 ± 0.22	2.37 ± 0.13	2.64 ± 0.29	2.43 ± 0.30
Weight (g)	308.3 ± 26.7 [c]		277.5 ± 21.1	

[a] Significant difference from SHAM (Operated LF) ($p<0.05$) by one-way ANOVA , Bonferroni post hoc analysis.
[b] Significant difference from SHAM (Intact RF) ($p<0.05$) by one-way ANOVA, Bonferroni post hoc analysis
[c] Significant difference from SHAM ($p<0.05$) by paired t-test, $p <0.05$

Local nanomechanical property changes of LYTIC group on the other hand, have shown a significant decrease in cortical hardness (-13.3%) and a general trend of decrease across other parameters with the exception of trabecular viscosity η_t (which was slightly higher) as compared to SHAM (Table 2).

Metastatic cancer affected trabeculae has been shown to have a significant decrease (-50%) in local tissue hardness H_t and in elastic modulus E_t (Nazarian et al 2008). Thus, the trend of reduced elastic mechanical properties observed from nanoindentation results appeared to be in agreement, except that it was cortical hardness that was significantly changed and not trabecular hardness. It was a little unexpected since osteolysis effects are more likely to affect trabecular bone faster than cortical bone (Mann et al, 2008) and it was trabecular content which was significantly decreased for LYTIC group.

Table 2. Nanomechanical property changes of LYTIC and SHAM as measured by nanoindentation. Group averages are represented as mean ± SD.

Variables	50^{th} day after surgery	
	LYTIC (Operated LF)	SHAM (Operated LF)
E_c (GPa)	16.38 ± 3.31	16.45 ± 2.68
E_t (GPa)	13.85 ± 3.00	14.03 ± 1.56
H_c (GPa)	0.52 ± 0.15 [a]	0.60 ± 0.14 [b]
H_t (GPa)	0.54 ± 0.16	0.56 ± 0.12
η_c (GPa S)	27456 ± 11234	30370 ± 10555
η_t (GPa S)	28203 ± 10166	27870 ± 8111

E_c = cortical elastic modulus, E_t = trabecular elastic modulus, H_c = cortical hardness, H_t = trabecular hardness, η_c = cortical viscosity, η_t = trabecular viscosity, LF = Left Femur, RF = Right Femur.
Statistical Test: One way ANOVA with Bonferroni corrections (SPSS v.16)
[a] Significant difference from SHAM (Operated LF) ($p<0.05$)
[b] Significant difference from LYTIC (Operated LF) ($p<0.05$)

It could be that there is a need for longer time for the manifestation of osteolytic effect for these rats with lower tumor growth rates. The model thus has its limitations in terms of reproducibility i.e. high variability in osteolytic lesions and limited tumor cell survival which depended on escaping immune surveillance and forming symbiotic interactions with host cells (Fidler 2003).

On the other hand, since the model provides sclerotic response, it could be ideal for examining sclerosis development (Chapter 3). With a primary tumor culture derived from *in-vivo* model, the direct effects of primary tumor cells on bone cells mechanical properties (Chapter 4) and mechanosensing (Chapter 5) could also be investigated in-vitro.

Chapter 3: Sclerotic response of bone tissue in immunocompetent model of osteolytic metastases

3.1 Summary of Chapter

Sclerosis (tissue hardening) development is a common occurrence in slow growing or benign osteolytic lesions. However, there is lack of knowledge on the mechanical and material property changes associated with sclerotic bone response. The immune system is postulated to play a relevant role in evoking sclerotic bone responses. In this chapter, localized sclerotic response in an immunocompetent model of Walker 256 breast carcinoma in SD rats showed a healing flare, with subsequent increase in new reactive bone formation. Sclerotic rat femurs showed significant increases in bone mineral density (BMD), bone mineral content (BMC), bone volume fraction (BV/TV), bone surface density (BS/TV), trabecular number (Tb.N) and a significant decrease in trabecular separation (Tb.Sp) and structural model index (SMI) as compared to control rat femurs. Significantly reduced creep responses were observed for both trabecular and cortical bone in sclerotic bones while no significant difference were observed in elastic modulus (E) and hardness (H) values, despite the active modeling. Therefore, we conclude that viscoelastic creep property using nanoindentation would serve as a more sensitive indicator of localized bone modeling than the elastic properties. Although enhanced microstructural changes and increased BMD contributes towards increased bone strength, reduced viscoelasticity could contribute towards increased microcrack propagation and therefore a reduced toughness. Since significant positive correlations between elastic properties (E) and (H) with viscosity (η) were also found, we can conclude that mechanical behavior of

sclerotic bone could shift towards a material with lowered damping and increased stiffness.

3.2 Introduction

For slow growing or benign lytic lesions, sclerosis (tissue hardening) development is a frequent occurrence (Priolo, & Cerase 1998) . In a study of 274 patients over 10 years, regression indicators in osteolytic bone metastasis based on radiological analysis were found to be recalcification of the lesion (11.6%), foci of sclerosis around the lesion (13.5%) which are apparent as low calcified spots and lack of deterioration of lesion (10.5%) over a period of at least 12 months (Huber et al 2002). Although sclerosis development in bone is seemingly favorable, little is known regarding its mechanism or its intrinsic material and mechanical property changes.

Bone is a hierarchical composite material comprising of macroscale bone cortex - trabeculae structure, microscale osteons - lamellae structure and nanoscale collagen fibers - hydroxyapatite crystals (Richie et al 2009, Chang et al 2011). As a composite material, bone exhibits viscoelastic behavior across different scales. Nanoindentation techniques could be used to study local tissue viscoelasticity, by analyzing the creep effect of the bone under constant load using rheological models such as Burger (Isaksson et al 2010a, Isaksson et al 2010b) and Voigt models (Kim et al 2013, Yang et al 2013, Kim et al 2011). It has already been used to monitor localized nanomechanical property changes in osteolytic bones (Nazarian et al 2008). Nano-level elastic properties could also be

assessed using semi-dynamic (Isaksson et al 2010a, Isaksson et al 2010b) and dynamic loading methods (Pathak et al 2011).

Dynamic mechanical analyses could be used after nanoindentation to assess tissue viscoelasticity from machined sections of bone. By monitoring tan δ (ratio of energy dissipated to energy stored in elastic component) across a range of frequencies, the comparative changes in tissue damping property could be provided. Together with peripheral quantitative computed tomography (pQCT) (Gasser 1995, Jamsa et al 2000) and micro-CT, these techniques could be used to assess the degree of bone repair and modeling occurring in sclerosis.

This chapter aims to assess the sclerotic response in an immunocompetent rodent model in terms of histological assessment, densitometric, micro-architectural indices and intrinsic tissue mechanical properties. It is a pertinent issue since changes in intrinsic material properties may affect the tissue level quality and strength. To the best of our knowledge, this is the first chapter to study the sclerotic response in an immunocompetent model of breast cancer inoculated into bone. The presence of the immune system in the animal model is postulated to play a relevant role in evoking sclerotic bone response.

The objectives of this chapter are therefore to: (1) characterize histomorphometric, densitometric, microarchitectural, elastic and viscoelastic property changes in a localized sclerotic response in an immunocompetent rat model and (2) to study whether viscoelastic nanomechanical properties can be used to detect localized changes due to bone modeling.

3.3 Methodology

Immunocompetent animal model

Thirty nine Sprague Dawley (SD) female rats, 8 -10 weeks old (Laboratory Animal Centre, National University of Singapore) were housed at 25^{o}C with a 12:12 hour light-dark cycle and were given standard rodent diet (Harland, Model T.2018S) and water *ad libitum.* All animal experiments were conducted in accordance with an approved protocol from Institutional Animal Care and Use Committee (IACUC) at National University of Singapore. Surgical procedures were carried out after 5 days of acclimatization of the rats at animal housing unit. The rats were randomly divided into 2 groups: one group (EXP, n=30), was subjected to surgical inoculation of 10^7 W256 cells in 0.1 ml M199 culture medium into the medullary cavity of left femur using a 22G needle, while the right femur was kept intact (Chen et al 2013a). The other group (SHAM, n=9) was surgically inoculated with M199 culture medium into the left femur while the right femur was kept intact. Based on preliminary radiographical diagnosis, 15 out of 30 in EXP group exhibited sclerotic bone responses and were allocated to SCL group (n=15).

Histological analyses

2 rats from SCL group were euthanized at 10 days interval until 50 days post-surgery and their femur bones were subjected to histological assessment. Histological analyses were performed using H&E staining for signs of tumor proliferation and bone cell response. While n=2 rats is insufficient to account for

inter-rat variability, histological analyses were meant to qualitatively shed light on the role of immune system, tumor cells and bone cells on the development of sclerosis. Given the limited number of samples, n=2 per time point was assigned. Additional Masson trichrome staining of collagen in a 50 days post-surgery SCL bone sample was performed by the Advanced Molecular Pathology Laboratory, IMCB, A*STAR, Singapore.

The remaining rats from SCL (n=5) and SHAM groups were sacrificed at 50 days post-surgery and both femurs were harvested. The bones were wrapped in gauze soaked with phosphate buffered saline (PBS), stored at -20^{0}C until used for subsequent experiments. Prior to testing, the bones were thawed to room temperature (25^{o}C).

pQCT analysis

Geometric and densitometric properties of left-operated femurs and right intact femurs from both SHAM and SCL groups were measured using peripheral quantitative computed tomography (pQCT) (XCT Research SA+; Stratec, Germany). The bone was scanned from 1mm above the distal metaphyseal growth plate as determined from a prior scout scan, using a voxel size of 100 μm. The metaphyseal region is of interest because any modeling and/or repair of osteolysis, typically associated with trabecular bone loss (Mann et al 2008), could be best assessed at the trabecular rich metaphyseal area. All measurements were averaged across 4 cross-sectional slices, each with a thickness of 0.5mm and slice-to-slice distance of 0.75mm. A threshold of 280 mg/cm^3 was used to separate bone from

soft tissue and inner threshold of 550 mg/cm^3 was used to separate trabecular bone from sub-cortical and cortical bone during the analysis (Chen et al 2013a, Yang et al 2011). Bone mineral density (BMD), bone mineral content (BMC), cortical and trabecular density and bone area were calculated for both femurs of each animal.

Micro-CT analysis

The distal femoral metaphysis was scanned using the SkyScan micro-CT machine (SkyScan 1172, Konitch, Belgium) with standardized settings of 100KeV peak energy, 18 µm nominal resolution, with a fixed source to object distance of 121 mm and source to detector distance of 161 mm. The volume of interest (VOI), containing 200 micro-CT slices, was scanned from 1mm above the distal metaphyseal growth plate, same as the pQCT scans. The images were then analyzed using the CT Analyser program (Skyscan, Belgium). A semi-automated contouring method was employed to select trabecular from cortical bone and the morphological indices, namely bone volume fraction (BV/TV), bone surface density (BS/TV), trabecular number (Tb.N), trabecular separation (Tb.Sp), trabecular thickness (Tb.Th) and structure model index (SMI) were obtained. The degree of anisotropy (DA), which is defined as the ratio of the longest to the shortest axis of the ellipsoid could also be determined (Whitehouse 1974). Three-dimensional CT rendered images were obtained at a higher nominal resolution of 9 µm using adaptive rendering algorithm by using the ANT program (Skyscan, Belgium).

Nanoindentation Testing

Thawed femur bones were rehydrated for 16 hours and then embedded in epoxy resin overnight, with the femur positioned upright. The embedded sample was cut precisely using a diamond blade to expose the metaphyseal growth plate (Isomet 1000 precision saw, Buehler, USA) and rehydrated overnight. The bone was then ground using a series of grinding paper with increasing fineness: 320, 500, 1200 and 4000; then polished using micro-bead suspensions of 3 µm followed by 1 µm. The sample height was monitored to ensure that indentations were made within the same ROI, across different samples. Embedded femur specimens were placed in the testing chamber at room temperature for 2 hours prior to indentation to achieve thermal stabilization (Ishimoto et al 2001). A pyramidal Berkovich tip was used to indent on the bone specimen using continuous stiffness mode (CSM) (G200 nanoindentor, Agilent, US). This dynamic mode of indentation superimposes a small oscillation at 45Hz, $0.01s^{-1}$ on loading signal, to provide a continuous measure of elastic modulus (E) and hardness (H) up to a maximum indentation depth of 1200 nm.

A total of 50 indentations were carried out on the trabecular and cortical regions, where neighboring indents were spaced more than 60 µm apart. Indentations were placed away from the cortical bone/epoxy interface and towards the inner cortex in order to minimize interference due to penetration by epoxy. E and H were determined at a depth of 700-800nm, to avoid interference due to surface roughness. Thermal drift was corrected for each indentation experiment, by calculating the drift rate due to thermal expansion or contraction

in the test material or equipment, near the end of each experiment. In this study, bone was assumed to be isotropic with Poisson ratio of 0.3.

A separate creep test was carried out in the cortical and trabecular regions at a maximum load of 6.3mN and hold time of 400s. The indenter tip was then unloaded to 10% of the maximum load and held another 50s for thermal drift measurement. Viscosity (η), which is defined as a parameter reflecting viscous-like deformation in a solid under loading, was evaluated using Equation (3) below (Kim et al 2010):

$$h^2(t) = \left(\frac{\pi}{2}\right) P_o \cot\alpha \left[\frac{\left(1 - e^{(-tE/\eta)}\right)}{E}\right] \quad \text{.....Equation (3)}$$

where *h(t)* is the creep displacement under maximum load as a function of time, α is an equivalent cone semi-angle (70.3 °) to the face angle of the Berkovich indenter (65.27 °), *E* is an elastic element of the Voigt model and P_o is the maximum load.

Pearson's correlations were established between η and E values and between η and H values. The indentations for creep and CSM modes were distanced sufficiently close to each other for a valid correlation.

Dynamical Mechanical Analysis

Rectangular strips of cortical bone in the posterior section (width 1.55 ± 0.05 mm, thickness 0.35 ± 0.018mm) were sectioned from earlier nanoindentation samples, with SHAM (n=5) and SCL (n=4) . The bones were tested in single cantilever bending (Fig. 9A) with a span of 5mm, in phosphate buffered saline

solution at 37 ℃ using a Dynamic mechanical analyzer (DMA8000, Perkin-Elmer, USA). Each bone was tested in triplicates, with at least 40 min between each test, which consisted of a frequency scan from 0.01 to 20 Hz. Dynamic mechanical analysis assesses viscoelastic properties of bone by applying oscillating stress σ (Fig. 9B) with angular frequency ω to a material (Equation 4). Resulting strain ε was then recorded as with Equation 5.

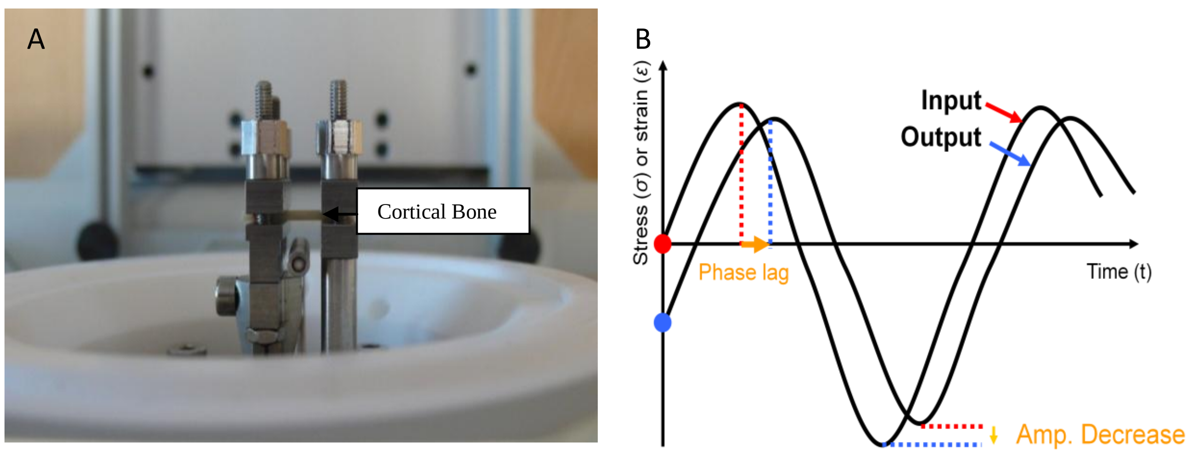

Figure 9: (A) Dynamic mechanical analyzer single cantilever set up, showing fixation of the cortical bone section (black arrow) and (B) Sinusoidal stress applied on linear viscoelastic material and showing phase lag δ.

Equations (Les et al 2005):

$$\sigma = \sigma_o \cos \omega t \quad (4)$$

Measured strain ε:

$$\varepsilon = \varepsilon_o \cos(\omega t - \delta) \quad (5)$$

where δ is the phase angle between stress σ and strain *ε* in response to a sinusoidal stress σ (t) as shown in Figure 9B. The complex modulus of the material under these conditions, *E** can be defined as

$$E^* = E' + iE'' \quad \ldots\ldots\ldots\ldots\ldots\ldots\ldots\ldots\ldots\ldots\ldots\ldots\ldots \quad (6)$$

where *E'* is the real or storage modulus (approximated to the Young's modulus)

$$E' = (\sigma_o/\varepsilon_o) \cos \delta \quad \ldots\ldots\ldots\ldots\ldots\ldots\ldots\ldots\ldots\ldots\ldots\ldots \quad (7)$$

and E*''* is the loss modulus:

$$E'' = (\sigma_o/\varepsilon_o) \sin \delta \quad \ldots\ldots\ldots\ldots\ldots\ldots\ldots\ldots\ldots\ldots\ldots\ldots \quad (8)$$

The loss tangent, or tan δ, is defined as

$$\tan \delta = E''/\, E' \quad \ldots\ldots\ldots\ldots\ldots\ldots\ldots\ldots\ldots\ldots\ldots\ldots\ldots \quad (9)$$

Tan δ that indicates amount of energy dissipated relative to energy stored in elastic component (Yeni et al 2007) may then be derived using Equation (9). There is an implicit assumption of bone being a linearly viscoelastic material which is not reflective of true bone material property. Nonetheless, it was adopted as a model in DMA to assess changes in viscoelastic responses in control and test samples.

Statistical analysis

All statistical analysis was conducted using SPSS v16, with results reported as mean ±SD (standard deviation). One-way ANOVA analysis ($p<0.05$) for SHAM, SCL groups were carried out with post-hoc tests of Bonferroni for

equal variances and Tamhane' T2 for unequal variances. Bivariate linear Pearson's correlation coefficients were also established with $p<0.05$ (2 tailed) for significance. For DMA results, paired t-test was used for comparisons between SHAM and SCL bone per frequency point, with $p<0.05$ (2 tailed) for significance.

3.4 Results

Different responses of bone metastasis

A combination of factors including different host conditions and heterogeneity in metastatic potential of tumor cells induces different bone responses (Nicolson & Poste 1983). In the group surgically inoculated with W256 cells (n=30), there were predominantly sclerotic response (n=15), variable osteolytic effect (n=7), mixed (n=2) and no responses (n=6) based on preliminary radiography examinations.

As observed from histological assessment (Fig. 10A), a cascade of healing activities involving osteoblast cells was observed at the 10^{th} day post-surgery for sclerotic group. Presence of any prominent inflammatory response to W256 cells appeared to have receded by 10^{th} day. As shown in Fig. 10B, there were no signs of tumor cells on day 50 post-surgery (or at earlier time-points) for sclerotic femurs but there were active osteoblastic cells which formed immature bone extending to the medullary cavity. The lamellar bone tissue in this region of interest displayed no qualitative difference in collagen organization from the surrounding tissues (Fig. 10C).

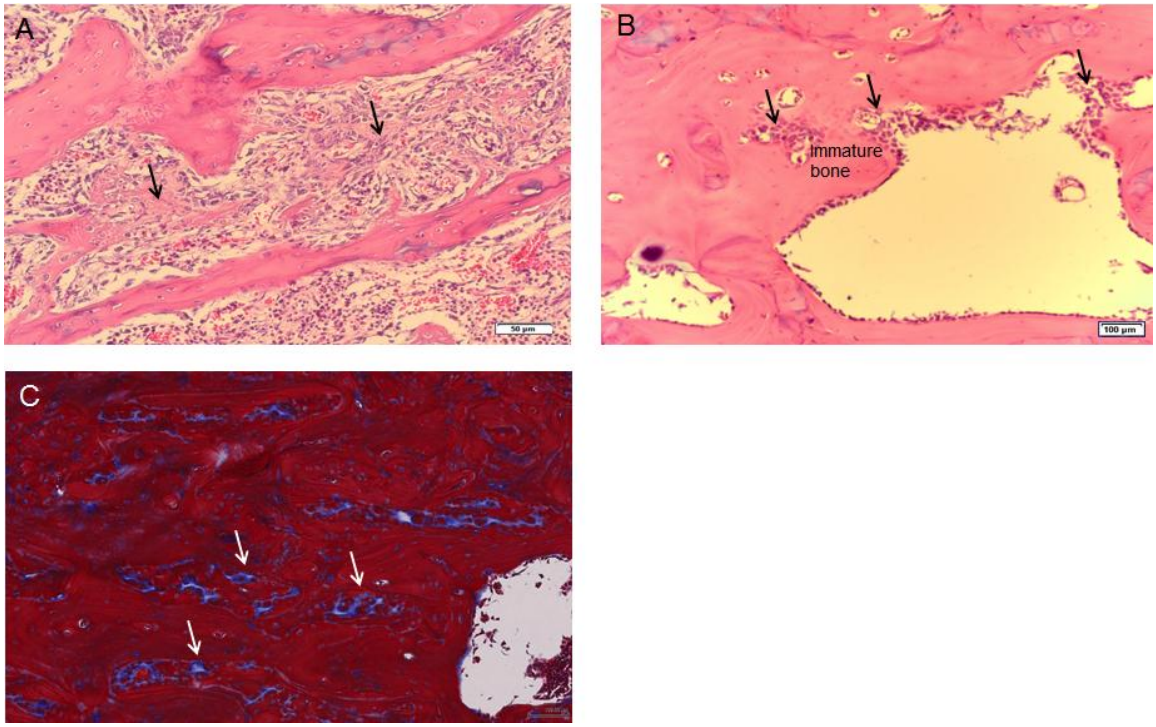

Figure 10: (A) Healing cascade (black arrows) at 10th day at 20x magnification; (B) Immature bone formation and osteoblasts activity (black arrows) at 50th day, 10x magnification for sclerotic bone and (C) Collagen staining (white arrows) of sclerotic bone at 50th day, at 10x magnification with Masson's Trichrome stain.

Densitometric and morphological changes

Fig. 11A shows 4 sequential slices of pQCT rendered images of distal femur where an infiltration of bone (indicated by white and highly mineralized regions) into the medullary cavity was prominent in sclerotic femur at 50 days. This was increasingly obvious in slices closer to the diaphyseal region. Fig. 11B, C and D represents averaged BMD, BMC and trabecular density of SHAM and SCL groups at 50th day. Significant increases in BMD (+12.8%, $p<0.001$) and BMC (+17.4%, $p=0.039$) were found in the SCL femur as compared to SHAM

femur. Trabecular density was observed to have increased in SCL bone but this increase was not significant (+6.42%, p=0.236). Cortical density (+0.14%, p=1.0) and bone area (+4.31%, p=1.0) of both groups (SCL compared to SHAM) were not significantly different from each other.

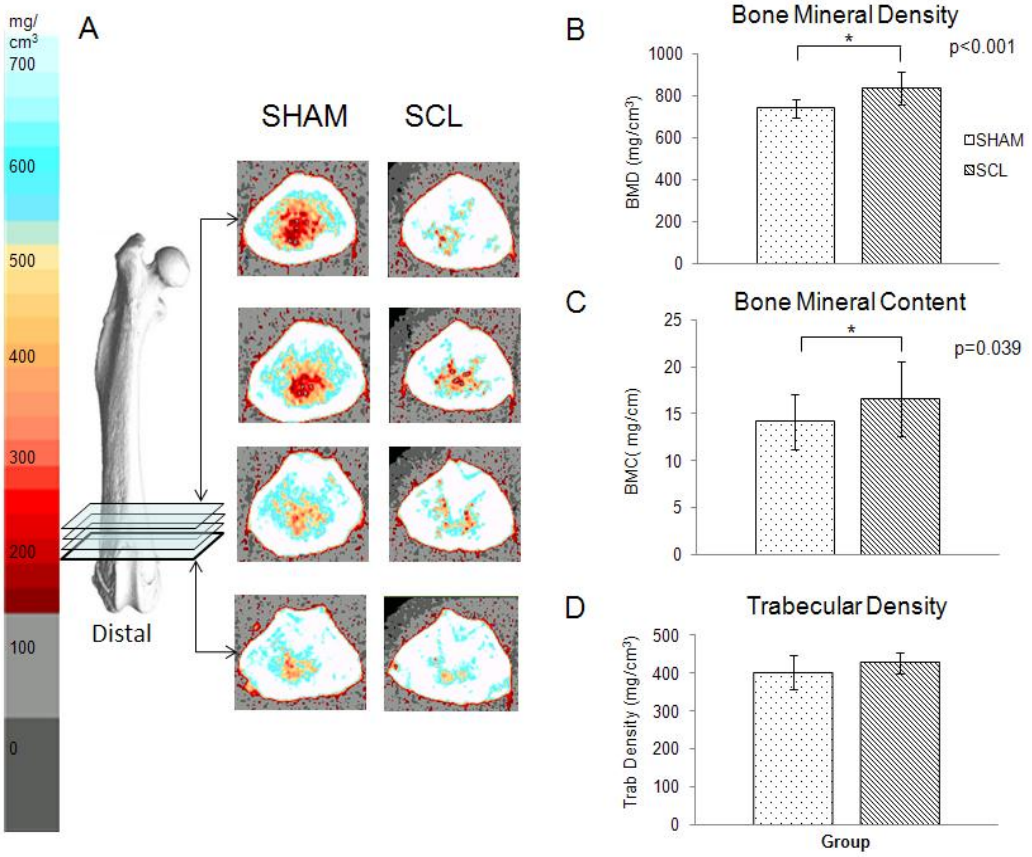

Figure 11: (A) pQCT sequential sections at metaphyseal region showed infiltration of new bone into the medullary for SCL bone in sections closer towards diaphyseal region, (B) Bone Mineral Density (BMD), (C) Bone Mineral Content (BMC) and (D) mean Trabecular Density. * -indicated $p<0.05$, one way ANOVA with bonferroni corrections

Fig. 12 shows the micro-CT rendered image of SHAM and SCL femurs with a nominal resolution of 9 µm. It was observed that there was an increase in trabecular bone structure and volume in the medullary region of SCL bone as compared to SHAM bone.

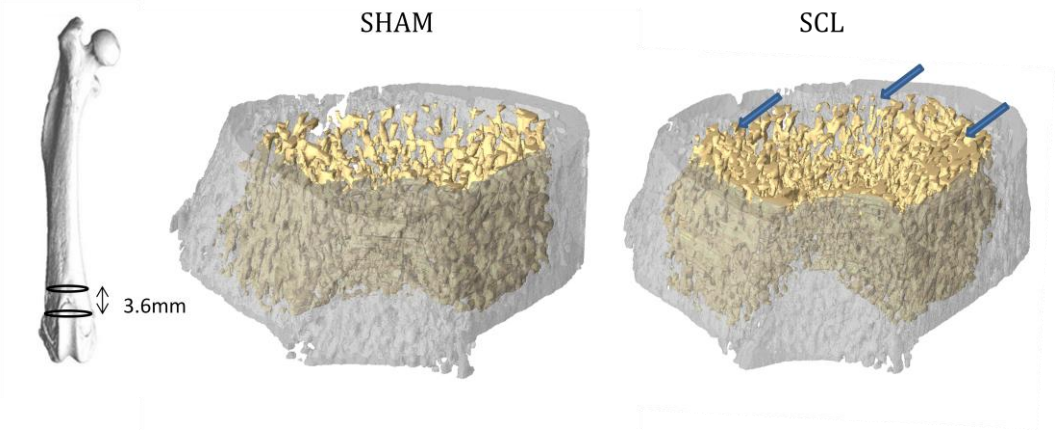

Figure 12: Micro-CT images of SHAM and SCL, with isotropic voxel at 9µm. SCL showed enhanced trabecular microarchitecture (arrows) compared to SHAM.

Fig.13 shows the microstructural indices for SHAM and SCL group for mean BV/TV, BS/TV, Tb.N, Tb.Th, Tb.Sp and SMI. Significant increases in BV/TV (+179.3%, $p<0.001$), BS/TV (+83.3 %, $p=0.002$), Tb.N (+99.3%, $p=0.001$) and decreases in Tb.Sp (-48.9%, $p=0.006$) and SMI (-29.1%, $p=0.001$) were observed in SCL left femurs as compared to the SHAM left femurs. An increase in Tb.Th was also observed in SCL left femur, but the difference was not significant (+321.1%, $p = 0.886$). Similarly, there was no significant difference in degree of anisotrophy between SHAM (2.81 ± 0.45) and SCL left femur groups

(2.66 ± 0.19). It also indicated that trabecular microstructure in both groups were anisotropic.

On the other hand, as shown in Table 3, the mean linear attenuation coefficient (per pixel) of SCL bone was significantly higher than that of SHAM for trabecular bone (+ 7.76%, p = 0.026) and not significant for cortical bone (+ 4.13%, p = 1.0).

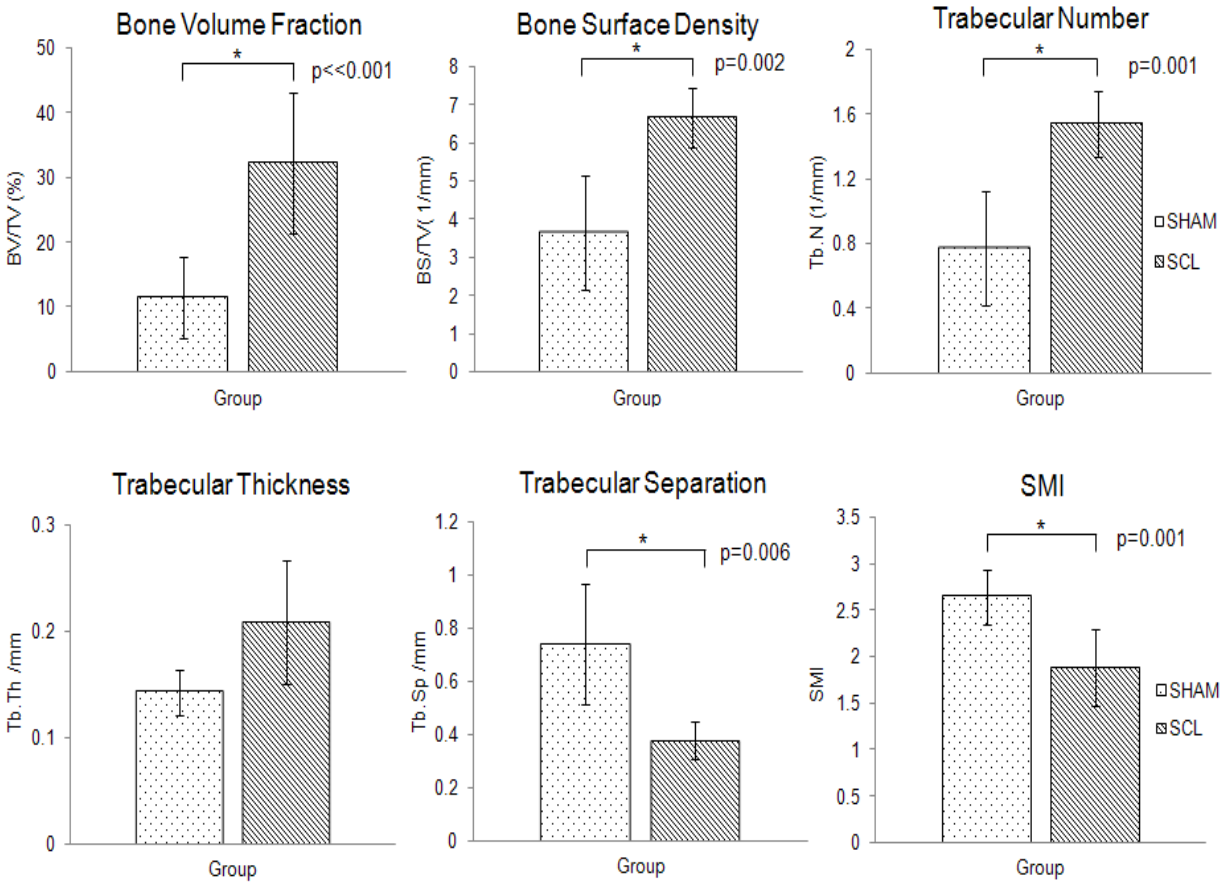

Figure 13: Micro-CT indices of SHAM and SCL: Bone volume fraction (BV/TV), Bone surface density (BS/TV), Trabecular number (Tb.N), Trabecular thickness (Tb.Th), Trabecular separation (Tb.Sp) and Structural model index (SMI). * indicated p<0.05

Nano-level elastic and viscoelastic properties

There were no significant differences found in either cortical or trabecular E and H values between SCL and SHAM operated bones (Table 3).

Table 3. Nanomechanical properties changes and mean linear attenuation coefficients. Group averages are represented as mean ± SD.

Variables	50^{th} day after surgery			
	SHAM (Operated LF)	SCL (Operated LF)	SHAM (Intact RF)	SCL (Intact RF)
E_c (GPa)	16.45 ± 2.68	16.19 ± 2.92	16.79 ± 2.92	16.16 ± 2.67
E_t (GPa)	14.03 ± 1.56	14.27 ± 2.33	14.51 ± 2.87	13.77 ± 2.51
H_c (GPa)	0.60 ± 0.14	0.56 ± 0.15	0.61 ± 0.14	0.57 ± 0.15
H_t (GPa)	0.56 ± 0.12	0.59 ± 0.14	0.61 ± 0.13	0.56 ± 0.16
η_c (GPa S)	30370 ± 10555 [b]	38365 ± 11319 [a,c,d]	33629 ±10474 [b]	31095 ±10076 [b]
η_t (GPa S)	27870 ± 8111 [b]	36109 ± 11109 [a]	34333 ±11330	30250 ±11049
μ_c (cm^{-1})	0.029 ± 0.0019	0.030 ± 0.0009	0.031 ± 0.0013	0.032 ± 0.0009
μ_t (cm^{-1})	0.0206 ± 0.0009	0.0222 ± 0.005 [a]	0.0212 ± 0.0008	0.0220 ± 0.0004

E_c = cortical elastic modulus, E_t = trabecular elastic modulus, H_c = cortical hardness, H_t = trabecular hardness, η_c = cortical viscosity, η_t = trabecular viscosity, μ_c = cortical mean linear attenuation coefficient, μ_t = trabecular mean linear attenuation coefficient. LF = Left Femur, RF = Right Femur.

[a] Significant difference from SHAM (Operated LF) ($p<0.05$)

[b] Significant difference from SCL (Operated LF) ($p<0.05$)

[c] Significant difference from SHAM (Intact RF) ($p<0.05$)

[d] Significant difference form SCL (Intact RF) ($p<0.05$)

Statistical Test: One way ANOVA with Bonferroni corrections (SPSS v.16)

However, a significant increase in η was observed in SCL group in both cortical (+26.32%, $p <0.001$) and trabecular bones (+29.56%, $p=0.032$) as compared to SHAM group (Fig. 14A and B). The creep data from SCL and

SHAM bones fitted well with Voigt model with all indentations having R^2 >0.99.

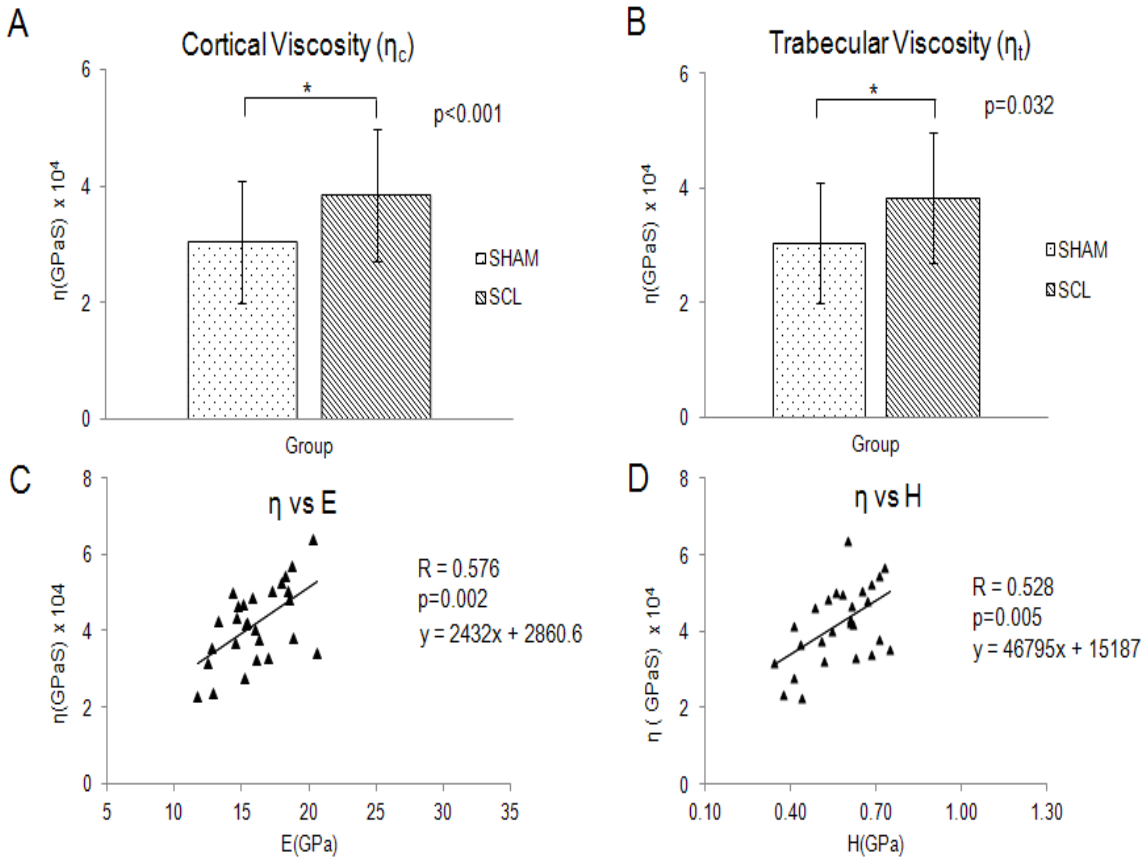

Figure 14: (A) Cortical and (B) Trabecular viscosity of SHAM and SCL with * indicating significant difference between groups, (C) Correlation between η and E and (D) Correlation between η and H

Significant positive Pearson's correlations between η vs. E and η vs. H were observed and the corresponding correlation coefficients were found to be 0.576 (p=0.002) and 0.528 (p=0.005) respectively. The corresponding linear slopes of correlation (m) were of high values, with m=2432 s and m=46795 s respectively (Fig 14 C, D). This suggested that when viscosity values increased

with sclerosis development in both cortical and trabecular bones, indentation modulus (E) and hardness values (H) also increased, but to a much smaller extent.

Tissue level viscoelastic properties

As observed from Fig. 15, no significant changes in tan delta or damping were found across different frequencies from 1-20Hz. Nonetheless, there was an observed sharper decline in tan delta at 15.85 Hz for SCL bone than for SHAM bone.

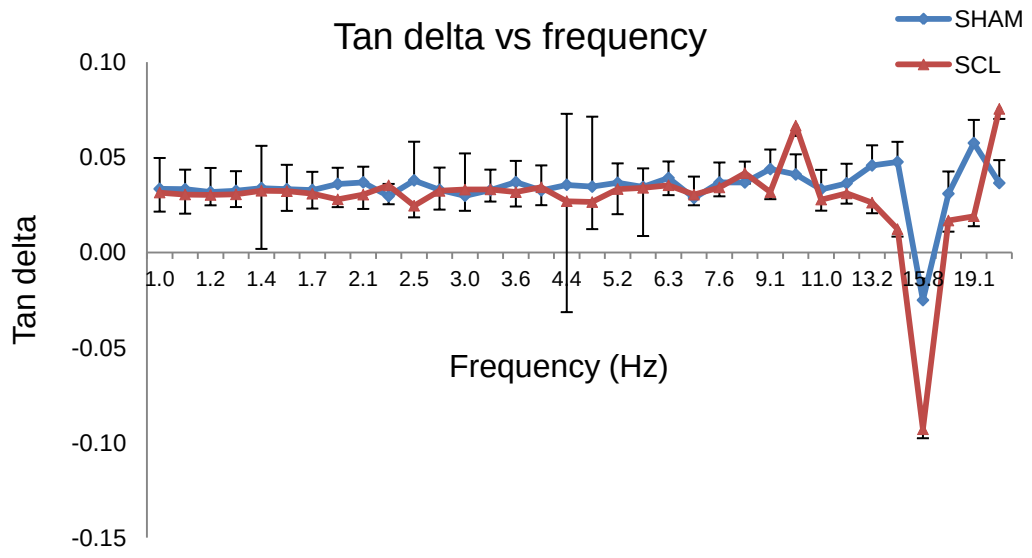

Figure 15: Tan delta of SHAM and SCL groups across different frequencies (1-20 Hz).

Similarly for storage modulus, no significant differences were found between the two groups (Fig. 16).

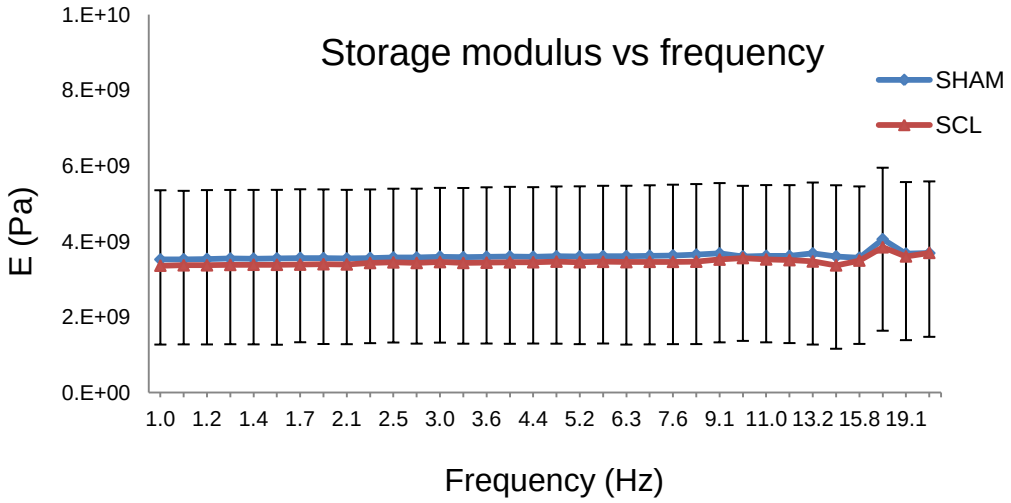

Figure 16: Storage moduli of SHAM and SCL groups across different frequencies (1-20 Hz)

Since E and H did not change at the nano-level and sclerosis effect appeared to be localized, there was less likelihood for cortical bone storage modulus at the tissue level to be affected. Furthermore, since tan delta, a ratio of storage modulus and loss modulus did not vary, it was also within expectation that loss modulus did not vary between the two groups (Fig. 17).

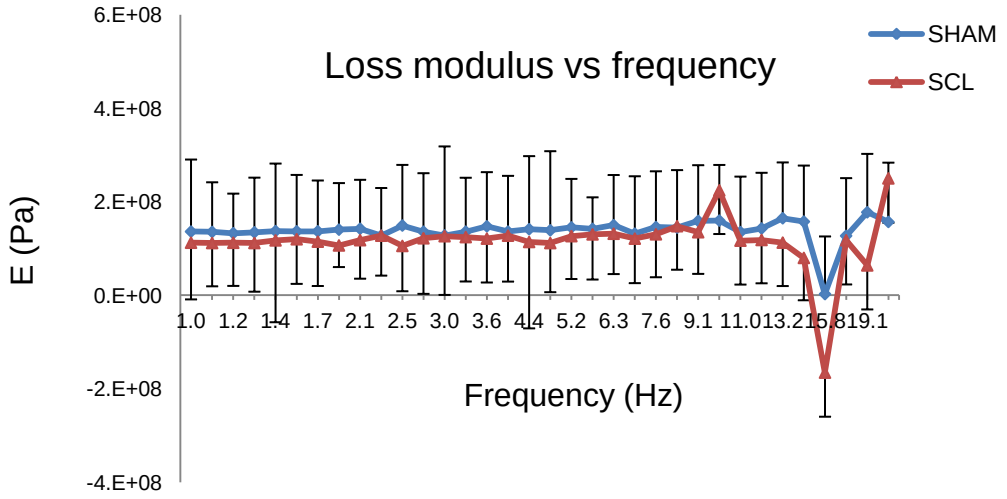

Figure 17: Loss moduli for SHAM and SCL across different frequencies (1-20 Hz)

Nonetheless, it could be observed that the decrease in tan delta at 15.85Hz corresponded to the decrease of loss modulus at the same frequency.

3.5 Discussions

There is a lack of knowledge in the mechanical property changes associated with sclerotic development since earlier models of osteolytic bone metastasis did not involve sclerosis (Neudert et al 2003, Bauerle et al 2005, Arrington et al 2006, Song et al 2008). In this study, a sclerotic bone response in an immunocompetent animal model was characterized using its histomorphometric, densitometric, microarchitectural, as well as elastic and viscoelastic property changes. The trends of changes across these different properties are summarized in Table 4, where it showed significant increases in BMD, BMC, enhanced trabecular microarchitecture (increased BV/TV, BS/TV and Tb.N, with reduced Tb.Sp and SMI) and mean attenuation coefficient as well as reduced creep responses in cortical and trabecular bone (increased η_c and η_t).

Table 4. Summary of effects on various parameters of bone quality at 50th day post surgery.

Variables	Animal Groups		
	SCL (Operated LF)	SHAM (Intact RF)	SCL (Intact RF)
η_c	↑	↔	↔
η_t	↑	↔	↔
E_c	↔	↔	↔
E_t	↔	↔	↔
H_c	↔	↔	↔
H_t	↔	↔	↔
BMD	↑	↔	↔
BMC	↑	↔	↔
Trab.BMD	↔	↔	↔
BV/TV	↑	↔	↔
BS/TV	↑	↔	↔
Tb.N	↑	↔	↔
Tb.Th	↔	↔	↔
Tb.Sp	↓	↔	↔
SMI	↓	↔	↔
D.A	↔	↔	↔
μ_c	↔	↔	↔
μ_t	↑	↔	↔

η_c = cortical viscosity, η_t = trabecular viscosity, E_c = cortical elastic modulus, E_t = trabecular elastic modulus, H_c = cortical hardness, H_t = trabecular hardness, BMD =bone mineral density, BMC = bone mineral content, Trab.BMD= trabecular bone mineral density, BV/TV= bone volume fraction, BS/TV= bone surface density, Tb.N= trabecular number, Tb.Th= trabecular thickness, Tb.Sp = trabecular separation, SMI = structural model index, D.A= degree of anistrophy, μ_c = cortical mean linear attenuation coefficient, μ_t = trabecular mean linear

attenuation coefficient. Arrows indicate significant changes with respect to SHAM (Operated LF).

As seen from histological results (Fig. 10), sclerotic responses have been stimulated as a form of healing flare in this model, with a cascade of osteoblast activities. Jaganjac et al (2008) has reported prominent inflammatory response and regression of W256 carcinoma in the muscle as a consequence of granulocytes response, from day 1 to 6 post-innoculation. Thus, the 10 days histological assessment of increased osteoblast activities observed in our study could have been brought about as an inflammatory response to the presence of W256 cells. Given that this is a preliminary study to investigate the sclerotic development, further investigation is required to demonstrate the role of immune system in sclerosis development. Nonetheless, it is logical that the presence of an intact immune system in bone metastasis animal model is relevant not only for the selective growth of tumor types but also for the regulation of bone modeling during diseased state.

Increase in new bone formation in the trabecular region

Micro-CT provides the advantage of non-invasive assessment of bone morphology and microstructure, with an established high correlation with traditional histomorphometric analysis (Barbier et al 1999). Histological observation of enhanced osteoblast activity in sclerotic bone concurred with micro-CT indices, indicating enhanced trabecular microstructure. Furthermore, micro-CT also provides additional topological parameters such as structural

model index (SMI), which is a representative scale between 0 (for ideal plate) and 3 (for ideal rod) (Lespessailles et al 2006). SMI was shown to have decreased significantly in SCL compared to SHAM. This suggests a shift towards more plate-like structures of trabeculae in distal metaphyseal area and a plausible alteration in mechanical stress distribution in SCL group. Relative magnitudes and locations of high principal strains and stresses could differ from that of SHAM group, to the possible extent of enhancing load bearing. pQCT parameters (BMC, BMD) indicated an overall increase in bone mass and since no significant difference in total bone area were found between SCL and SHAM, bone modeling mainly affected trabecular microarchitecture and bone mass.

Viscoelastic nano-mechanical properties as a sensitive indicator of bone modeling

SCL bones showed reduced creep effect with significantly increased cortical and trabecular viscosity as compared to SHAM. The increased cascade of osteoblast activities as observed from histological results could also possibly speed up the process of secondary mineralization, with 'spill-over' to cortical areas. Accordingly, the average linear attenuation coefficient per pixel (measured by micro-CT) in SCL bone was higher than SHAM bone and was significantly increased for trabecular bone. Linear attenuation coefficient can be considered proportional to local degree of mineralization (Cox et al 2012, Shahnazari et al 2010). A higher linear attenuation coefficient per pixel could correspond to increased mineralization, contributing to changes in local creep response of SCL

bone. It was less likely that collagen organization could have affected the creep response, since no abnormalities in collagen fibers or organization was observed.

This trend of a reduced nano-level creep response with an increased mineralization could positively correspond to an earlier work demonstrating a similar trend in macroscale viscoelastic behavior of compact bone due to changes in mineralization levels (Currey 1975, Les et al 2004). This indicates that changes in mineralization levels could have an inverse effect on viscoelastic behavior across different scales.

The positive correlations established between η versus E and η versus H are in accordance with an earlier study on canine osteonal tissue (Kim et al 2010), although the correlation strength (R=0.576 and 0.528 respectively) in our study was not stronger. This could be due to factors such as the presence of cement lines and the difference in orientation of collagen fibers that contribute to greater degree of heterogeneity. Since rodent femur microstructures typically do not contain secondary osteons (Martiniakova et al 2006), a direct comparison with the canine study is not feasible. It is also worth noting that the slopes of correlation between η versus E and η versus H were high (m=2432s and m=46795 s respectively), indicating that both viscoelastic and elastic parameters have not increased together to the same extent. For a smaller increase in E and H, η exhibited a greater increase. Accordingly, at the time point of our study both the cortical and trabecular E and H did not exhibit a significant difference between SCL and SHAM. However, as seen from the correlation study, it is possible that

there could be a significant change in E and H with further increases in η at a later time point than our study. Nonetheless, viscoelastic nanomechanical property (η) changes were found to be a more sensitive indicator of bone modeling than elastic nanomechanical properties (E, H).

Tissue viscoelastic behavior

The sclerosis effect appeared to affect a localized level (nano-level viscosity) rather than tissue level as shown in DMA analysis. However, there was a sharp decrease in tan δ and loss modulus at 15.85 Hz in SCL compared to SHAM group. Since energy dissipation mechanisms activated at higher frequencies (e.g. 15.85 Hz) are associated with ultra and molecular structures (Yeni et al 2007), there might be minor changes at these scales (e.g. mineralized collagen fibril) in the cortical bone that have reduced damping efficiency. Reduced tan δ was also found in sclerotic bone samples with osteoarthritis (Fortis et al 2004), which is in agreement with the noted trend observed from this study.

Implications for bone material behavior

Reduced creep response at the tissue level and the indicative changes in the microarchitecture of trabecular bone may bear implications for microcrack propagation and altered mechanical load distribution respectively in sclerotic bone. Viscoelastic behavior (e.g. collagen deformation) helps to dissipate local high stresses around microcracks and provide fracture resistance (Ritchie et al 2009). The material characteristic to undergo limited deformation contributes to bone toughness (Ritchie 2011). Thus, reduced creep response in the sclerotic bone

tissue would correspond to more microcrack propagation, thereby implying reduced bone toughness during cyclic loading (Ritchie et al 2009, Chang et al 2011). The viscoelastic parameters measured by macroscopic torsion test and that of nanoindentation were found to have weak or no correlation, because the macroscopic viscoelastic behavior depends on other factors such as fluid flow and hierarchical structure of bone bone (Ritchie et al 2009, Shepherd et al 2011). Therefore, it is uncertain if the decrease in nanolevel viscoelastic creep property associated with sclerotic response in our study would correspond to overall bone viscoelastic characteristics. Moreover, despite the decrease in tan δ and loss modulus at 15.85Hz, no significant change was established in tan δ or damping property at the cortical tissue level. Since sclerosis is a localized development in this study, it is still within expectation that there might not be drastic changes at the bone tissue level.

Overall, it is worth noting that sclerosis induces likely changes in load distribution and a reduction in intrinsic damping property that could be related to changes in overall bone mechanical behavior. Since significant positive correlations between elastic properties (E) and (H) with viscosity (η) were also found, we can conclude that mechanical behavior of sclerotic bone would shift towards a material with lowered damping and likely with increased stiffness.

Study limitations

The drying of samples during nanoindentation could affect both elastic and viscoelastic mechanical properties that could be attributed to fibril shrinkage

(Rho & Pharr 1999). For instance, E and H were found to be higher in dry specimens than wet specimens (Bushby et al 2004, Wolfram et al 2010) and state of hydration could be important for determining treatment differences in E, H and dissipated energy between groups (Ammann et al 2007). As such, the bone samples were kept hydrated as much as possible during the sample preparation. To reduce the effect of drying during indentation, experimental time for each sample was kept constant. In DMA, the bone sample is kept hydrated in a PBS bath during testing procedure.

The effect of embedding could possibly increase E (Bushby et al 2004) and H (Mittra et al 2006, Ferguson 2009). Since embedding is needed as mechanical support for cutting rodent bones and surface polishing, to minimize any interference, indentations on the bone were placed away from epoxy-bone interface (Wolfram et al 2010). The time duration from embedding to completion of testing was also kept consistent between samples.

One important limitation of the study is the relatively smaller sample size (n=5) for the sclerotic group. Given that this is only a preliminary study, more experiments are required to further confirm the involvement of the immune system in the development of sclerosis in tumor metastasis. Another limitation is the duration of the study that accounts for the earlier changes in bone quality induced by tumor metastasis and did not take into account the possibility of modeling over longer time period. The ultimate strength and yield of sclerotic bones were not measured in this study as well, due to the limited samples.

Nonetheless, this is a novel study that centred on possible mechanical and material property changes associated with sclerosis that requires further exploration for clear understanding. Since sclerosis development is common in clinical cases of benign and slow-growing lesions, as correborated by this model, it is believed that the results of this study would also be translatable to clinical cases.

3.6 Conclusions

In this study, sclerotic response was found to be reactive new bone formation and mineralization as a healing flare likely in response to presence of W256 carcinoma cells. Here, the immune system is postulated to be responsible for the evocation of varying bone responses similar to the clinical scenario. Microstructural and densitometric changes showed increased bone formation and enhanced trabecular microarchitecture. Significantly reduced creep effect was observed in both trabeculae and cortical bone, whereas nanolevel elastic properties did not show a significant difference. Therefore, we conclude that viscoelastic nanomechanical property would serve as a more sensitive indicator of modeling in bone than elastic properties. Reduced viscoelasticity may contribute towards microcrack propagation and therefore a reduced toughness. Since significant positive correlations between elastic properties (E) and (H) with viscosity (η) were also found, it can be postulated that sclerotic response would result in lowered damping response with increased stiffening of material.

Chapter 4: Mechanical property changes of tumor affected bone cells

4.1 Summary of Chapter

Metastatic cancer cells were found to exert inhibitive effects in vitro on osteoblastic cells in terms of proliferation, differentiation and morphology. However, there is no prior study on changes of mechanical properties of bone cells affected by tumor cells, which could reflect cellular physiological state and affect the role of bone cells in mechanosensing and osteogenic response. Moreover, earlier in-vitro studies have involved the use of immortalized cell lines that may exhibit altered cellular characteristics.

In this chapter, atomic force microscopy (AFM) indentations on primary bone cells exposed to 50% conditioned medium from Walker 256 carcinoma cell line (W) or primary tumor (T) (derived from W256 tumor in SD rat) were carried out. Bone cell elastic moduli in W and T-groups were found to decrease significantly by 61% and 69.6%, respectively compared to control and corresponded to f-actin changes. It could also be associated with the variation in bone cell differentiation. There was also a significantly higher inhibition of growth rate (%) and higher inhibition of alkaline phosphatase activity (%) at 7 days exposure in T group compared to W group. Inhibition of bone nodule formation and mineralization was more apparent in T group than W group.

This is the first study to demonstrate that there was a significant reduction in stiffness of bone cells exposed to tumor conditioned medium, which could in turn affect its mechanosensing properties. It also demonstrated that there was a stronger sustained inhibitive effect on bone cells viability and differentiation by adaptive tumor cells than of its cell line was demonstrated. This could be

attributed to the higher levels of TGF-β1 in the T-conditioned medium compared to W-conditioned medium.

4.2 Introduction

In osteolytic metastasis, osteoblast cells affected by tumor cells have a role in enhancing osteoclast resorption through the release of receptor activator of nuclear factor-κB ligand (RANKL) and reduction in osteoprotegrin (OPG) expression (Kozlow & Guise 2005). Evoked inflammatory cytokines responses (IL-6, IL-8 and MCP-1) by osteoblasts cells can promote osteoclast differentiation and activation (Kinder et al 2008). However, further evidence from *in-vitro* studies suggests that there are more prominant effects on osteoblasts due to metastatic cancer cells. This may further explain the *in-vivo* decrease in osteoblast number and bone formation (Phadke et al 2006) as well as lack of healing reported even after bisphosphonate treatment (Sasaki et al 1995).

Osteoblastic cells were found to exhibit increase in apoptosis (Mastro et al 2004), reduced differentiation in terms of alkaline phosphatase activity, osteocalcein, bone sialoprotein and mineralization (Mercer et al 2004, Zhu et al 2009) after exposure to tumor cell conditioned medium. Morphological changes in osteoblastic cells from cuboidal to elongated spindle-like morphology were observed (Zhu et al 2009) with punctuated f-actin fibers (Mercer et al 2004, Mercer & Mastro 2005) and reduction in focal adhesion plaques (Mercer & Mastro 2005).

However, there was no report on the mechanical property changes of tumor affected bone cells, which could be present given the cytoskeletal changes.

Changes in bone cell mechanical properties could impact its mechanosensing (Bacabac et al 2008) and also be used to reflect physiological state of cells (Zhou et al 2012, Sugawara et al 2008). Atomic force microscopy (AFM) being a sensitive force sensor with piconewton resolution could be used to probe and quantify cell elasticity (Lim et al 2006).

Furthermore, earlier in-vitro studies are mainly done on osteoblast-like (MC3T3-E1) cells or with established breast cancer cell lines (MDA-MB-231 and MCF-7), which could possibly exhibit altered phenotype characteristics from the originating tumor with continuous culture (Burdall et al 2003). Therefore, this chapter aimed to investigate the inhibitive effects of primary tumor culture (derived from Walker 256 inoculated tumor in SD rodent) and original cell line used (Walker 256) on primary SD rodent bone cells culture.

Differences in terms of mechanical properties of bone cells exposed to tumor conditioned medium as compared to control medium were quantified using AFM indentation. Proliferation, differentiation (alkaline phosphatase activity), mineralization and morphology of bone cells with exposure to primary tumor conditioned (T) medium or W256 (W) conditioned medium were also determined.

The aims of this chapter were to determine whether: (1) tumor conditioned medium adversely affected the mechanical properties of bone cells, (2) there were differences between the inhibitory effects of adaptive tumor cells and established tumor cell line on primary bone cells.

4.3 Methodology

Primary tumor and bone explant culture

Tumor inoculation of 10^7 W256 cells in 0.1 ml M199 culture medium into the medullary cavity of left femur was performed, while the right femur was kept intact (n=30) (Chen et al 2013a). Three remaining rats were kept intact for bone cell harvesting. In the tumor group, there was invasive soft tissue tumor formation, from which tumor tissue was excised at 50^{th} day.

Tumor tissue was sliced into smaller pieces under sterile conditions and placed in 6 well plates with incubation using M199 medium and 5 % horse serum. The plates were left undisturbed, with minimal changes of medium during initial phases of growth (Masters 2012).

Soft tissues were thoroughly removed from the harvested bones (n=3 rats) and bones were sectioned into smaller pieces. Bone pieces were washed with PBS with 2 x antibiotics before being added to 6 well plates and incubated with osteogenic medium consisting of DMEM (Invitrogen), 10% fetal bovine serum (FBS), 1 x antibiotic-antimyosin and 100 µM L-ascorbate (A4403, Sigma). The bone explants were maintained undisturbed for 3-4 weeks, until confluency of bone cells was achieved (Fig.18). Following which, the bone cells could be trysinized and utilized for experimental use.

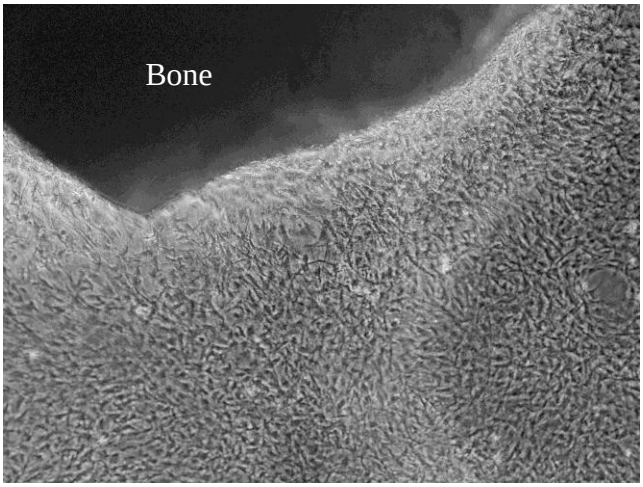

Figure 18: Confluent bone cell culture at 4x magnification under bright-field imaging.

Conditioned medium preparation and conditioned treatment of bone cells

W256 cells (W) and the primary tumor culture cells (T) were individually cultured in M199 with 5% Horse serum and replaced with DMEM (5 ml in T-25 flask, for cell concentration of 2.0 x 10^6 cells/ml) for 24 hours. W and T-conditioned medium were collected, with supernatant stored in aliquots at -20^0C. 10% FBS and 100 µM L-ascorbate were added to the treatment medium prior to treatment of bone cells. Bone cells were treated with 50% of either W or T-conditioned medium and no treatment for control cells (100% osteogenic medium).

W and T-conditioned mediums (without FBS) were assayed for TGF-β1 production. Culture medium at 3rd day of culture from respective T-conditioned and W-conditioned wells were also collected and centrifuged for supernatant. Activation of latent TGF-β1 and measurement in duplicates were carried out

according to instructions in Rat TGF-β1 Quantikine ELISA kit (R&D Systems, USA) (n=3). Osteogenic culture medium was similarly treated and measured as control.

Growth inhibition assay

2.0 x 10^3 cells/well were seeded into 96 well plates and after addition of conditioned or control medium, cells were left to culture for 3, 5 and 7 days. 10 µl of MTT (5mg/ml in PBS) was added to each well and after 4 hours, the medium was removed and 100 µl of DMSO added. Absorbance values at 595nm were read on the microplate reader. Growth Inhibition rates (%) were calculated as follows in Equation 10 (Chen et al 2013b):

$$\left(1-\frac{\text{Absorbance of sample}-\text{Absorbance of blank}}{\text{Absorbance of control}-\text{Absorbance of blank}}\right)\times 100\%$$

Alkaline phosphatase (ALP) activity

2.0 x 10^4 cells/well were seeded onto 24-well plates and with addition of conditioned or control medium, cells were left to culture for 3, 5 and 7 days. ALP activity was monitored with incubation of bone cells with 200 µl pNPP liquid substrate (P7998, Sigma Aldrich) for 30 mins, with 50 µl of 3 N NaOH solution added to stop the reaction. Absorbance measurements at 405nm were made using a microplate reader. Inhibition rates (%) were calculated as with equation (10).

Von Kossa Assay

2.0×10^4 cells/well were seeded onto 24-well plates and after exposure of conditioned or control medium for 7 days, the medium was replaced with fresh osteogenic medium with addition of 10 mM sodium-glycerophosphate (Sigma Aldrich, USA) for 2 weeks. The cells were then washed with PBS and stained with 1% Silver Nitrate (Sigma) under UV exposure for 40 mins. The cells were then washed with distilled water and 3% sodium thiosulphate was added for 5 mins, before being removed and washed with distilled water. Images were captured using optical inverted microscope (Olympus IX-71 Microscope).

Fluorescence Microscopy

2.5×10^3 cells/well were grown for 3 days with conditioned medium or control medium in a 24-well plate. The cells were fixed using 4% paraformaldehyde (Sigma Aldrich, St. Louis, USA), followed by labeling with 0.1 µg/ml TRITC-Phalloidin (Sigma Aldrich, St. Louis, USA) for f-actin and 5 µg/ml DAPI (Sigma Aldrich, St. Louis, USA) for cell nucleus. Fluorescence imaging was then conducted using Olympus FV1000 confocal imaging system. Cell morphology analysis (N = 7 cells per group) was conducted using Image J software (NIH, MD, USA) by determining projected cell area and aspect ratio i.e. ratio of maximum length to maximum width (Jaasma et al 2006).

Atomic Force Microscopy

1.0 x 10^4 cells were seeded on sterile 13 mm glass cover slips (Heinz glass) and after growing for three days, the live cells were subjected to AFM indentation using nanoscope IV multimode AFM with a picoforce scanner (Digital Instruments Inc, USA) The cells were kept immersed in phosphate buffered saline using a fluid cell (Digital Instruments Inc) throughout the experiment (Fig. 19).

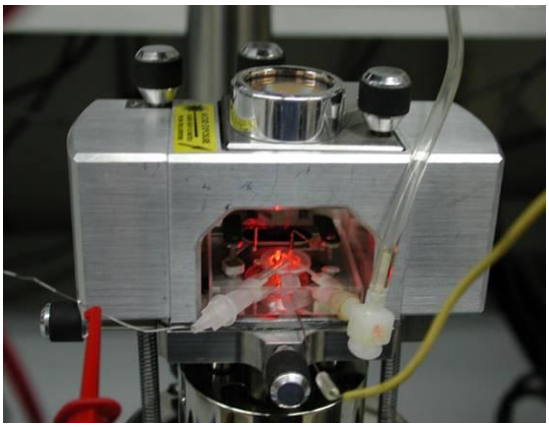

Figure 19: AFM fluid cell set-up where cells can remain hydrated in phosphate buffered saline under experiment loading conditions

For measuring cell mechanical property (n=30 cells per group), a silicon nitride cantilever of spring constant 0.03 N/m with a spherical polystyrene bead of diameter 4.5 μm adhered to the tip (NovaScan technologies) was used for indentation at 200pN, 0.1 Hz (Muthukumaran et al 2012). The indentation was done at the centre of cell, to minimize influence of the substrate. The apparent elastic modulus (E) of the sample can be determined from the force (F) versus indentation depth (h) curve. Hysteresis was calculated by subtraction of area under curve for retraction from approach curve, which gave energy dissipated into

the cell from AFM tip indentation (Lieber et al 2003) and also provided an indirect measurement of the apparent viscosity of the sample (Rebelo et al 2013).

Deflections in the AFM tip arising from interactions with the sample placed on a piezoelectric platform are detected through changes in position of reflected laser beam on the 4-point photodetector system. Force (F) versus displacement (Z) curves (Fig. 20) can be obtained from AFM force mode, where force is calculated using Hooke's law, $F = K*d$, where K is elastic spring constant and d is deflection of cantilever. Before coming into contact with the sample, force remains at zero value. As the sample is shifted up towards the fixed AFM tip i.e. Z increases, there comes a point at which the AFM tip comes into contact with the sample. Beyond the contact point, Z continues to increase, but there would be deflection of the cantilever (reflected as increase in force values in the approaching curve) and indentation into the cell sample. Once the trigger force is reached (pre-determined by user), the sample is retracted downwards i.e. Z decreases. A non-zero force F_{adh} (adhesion force) may be required to remove the tip from the sample. At point of contact, $Z = 0$ and penetration depth into the cell (h) is given by $h = Z- d$. Determination of point of contact is critical for deriving values of h and therefore E, stiffness values for cell, as shown in subsequent paragraph.

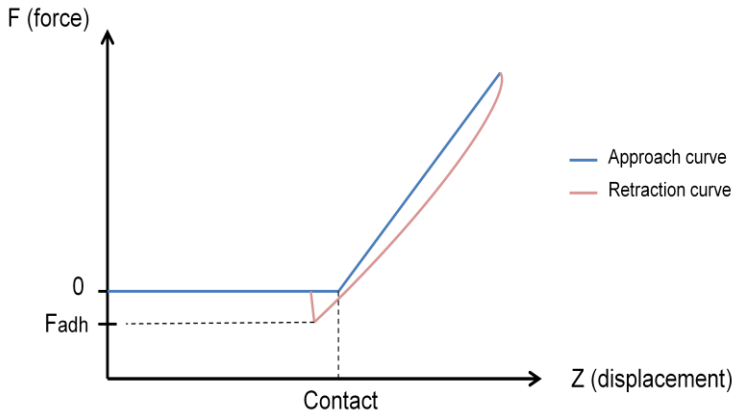

Figure 20: Force-displacement curves obtained from AFM elastic tests.

From Hertz-Sneddon model, the force can be related to the indentation as in equation (11):

$$F = \frac{4}{3}\frac{E_{cell}}{1-\nu^2}R^{\frac{1}{2}}h^{\frac{3}{2}}$$

where R is the radius of the spherical bead (2.25 μm) on the indent tip, ν is the Poisson's ratio, assumed to be 0.5 for biological samples (Darling et al 2008). E_{cell} is Elastic modulus of cell and h is indentation depth into cell. Fig 21 illustrates indentation into the cell using an AFM probe.

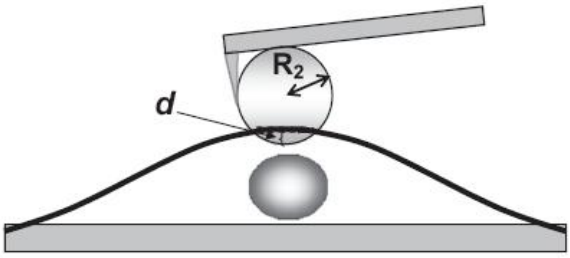

Figure 21: Spherical AFM tip on adhered cell (Bacabac et al 2008).

Statistical Analysis

SPSS 16.0 software was used to conduct one-way ANOVA analysis among different group comparisons, with $p < 0.05$ used for significance. Results

were shown as mean ± SD and for AFM experiments, results were represented as mean ± SEM (Standard Error of Mean). For equal variances, Tukey's HSD post hoc test was used for comparisons between 6 groups. For non-equal variances, Tamhane's post hoc test was used. Bivariate linear Pearson's correlation coefficients were also established with $p<0.05$ (2 tailed) for significance.

4.4 Results

Radiography and histological analyses

W256 carcinoma cells were injected in the medullary approximately 5mm from the distal growth plate of the left femur (Fig. 22A). Radiograph of the distal left femur showed a large soft tissue mass, with parts of bone cortex having eroded at distal growth plate (Figure 22B). Elevated periosteal reaction at the proximal margin of tumor or 'Codman's triangle' (Bullough 2012) was also observed. In histological results, growth and expansion of the tumor cells into the soft tissue surrounding the bone and degradation of bone tissue at the distal growth plate was observed (Fig. 22D) as compared to sham operated bone (Fig. 22C), concurring with radiographical results. It demonstrated the osteolytic effect of the injected W256 cells that have selectively adapted to the host environment.

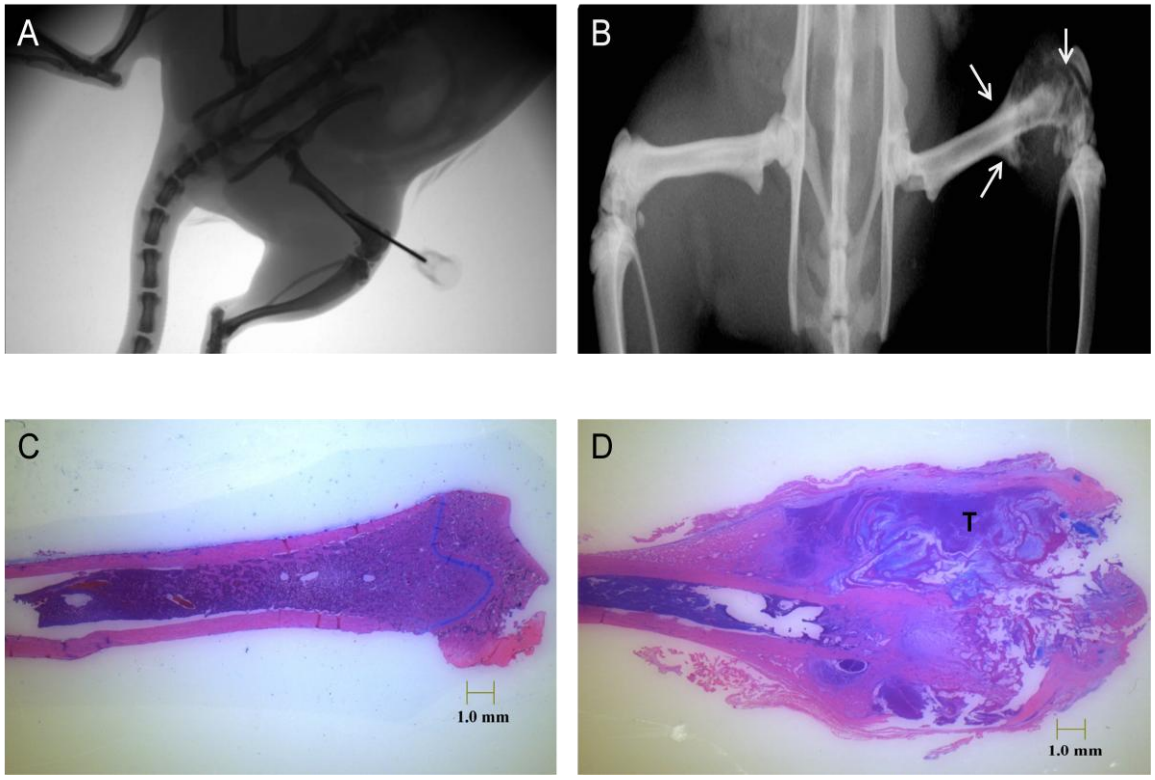

Figure 22: (A) Immunocompetent SD rat injected with W256 carcinoma cells, (B) aggressive malignant lesion (white arrow) induced with elevated periosteal reaction and a soft tissue mass with aneurysmal features (C) histological image of sham operated bone and (D) of tumor (T) burdened bone at same magnification.

TGF-β1 production

TGF-β1 in acid-activated T- and W-conditioned medium (without FBS) were found respectively, to be 20.2 pg/ml and 14.3 pg/ml. Acid activated medium collected at 3rd day of culture from T- and W-conditioned wells showed that TGF-β1 levels were 113.3 pg/ml and 65.9 pg/ml respectively, after correction for basal

medium TGF-β1 levels. It appeared that there was a dose-dependent effect on TGF-β1 production by bone cells through exogenous TGF-β1 conditioning, which agreed with an earlier report (Dallas et al 1994).

Growth inhibition rates

As observed from Fig 23A, T-conditioned medium had a twofold higher inhibition of bone cells growth than that of W conditioned medium at 3 days of exposure (+12.93%, $p<0.001$) and at 7 days of exposure (+13.34%, $p=0.008$). There was no significant difference in inhibition rates for T group from 3 to 7 days. By two way ANOVA analysis, only the treatment medium was indicated to have significant effect ($p<0.001$).

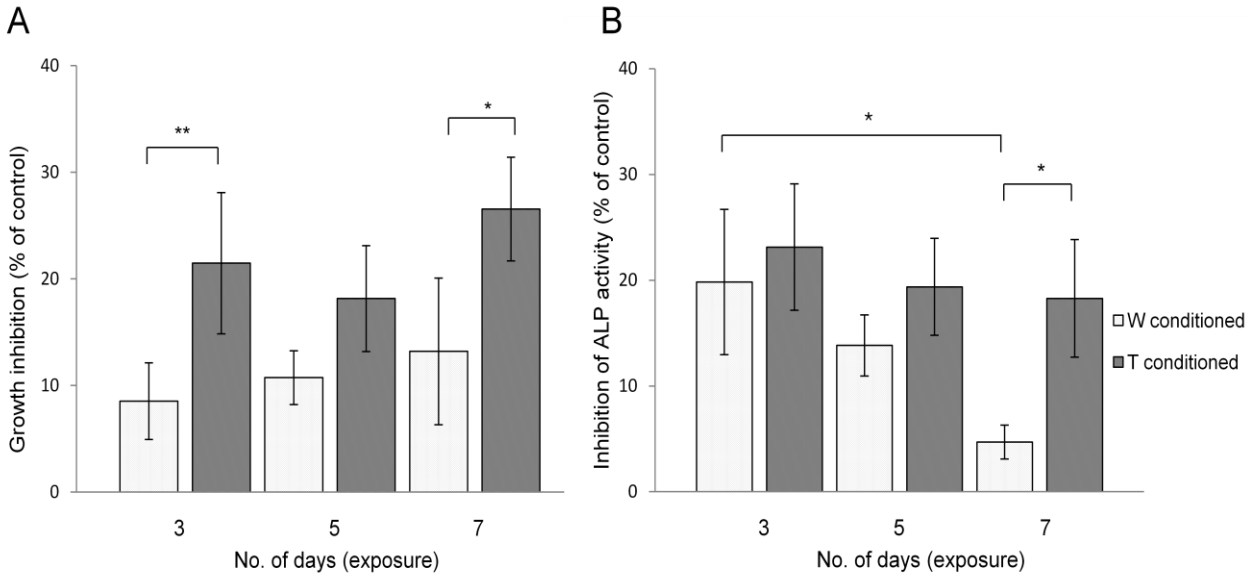

Figure 23: (A) Growth inhibition of bone cells and (B) Alkaline phosphatase activity inhibition of bone cells by W and T conditioned medium for 3, 5 and 7

days of exposure. * indicated $p < 0.05$ and ** indicated $p < 0.001$ for one way ANOVA analysis, with Tukey's HSD post hoc test.

Alkaline phosphatase (ALP) activity inhibition

T group had a significantly higher inhibition of ALP activity than W group at 7 days exposure (+13.57%, $p = 0.016$). While there was no change in inhibition rate of ALP activity by T conditioned medium, there was decreasing inhibition by W conditioned medium on ALP activity from 3 to 7 days (Fig. 23B). W group inhibition rate at 7^{th} day was significantly lower than that on 3^{rd} day (-15.12%, $p=0.008$). The two main effects, number of days of exposure ($p=0.002$) and the treatment medium ($p = 0.002$) was each indicated to be significant by two-way ANOVA analysis.

Mineralization

T conditioned bone cells after 7 days exposure (Fig. 24C) did not form brown stained mineralized nodules, as compared to the control bone cells (Fig. 24A). The degree of mineralization was reduced, as seen from the lower presence of brownish stains. The size of nodule formed was smaller for bone cells exposed to W conditioned medium (Fig. 24B) as compared to control well.

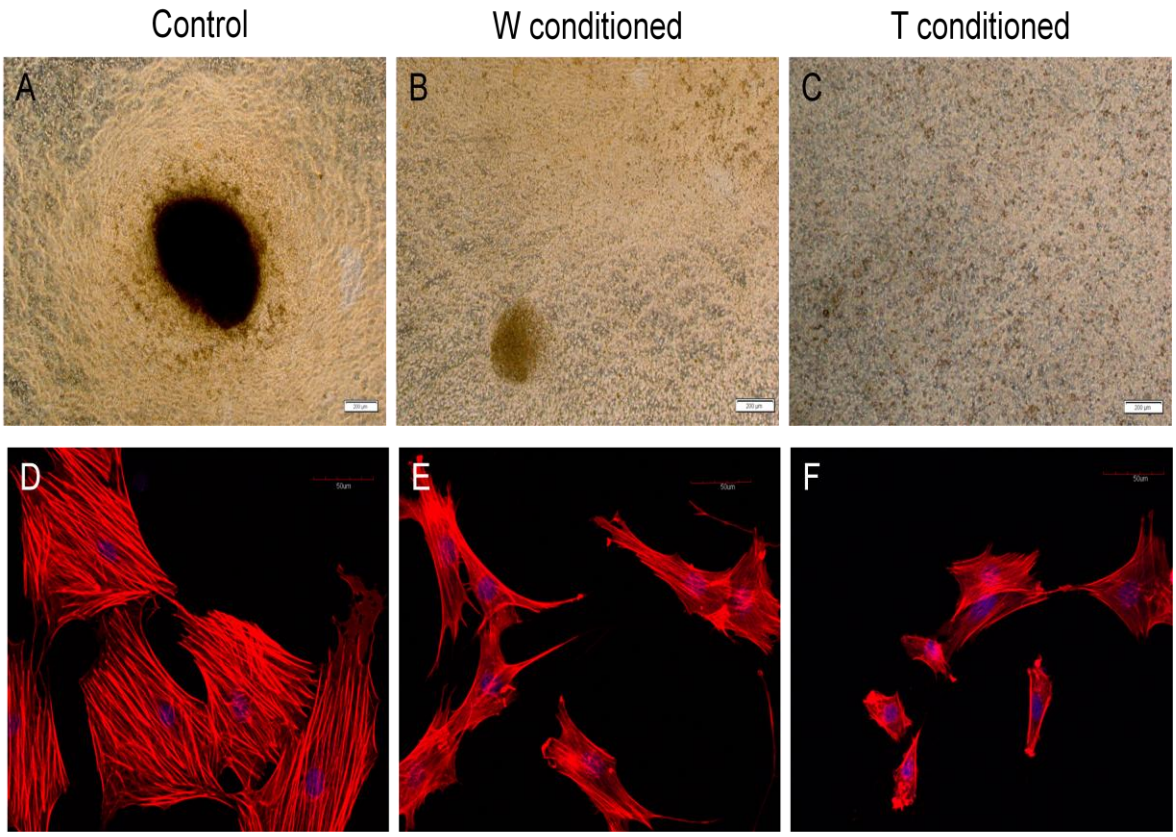

Figure 24:(A) Von Kossa staining of Control well, (B) W conditioned well (C) T conditioned well at 4x magnification; corresponding F-actin staining of (D) control well, (E) W-conditioned well and (F) T-conditioned well at 40x magnification, scale bar: 50µm. Cell nucleus was counterstained with DAPI.

Morphological changes

Control bone cells retained their cuboidal morphology with dense actin fibers (Fig.24D), with mean cell area 2322 ± 1362 μm^2 and aspect ratio 1.68 ± 0.46. Exposure to W and T conditioned medium for 3 days induced morphology changes, with reduced cell area (1158 ± 481 and 1004 ± 614 μm^2 respectively for W and T groups) and significant elongation i.e. higher aspect ratio 3.55 ± 1.67 (p

=0.046) and 2.71 ± 0.917 (p =0.0.36) respectively for W- (Fig. 24E) and T-conditioned groups (Fig. 24F).

Density of f-actin fibers was observed to be reduced across centre of cell in W-conditioned group and punctuated stress fibers of bone cells in T-conditioned group were noted. F-actin fluorescence levels across groups were quantified using micro-plate reader (data not shown) and no significant differences were observed. Thus, changes of cytoskeleton occurred in the reorganization of f-actin fibers and not as a reduction of f-actin expression levels.

Elastic modulus and hysteresis values of bone cells

It was observed that there were higher indentation depths for the same indentation load for both W- and T-conditioned groups compared to control (Figure 25A). For the same given loading force, the indentation depth will be larger given that the resistance against the mechanical load is reduced for both W and T group bone cells. Correspondingly, E was shown to have decreased significantly for W- and T- conditioned groups by 61.0% ($p < 0.001$) and 69.6% ($p < 0.001$) respectively, compared to control (Figure 25B). Hysteresis values or energy dissipated during indentation were shown to have increased by 152.9% ($p = 0.027$) and 161.3% ($p = 0.001$) for W- and T- conditioned groups respectively, compared to control (Figure 25C). There was also a significant negative Pearson's correlation between E and hysteresis values with correlation coefficient -0.485 ($p < 0.001$)

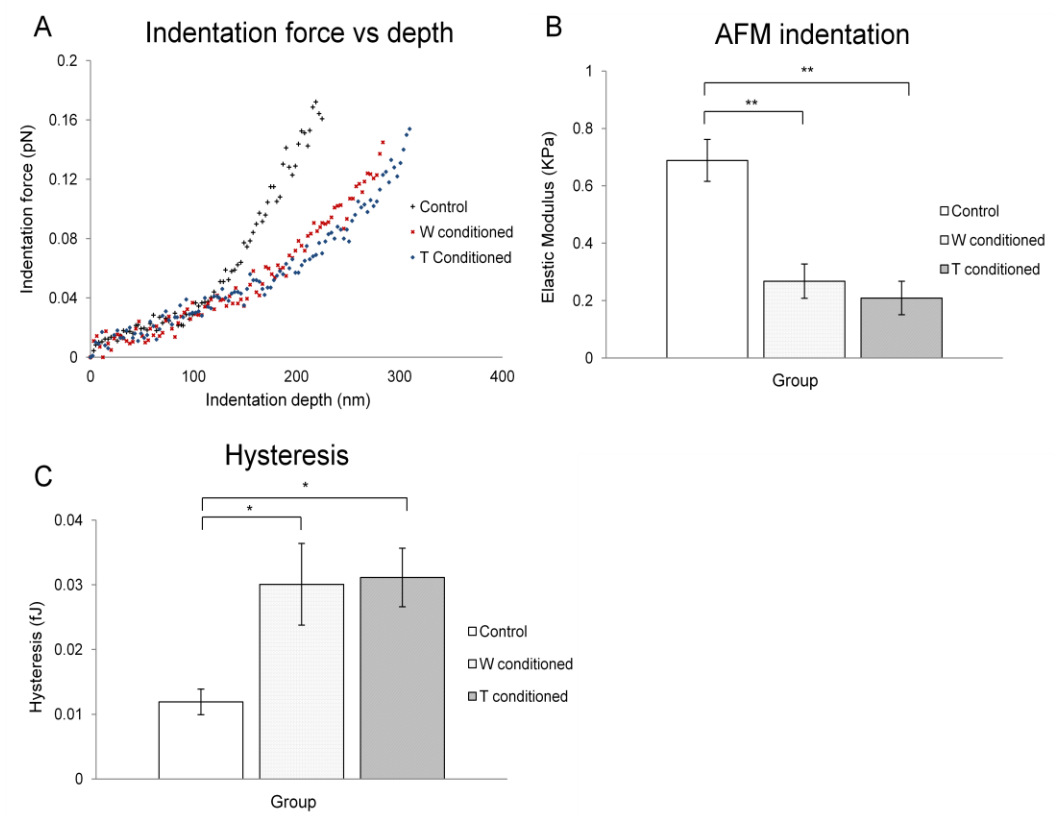

Figure 25: (A) Graph of indentation force versus depth, (B) Bar plot of elastic moduli and (C) Bar plot of hysteresis values for control, W conditioned and T conditioned groups. **-indicated $p<0.001$, * -indicated $p<0.05$.

4.5 Discussions

In this first study to look into mechanical property changes of bone cells conditioned by tumor cells, there was also an emphasis on the comparison of effects of primary tumor cells with original cell line. It is well understood that the selective adaptation of tumor cells and osteolysis development depended on inherent tumor characteristics to form symbiotic interactions with host cells in the

bone microenvironment (Fidler 2003). Moreover, new variants of tumor could result from differential propagation of tumor subpopulations in a process involving the immune system (Khong & Restifo 2002). As such, it is postulated that a primary tumor cell culture established from an in-vivo model of tumor burden, could have selectively different characteristics from that of the immortalized tumor line. Therefore, it would be pertinent to examine any possible contrasts in effects for primary tumor conditioned medium on bone cells, since earlier in-vitro studies have used tumor cell line conditioned medium.

Overall, it was demonstrated that there was a stronger and sustained inhibitive effect on bone cells viability, differentiation i.e. alkaline phosphatase activity as well as mineralization by primary tumor conditioning compared to W256 conditioning. This could be directly attributed to the higher levels of TGF-β1 in the T-conditioned medium compared to the W-conditioned medium. An earlier study has corroborated with this observation, demonstrating that the presence of TGFβ in the conditioned medium of MDA-MB-231 was in part, responsible for the inhibition of osteoblast differentiation (Mercer et al 2004).

TGF- β has been shown to play both positive and negative influences over osteogenic differentiation (Li et al 2012a, Zhou 2011, Zhao et al, 2010) and cell viability (Li et al 2012a, Dufour et al 2008) and its effects vary based on concentration and cell types (Li et al 2012a, Ochiai et al 2012, Zhou 2011). Nonetheless, it has been shown that repeated exposure to low dosage of TGF-β1 could reduce IGF-1 expression and down regulation of PI3K/Akt pathway, resulting in the inhibition of osteoblast differentiation (Ochiai et al 2011). As such,

the concentration differences of growth factors in different conditioned mediums could contribute to the varied inhibitive effects on bone cells.

It was further shown in this study that there was significantly reduced elasticity and increased energy dissipation of the bone cells exposed to the tumor-conditioned medium. This suggested the potential of cell mechanical property changes as an indicator of physiological health of bone cells. The actin network is demonstrated to be important for cell mechanical stability and directly affects cell elastic modulus (Rotsch & Radmacher 2000, Li et al 2008, Muthukumaran et al 2012). Thus, the observed reduction in elastic modulus and increased hysteresis could be associated with the changes in f-actin organization with tumor conditioning; where f-actin density was not only reduced across centre of cell (indentation location) but also more punctuated.

The reduced stiffness could also be linked to variation in degree of cell differentiation, since alkaline phosphatase activity (an early differentiation marker) was inhibited in both types of tumor conditioned medium. Darling et al showed that there were distinct mechanical property differences between different phenotypes of differentiated cells and of undifferentiated bone marrow derived mesenchymal stem cells (Darling et al 2008). Thus, inhibition of differentiation by tumor conditioning could result in variation of stages of bone cell phenotypes from control, with differing mechanical properties and morphology.

There could be another contributing factor to the altered cell stiffness i.e. the substrate, since actin network rearranges on attachment to extracellular matrix (Takai et al 2005). With 7 days exposure to W and T conditioned medium, there

was inhibition in terms of the degree of mineralization and formation of bone nodules after 2 weeks. Therefore, it was possible that at the time-point of the AFM study (3 days exposure) there could be differences in mineralization that could contribute to variation in cell cytoskeletal arrangement and thus stiffness. However, quantification of mineralization at 3 days time point did not indicate a significant difference in mineralization between the groups. Thus, substrate mineralization may not contribute to the observed differences in cell stiffness.

The ability of bone cells to detect mechanical signals and respond with appropriate biochemical signals is dependent on the cytoskeleton (Myers et al 2007, Li et al 2007). For instance, through microfilament disruption, osteoblasts under cyclic compression loading were inhibited in c-Fos mRNA and protein expression that is important for bone growth and mineralization (Li et al 2007). Changes in bone cell mechanical properties could also impact its mechanosensing (Bacabac et al 2008). Changes in F-actin organization and increased deformability of T- and W-conditioned bone cells (lowered stiffness) could therefore affect their mechanosensing properties and contribute to changes in remodeling events.

Nonetheless, there were some limitations in this study, namely experiment time-point i.e. 3 day tumor conditioning for AFM indentations and experimental conditions e.g. temperature and substrate. Since this is only a preliminary study to examine mechanical properties of tumor conditioned bone cells, it will be part of future work to examine if the reduced bone cell stiffness would be sustained over a longer periods of tumor conditioning. Given that cell mechanical properties

were demonstrated to have changed significantly, it is also of interest to examine whether bone cell mechanosensing properties would be similarly affected in future experiments (Chapter 5).

All AFM indentations were conducted on hydrated glass slips under room temperature. Since differences in cell cycle could also contribute to the inherent differences in cell mechanical properties (Kelly et al 2011), confluent cells were used for AFM assessment, similar to the cell preparation used by Muthukuraman et al to control the cell cycle for assessment of cell E across the groups. As relative cell attachment could affect cellular mechanical properties, experimental durations were controlled to ensure that analyzed cells from all 3 groups remained attached during experiment to ensure consistent comparisons.

The Hertz-Sneddon model used here for quantification of cell stiffness has three main assumptions: (1) the rigidity of the probe is much higher than the sample, (2) probe penetration is much smaller than radius of probe and (3) there is lack of adhesion between probe and sample. Since the probe is typically more rigid than the cell sample, radius of sphere (2.5μm) is much higher than depth of penetration (controlled at 100-300nm) and the adhesion forces were negligible (as observed from the retraction curve), this model is still valid for comparisons between samples.

4.6 Conclusion

In our study, it was demonstrated that there was stronger sustained inhibition of bone cells viability, differentiation, mineralization by primary tumor conditioned medium than the original cell line conditioned medium. This could be attributed to higher levels of TGF-β1 in the T-conditioned medium than that of W-conditioned medium. There was significantly reduced stiffness and increased hysteresis of bone cells exposed to tumour conditioned medium, which could be associated with the changes in cytoskeleton and possibly differences in differentiation. This suggested the potential of cell mechanical property changes as an indicator of physiological health of bone cells. Moreover, since changes in bone cell mechanical properties could impact its mechanosensing, it will be interesting to examine changes in mechanosensing property of bone cells in the following chapter (Chapter 5).

Chapter 5: Mechanosensing of tumor conditioned bone cells to vibration

5.1 Summary of the chapter

It was earlier demonstrated that there were significant reduction in cell stiffness and increased hysteresis with tumour conditioned bone cells, associated with cytoskeleton changes and possibly cell differentiation stage. Since mechanosensing is mediated by cell cytoskeleton, it is postulated that there could be mechanosensing changes in bone cells affected by tumour conditioning.

Primary tumor cells were revealed to have anchorage independence, indicating their metatatic potential, as well as a similar phenotypic signature with the original W256 cell line. However, size difference in colony formation suggested varying tumor subpopulations being propagated, which may explain the differences in inhibitive effects on bone cells. Here, T-conditioned bone cells were shown to form defective matrix deposition that could reinforce negative feedback for differentiation, mechanical characteristics and thus mechanosensing of attached bone cells. Correspondingly, it was demonstrated in this study that only T conditioning exerted inhibitive effects on nitric oxide release in response to LMHF vibration. It could also be due to the higher levels of TGF-β1 in T-conditioned medium than that of W-conditioned medium.

LY294002, an inhibitor of PI3K signaling pathway through which TGF-β, IGFII and PDGF mediate their effects on cytoskeleton, was thus used at a dosage of 1μM. It was shown to alleviate the inhibition on mechanosensing properties of T-conditioned cells, possibly through the maintainence of cytoskeletal organization in tumor affected cells. It suggested that growth factors like TGF-β1 could be good pharmocological targets for osteoblast treatment in

osteolytic metastasis. The inhibition on mechanosensing by bone cells could thus contribute to the defunct bone formation activity.

5.2 Introduction

Earlier *in-vitro* experiments have demonstrated that tumor cells exert inhibitive effects on osteoblast proliferation (Mastro et al 2004, Zhu et al 2009) and differentiation (Zhu et al 2009) as well as affect their morphology (Mercer & Mastro 2005, Dhurjati et al 2008, Zhu et al 2009). LY294002, a PI3K/Akt inhibitor, has been shown to maintain the morphology of breast cancer conditioned bone cells, demonstrating that induced morphology changes were mediated through PI3K pathway (Mercer & Mastro 2005).

In the previous chapter, we further demonstrated that there was a significant reduction in stiffness and increased hysteresis of bone cells exposed to primary tumor conditioned medium. Bone cell mechanical property changes were found to be associated with f-actin structure changes and possibly with differentiation stages. Since mechanosensing of bone cells is mediated by the cytoskeleton (Willems et al 2011), it is postulated that there would also be inhibition of mechanosensing property with tumor conditioning.

Mechanosensing i.e. sensing of mechanical signals leading to biochemical responses (Adachi et al 2008), plays a vital role in bone cells functionality (Kreja et al 2008, Tanaka et al 2005) and thus, tissue level adaptation to mechanical loading (Li et al 2007). Osteoblastic cells have been demonstrated to express osteogenesis related factors with exposure to low amplitude, high frequency vibrations(Bacabac et al 2006, Patel et al

2009, Hou et al 2011, Pre et al 2011). The anabolic effect of low magnitude, high frequency (LMHF) vibration has also been demonstrated in sheep at 0.3g, 30 Hz (Rubin et al 2002), mice at 0.3g, 45 Hz (Xie et al 2008) and ovariectomized rats at 3g, 30Hz (Rubinacci et al 2008) and 0.3g, 35Hz (Shi et al 2010) . As such, mechanosensing changes of tumor conditioned bone cells to LMHF vibrations could be of interest, since it helps to elucidate the potential of LMHF vibrations in stimulating osteogenic response in tumor affected bone cells.

Nitric oxide is important in the signaling of bone cells for the regulation of bone remodeling and the addition of an inhibitor of nitric oxide (L-NAME) also inhibited mechanically induced bone formation in rodents (Turner et al 1996). This provided supporting evidence for the role of nitric oxide in mechanotransduction and as an indicator for mechanosensing by bone cells. Thus, monitoring of nitric oxide levels in response to LMHF vibrations could be used to reflect changes in mechanosensing and degree of bone cell activation to mechanical stimuli.

The bone matrix deposition of tumor conditioned bone cells i.e. mineralization pattern and the physical quality of collagen fiber formation would also be examined. It was found in osteoporotic bone matrix that there was increased amount of new collagen with increased lysine hydroxylation which contributed to the deterioration in bone quality (Knott et al 1995). Collagen synthesis has been shown to be down-regulated for tumor affected osteoblast cells (Dhurjati et al 2008), but the characteristics of collagen fibers deposited were not examined previously. Structural organization of collagen fibers and mineralization pattern could not only contribute to tissue integrity, but also affect mechanical characteristics and thus mechanosensing of attached bone cells.

Thus, the aims of our study were to determine whether: (1) tumor conditioned medium adversely affects the mechanosensing properties of bone cells to low magnitude high frequency vibration, (2) there were differences in bone matrix deposition in terms of collagen fiber organization and degree of mineralization for primary tumor cells (T) conditioned cells and that of W256 breast cancer cell line (W) conditioned cells.

5.3 Methodology

Tumor model

Tumor inoculation of 10^7 W256 cells in 0.1 ml M199 culture medium into the medullary cavity of left femur were performed using a 22G needle, while the right femur was kept intact (n=30) (Chen et al 2013a). 3 remaining rats were kept intact for bone cell harvesting from femur bones. All animal experiments were conducted accordance with an approved protocol from Institutional Animal Care and Use Committee (IACUC) at National University of Singapore.

Primary tumor and bone explant culture

Tumor tissue was sliced into smaller pieces under sterile conditions and placed in 6 well plates with incubation using M199 medium and 5 % horse serum. The plates were left undisturbed, with minimal changes of medium during initial phases of growth (Masters 2012).

Soft tissues were thoroughly removed from the harvested intact bones (n=3 rats) and bones were sectioned into smaller pieces. Bone pieces were washed

with PBS with 2 x antibiotics before being added to 6 well plates and incubated with osteogenic medium consisting of DMEM (Life Technologies, USA), 10% fetal bovine serum (FBS), 1 x antibiotic-antimyosin and 100 µM L-ascorbate (A4403, (Sigma Aldrich, St. Louis, USA). The bone explants were maintained undisturbed for 3-4 weeks, until confluency of bone cells was achieved. Following which, the bone cells could be trysinized and utilized for experimental use.

Immunostaining for cytokeratin and vimentin expression

2.0 x 10^4 W and T cells were seeded respectively into 24-well plates and at least 50% confluency was reached before cells were fixed with absolute methanol for 10mins in room temperature. Non-specific binding sites were blocked with 1:5 fetal bovine serum in PBS for 20 mins. Incubation with primary antibodies i.e. anti-vimentin produced in goat (V4630, Sigma Aldrich, St. Louis, USA) at1:100 and anti-pan cytokeratin produced in rabbit (C2562, Sigma Aldrich, St. Louis, USA) at 1:100 for 1 hour was then carried out. PBS was used to wash the wells for 3 times. Incubation with appropriate secondary antibodies anti-goat IgG- TRITC (Sigma Aldrich, St. Louis, USA) and anti mouse IgG-FITC (Sigma Aldrich, St. Louis, USA) at 1:100 and 1:32 respectively for 1 hour was carried out. PBS was again used to wash the wells and to incubate the wells for fluorescence imaging using Olympus FV1000 confocal system.

Soft agar assay for colony formation

Soft agar assay tests for anchorage independent growth in soft agar and is used for detecting in-vitro cellular transformation and predicting potential for inducing metastasis *in-vivo* (Li et al 1989). In brief, 0.6% bottom agar is prepared by mixing 1.3ml of 1.8% agar with 2ml of 2x M199 and 0.7ml of double distilled water. They were maintained at a temperature of 42 ^{0}C and plated in tissue culture plate to solidify. 0.3% top agar is similarly prepared, by mixing equal volume of 0.6% agar with equal volume of cells suspension (20,000 cells/ml) at 37 ^{0}C. The top agar was left to solidify before being placed in the incubator. Soft agar assay was maintained at least for 2 weeks, with topping up of medium if agar appeared dry.

Conditioned medium preparation and conditioned treatment of bone cells

W256 cells (W) and the primary tumor culture cells (T) were individually cultured in M199 with 5% Horse serum and replaced with DMEM (5 ml in T-25 flask, for cell concentration of 2.0 x 10^6 cells/ml) for 24 hours. W and T-conditioned medium were collected, with supernatant stored in aliquots at -20^{0}C. 10% FBS and 100 µM L-ascorbate were added to the treatment medium prior to treatment of bone cells. Bone cells were treated with 50% of either W or T-conditioned medium and no treatment for control cells (i.e. 100% osteogenic medium).

Type I Collagen staining

2.0 x 10^4 bone cells were seeded onto 24-well plates and after exposure to conditioned or control medium for 7 days, the medium was replaced with fresh

osteogenic medium for 3 weeks. Fixation of cells were first carried out using ice cold methanol (-20 ℃). 3% of bovine serum albumin (BSA) solution was added to each well for 30 mins before being removed. 200 µl of Mouse Anti-collagen I antibodies in 1:1000 dilution (C2456, Sigma Aldrich) was added to each well and incubated for 90 mins at room temperature. Phosphate buffered saline (PBS) was used to rinse the wells for 3 times. 200 µl of goat anti-mouse antibody in 1:400 dilution (Alexa Fluorophore 594, Life Technologies, USA) was added in the dark together with DAPI stain and incubated for 45 mins at room temperature. Each well was rinsed 3 times with PBS and final amount of 300 µl of PBS was added to each well for viewing under the fluorescence microscope. Image J was used to measure collagen fiber lengths, using a threshold function to identify fibers (Chen et al 2012).

Mineralization of extracellular matrix

Von Kossa assay is used to assess for in-vitro mineralization. 2.0×10^4 bone cells were seeded onto 24 well plates and after exposure of conditioned or control medium for 7 days, the medium was replaced with fresh osteogenic medium with addition of 10 mM sodium-glycerophosphate (Sigma Aldrich, St. Louis, USA) for 2 weeks. The cells were then washed with PBS and stained with 1% Silver Nitrate (Sigma Aldrich, St. Louis, USA) under UV exposure for 40 mins. The cells were then washed with distilled water and 3% sodium thiosulphate was added for 5 mins, before being removed and washed with distilled water. Images were captured using optical inverted microscope (Olympus IX-71 Microscope) with n= 3 sets of experiments.

Vibration protocol

2.0 x 10^3 cells were seeded into 96-well plate and after addition of conditioned medium or normal medium for three days, serum starvation (for 1 day with DMEM with 2.5% fetal bovine serum) for cell cycle synchronization was carried out before being maintained in normal osteogenic medium. Vibration was carried out for 20 mins at room temperature on a vibration platform (Juvent 1000R, Juvent Inc., USA) which provides vertical accelerations at 0.3g, 30 Hz. The non-vibrated well-plate was placed at room temperature for same period. The well plates were returned to the incubator at 37 ^{0}C for 1 hour before being quantified for nitric oxide. The vibration is repeated for another day, with experimental outline of cell preparation and other assays shown in Fig.26.

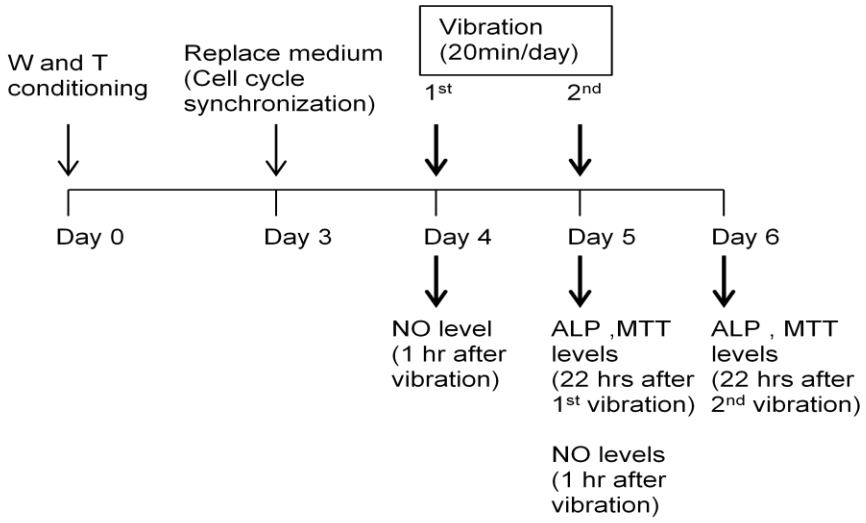

Figure 26: Experimental outline of cell preparation and analysis.

Nitric oxide detection

The nitric oxide concentration may be measured indirectly by nitrite and nitrate determination, since nitric oxide quickly metabolizes to the more stable

compounds of nitrite and nitrate. Briefly, 100 µl of medium from each well was removed and reacted with equal volume of Griess reagent (Sigma Aldrich, USA) at room temperature for 10 mins. Measurement of the absorbance at 550 nm was carried out and nitrite concentration was determined from a sodium nitrite standard curve using 0-100 µM of $NaNO_2$. Results were normalized by respective controls (non-vibrated cells), with n=6 sets of experiments.

Alkaline phosphatase assay

ALP levels were monitored by incubating bone cells with 200 µl pNPP liquid substrate (P7998, Sigma Aldrich, USA) for 30 mins, with 50 µl of 3 N NaOH solution added to stop the reaction. Absorbance measurements at 405nm were made using a microplate reader

Cell growth assay (MTT assay)

10 µl of MTT (5mg/ml in PBS) was added to each well and after 4 hours, the medium was removed and 100 µl of DMSO added. Absorbance values at 595nm were read on the microplate reader.

Effects of LY294002 (PI3K inhibitor) with vibration

LY294002, a PI3K/Akt inhibitor, has been shown to maintain the morphology of breast cancer conditioned bone cells, which implied that induced morphology changes were mediated through PI3K pathway (Mercer & Mastro 2005). To investigate the possible role of PI3K pathway and cell morphology on

mechanosensing, LY294002, a PI3K inhibitor was used to treat bone cells before conditioning.

2.0×10^3 cells were seeded into 96-well plate and treatment with or without 1μM of LY294002 (Sigma Aldrich, St. Louis, USA) was carried out prior to addition of conditioned medium or normal medium. The cells were subsequently incubated for three days, followed by serum starvation for cell cycle synchronization before being maintained in normal osteogenic medium. Vibration was carried out carried out for 20 mins at room temperature with vibration platform (Juvent 1000R, Juvent Inc., USA) at 0.3g, 30 Hz and nitric oxide levels were quantified 1 hour after one vibration (n=3). Morphological changes of cells at the same time point i.e. 1 hour after vibration was imaged using F-actin and DAPI staining using Olympus FV1000 confocal imaging system.

Statistical Analysis

SPSS 16.0 software was used to conduct one-way ANOVA analysis among different group comparisons, with $p < 0.05$ used for significance. For equal variances, Bonferroni post hoc test were used.

5.4 Results

Vimentin and Cytokeratin expression

There was intense positive stainings for vimentin in both tumor explants cells (T) and W256 (W) cells (Fig. 27), with light or minimal staining for cytokeratin expression. Immunophenotypic analysis indicated that both T and W cell types are hematopoietic in origin (Simpkins et al 1991), with minimal epithelial cell markers.

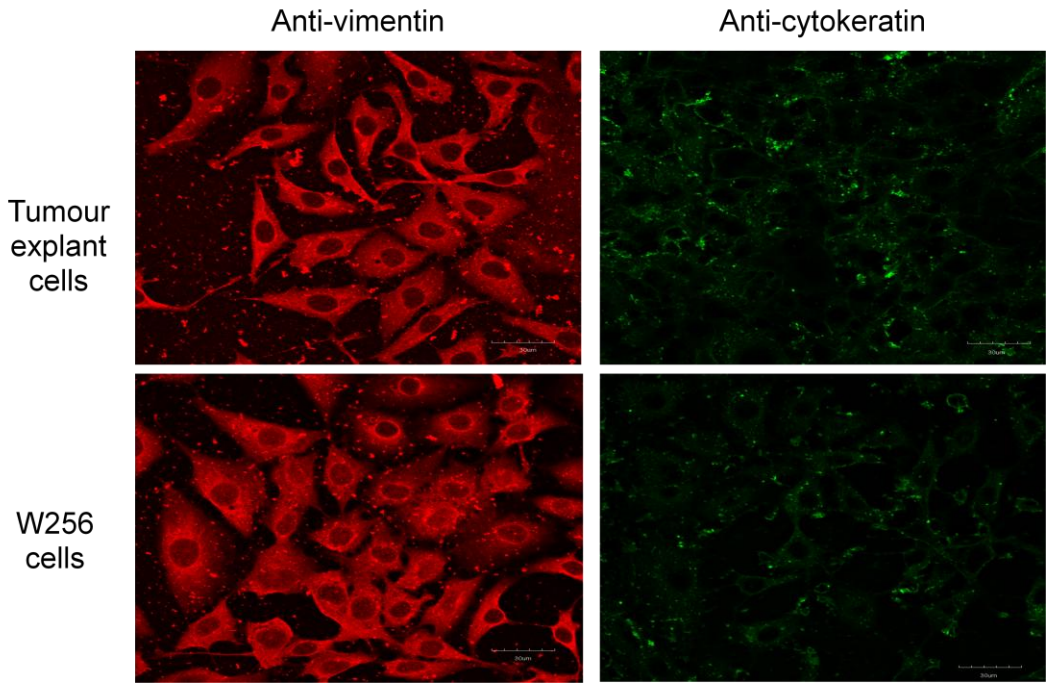

Figure 27: Vimentin and cytokeratin expression of (T) tumor explants and (W) W256 cells, at 60x magnification, scale bar: 30 μm

Anchorage independence

As observed from W256 and primary tumour cells colony formation, W256 (W) cells tended to form larger colonies (Fig. 28A) as compared to that of that of primary tumor cells (T) with numbers of smaller colonies (Fig. 28C and

D). Both W256 cells and primary tumor cultured cells demonstrated anchorage independence, which is one of the characteristics for cells with metastatic potential (Li et al 1989).

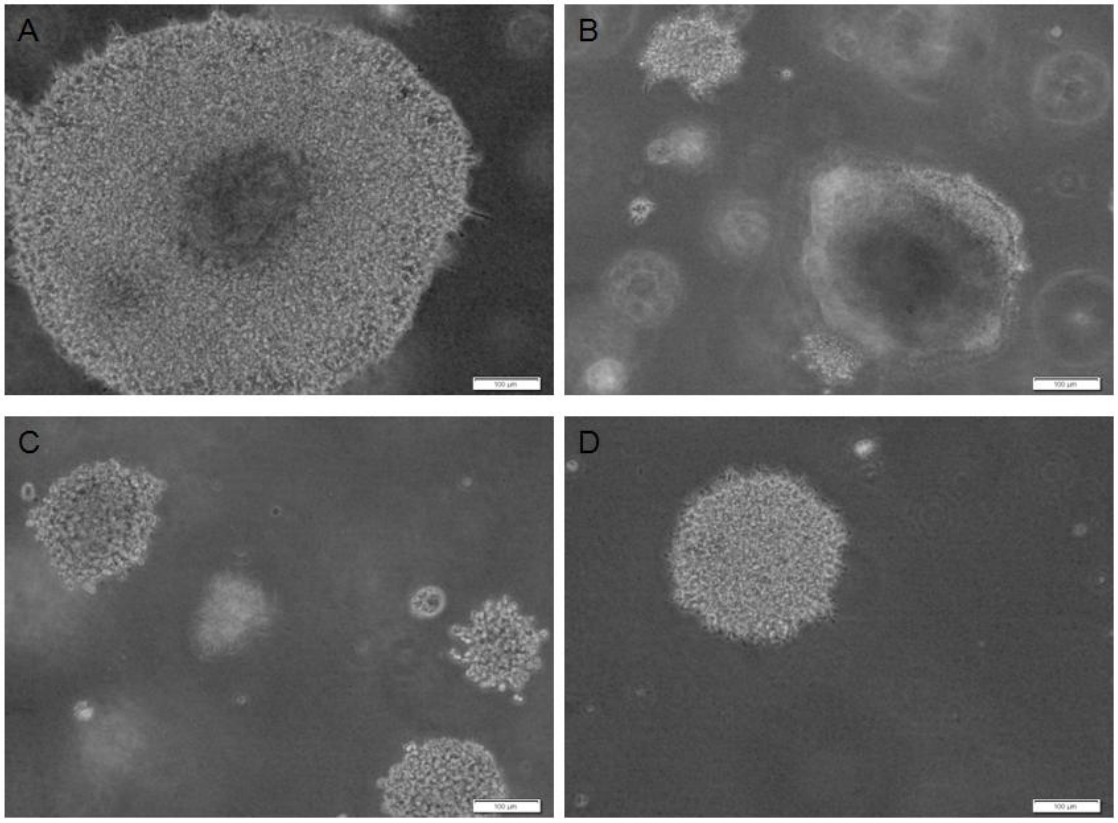

Figure 28: Soft agar assay of W256 cells, with (A) one large colony and (B) smaller colonies; (C, D) Tumor cells with smaller colonies at 10x magnification after 13 days.

Type I Collagen formation

The control bone cells tended to form more distinct fibers (Fig. 29A) than W- (Fig. 29B) and T-conditioned bone cells (Fig.29C). For T-conditioned bone cells, the type I collagen formed were observed to be more amorphous, without any distinctive fiber organization. Lengths of collagen fibers formed (Fig. 29D) in

control group (50.4 ± 15.6 μm) were also significantly longer by 69.1% (p=0.002) and 98.4% (p<0.001) respectively, compared to W-conditioned (29.8 ± 10.2 μm) and T-conditioned groups (25.4 ± 8.95 μm).

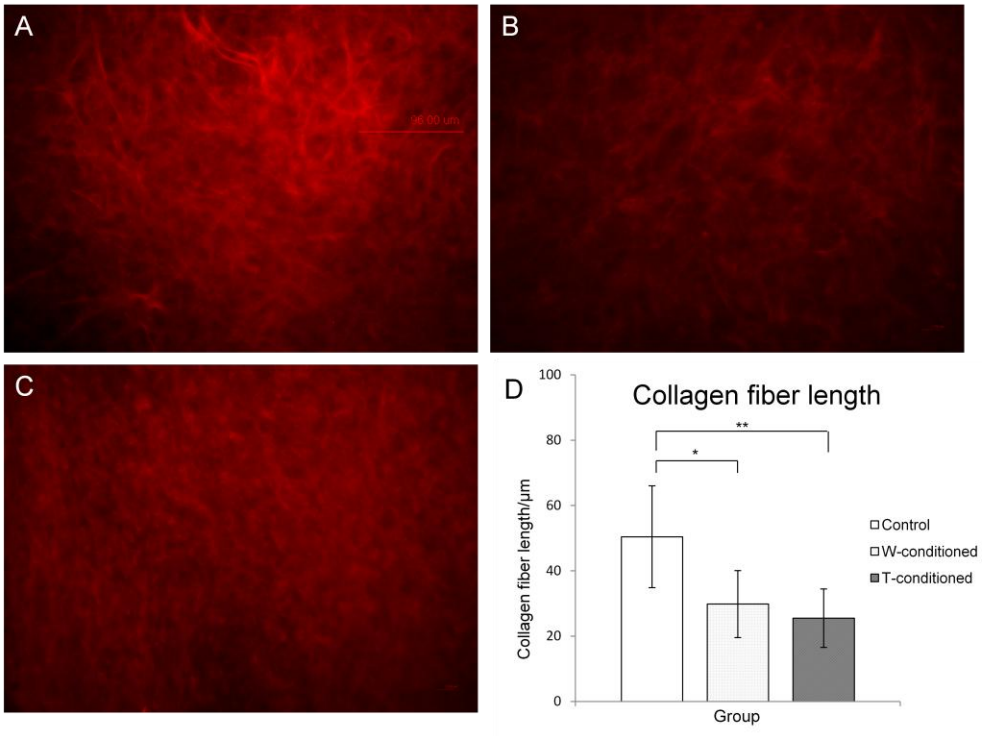

Figure 29: (A) Collagen I staining of control cells with distinct collagen fiber organization, (B) W conditioned cells with less distinct collagen fiber organization, (C) T conditioned cells with amorphous collagen formation at 20x magnification at 3 weeks and (D) Bar plot of collagen fiber length, *-indicated p <0.05 and **- indicated p <0.001

Mineralization

Control cells presented larger area of bone nodules and darker stainings of mineralization (Fig. 30A, B) than W conditioned cells (Fig. 30C, D) as well as T conditioned cells (Fig. 30E, F), which showed smaller area of bone nodules and less intense brownish staining. The pattern of mineralization was observed to be around the foci of nodules, with some dispersed mineralization present in all 3 groups.

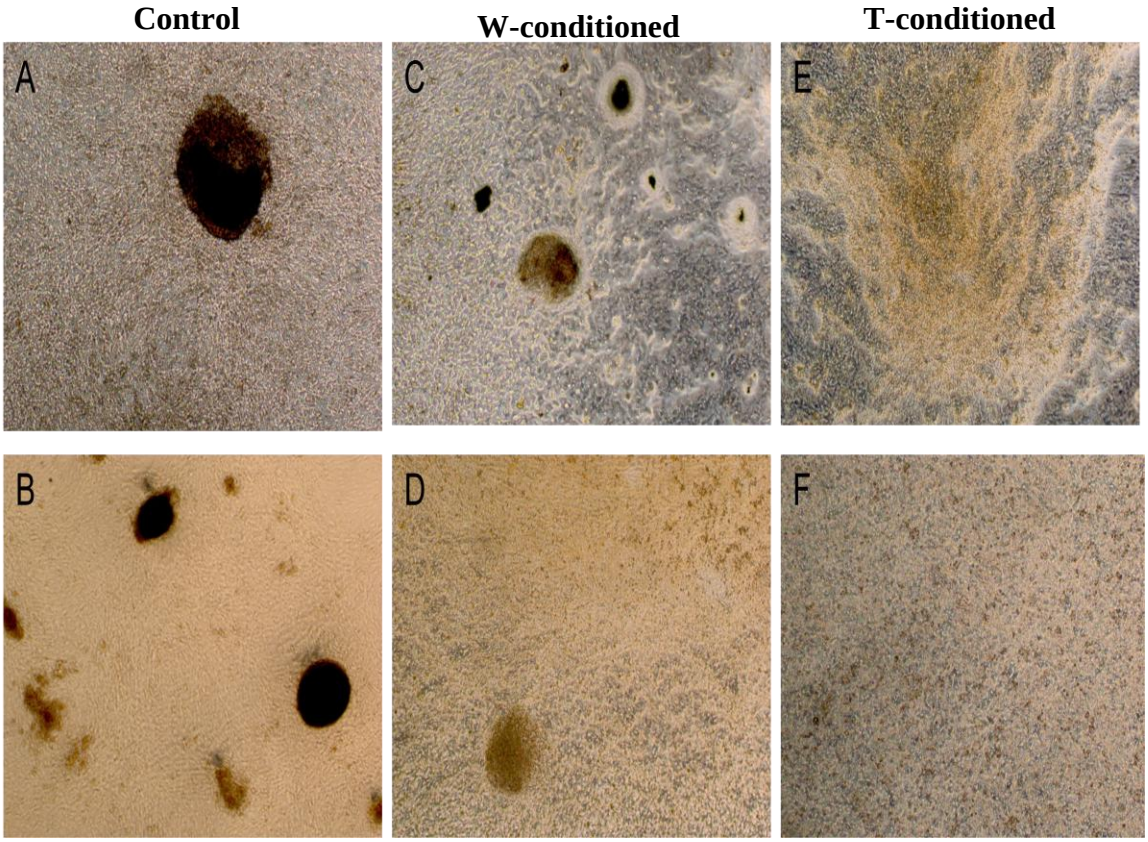

Figure 30: (A, B) Von Kossa staining of control cells with larger size of bone nodules formed and darker staining of mineralization; (C, D) W conditioned cells with smaller area of bone nodules and less intense staining and (E, F) T

conditioned cells, less intense stainings of mineralization. All pictures taken at 4x magnification at 2 weeks, with n=3 sets of experiments.

Nitric oxide changes

There was an observed increase in nitric oxide levels in vibrated control bone cells in Figure 30. There was significant lower nitric oxide levels (p=0.037) in vibrated T conditioned cells on day 1 vibration, suggesting that tumor conditioning inhibited bone cell activation and mechanosensing.

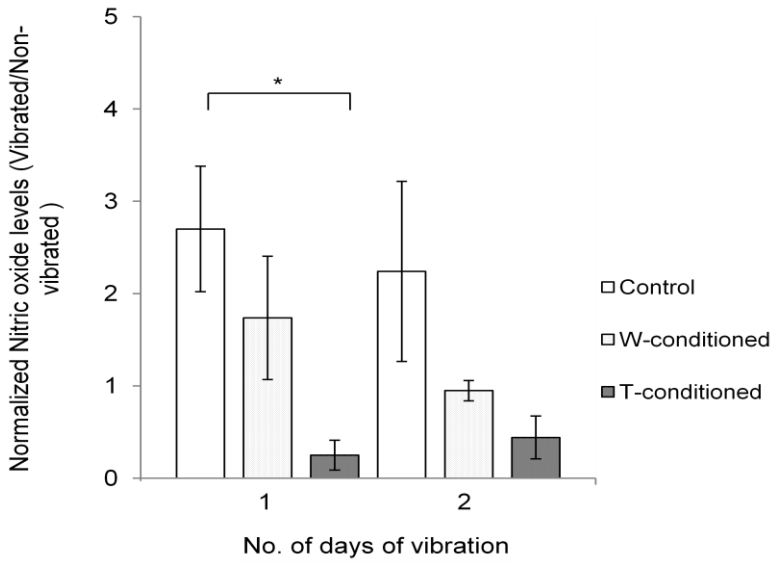

Figure 31: Normalized nitric oxide levels across 3 groups (control, W conditioned and T conditioned cells) in vibrated plates at 0.3g, 30 Hz. Results are presented in mean ± SEM, n=6 sets of experiment. * indicated $p<0.05$ for one way ANOVA, with bonferroni corrections.

Alkaline phosphastase activity and cell growth

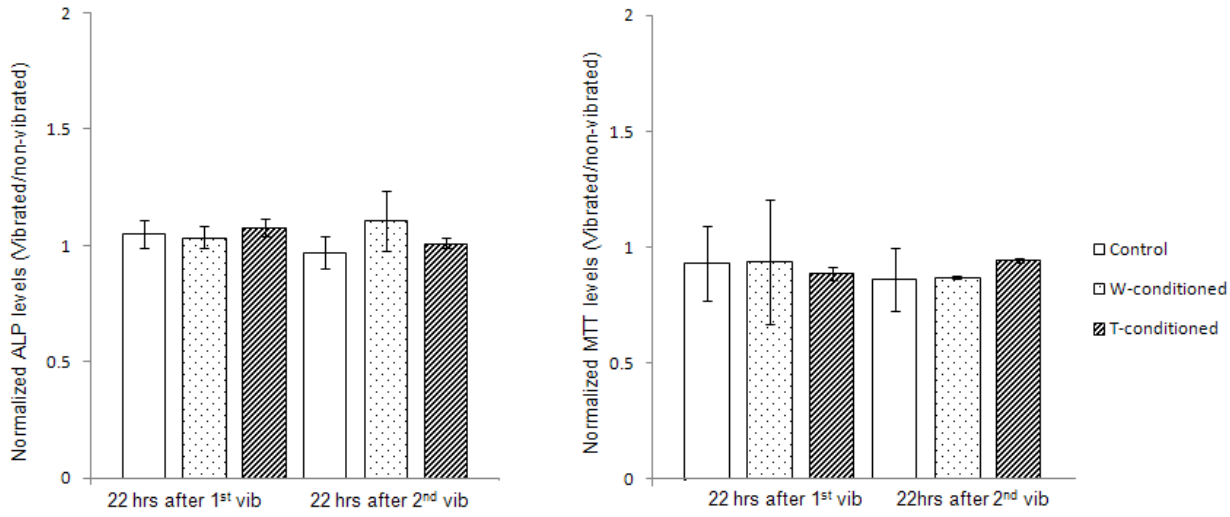

Fig. 32: Normalized ALP and MTT levels across 3 groups (control, W- and T-conditioned cells) in vibrated plates. Results are presented in mean ± SD, n=3 sets of experiment.

As shown in Figure 32, there were no significant changes in bone cell differentiation (ALP activity) and growth rates with vibration, with normalized ALP and MTT levels equivalent to respective non-vibrated groups at 22 hours after each vibration.

With LY294002 treatment (PI3K inhibitor)

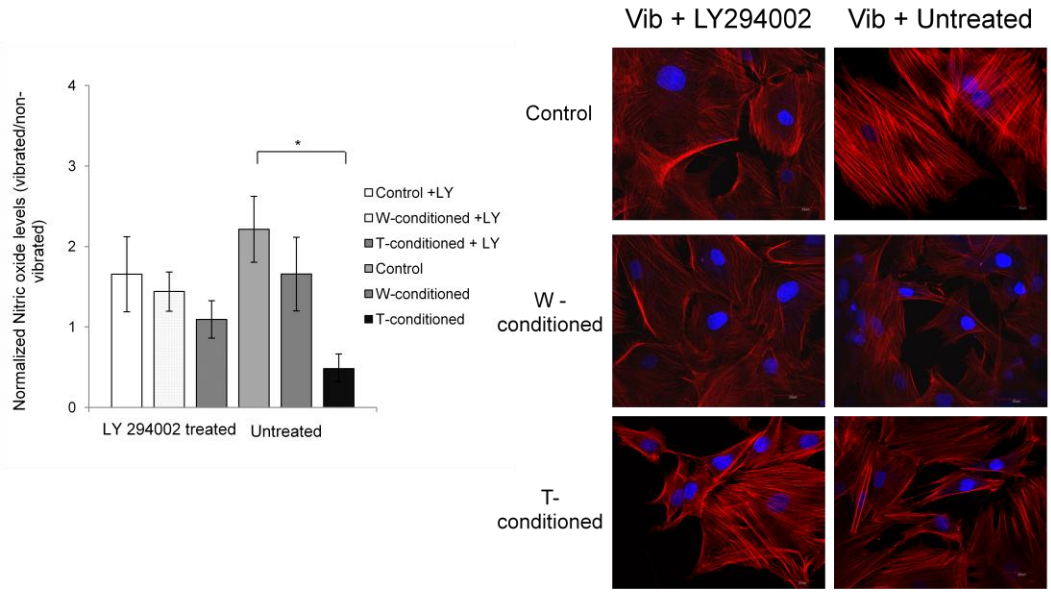

Figure 33: Bar chart of normalized NO levels in Control, W- and T-conditioned groups, with or without LY294002 treatment (PI3K inhibitor). F-actin staining at 60x magnification, for control (C), W256(W)- and T-conditioned groups (T) with or without treatment of LY294002, with vibration.

Nitric oxide (NO) response of bone cells to LMHF vibrations were significantly inhibited by 78.2% ($p = 0.013$) in untreated T-conditioned cells (Fig. 33) but not in untreated W-conditioned cells. On the other hand, no significant difference was found between LY294002 treated T-conditioned cell from both control groups (untreated and treated with LY294002), indicating that NO response with treatment is similar to that of control.

With vibration, LY294002 treated W-conditioned cells (Fig. 33) were morphologically similar to that of both treated and untreated control wells.

However, in LY294002 treated T-conditioned wells, there was still the appearance of elongated cells as with the non-treated T-conditioned wells.

5.5 Discussions

In this study, characterization of primary tumor cells using immunostaining and soft agar assay was first carried out. Both W256 cell line (W) and tumor explants derived cells (T) displayed similar immunophenotypic expression and exhibited anchorage independence that indicated metastatic potential. However, size difference in colony formation suggested varying tumor subpopulations being propagated.

Different types of tumor variants would induce differential effects on bone. For instance, W256/B variant cells were found to induce osteolytic cortical lesions with extension into soft tissues and woven bone was found in the subperiosteal area (Badraoui et al 2009). Furthermore, these variant cells were not capable of metastasizing to bone after subcutaneous implantation (Rizzoli, & Fleisch 1987), unlike the W256/A variant cells. Both observations were found to corroborate with the effects of tumor explants cells, suggesting that W256/B variant cells might have been derived here.

In Chapter 4, we demonstrated that there was significant reduction in the cell stiffness (and increased hysteresis) of tumor conditioned bone cells associated with cytoskeletal changes and possibly variation in bone cell differentiation. It was thus postulated that there could also be cytoskeletal mediated changes in

mechanosensing of bone cells, which could impact the bone tissue remodeling in response to mechanical loading.

Mechanosensing of tumor conditioned bone cells to low magnitude, high frequency (LMHF) vertical vibration of 0.3g and 30 Hz was investigated in this chapter. It was shown that there was lack of increase of nitric oxide levels in T-conditioned cells as compared to control bone cells. This implied an inhibition of bone cell activation to mechanical loading, given the importance of nitric oxide in bone cells biochemical signaling. Nitric oxide was found to inhibit bone resorption effect in-vitro, as it was positively associated with decrease in RANKL and increase in OPG protein formation by bone cells (Fan et al 2004). Thus, the lower release of NO by T conditioned cells could imply that there would be reduced inhibition of bone resorption, even with mechanical stimuli.

The significant reduction in the release of NO in response to vibration could be positively associated with the changes in f-actin organization and mechanical stiffness of the cell. For instance, it was demonstrated that cellular NO responses to AFM indentation corresponded to indentations at stiffer locations on the osteoblast membrane (McGarry et al 2008). Thus, it is possible that the reduced stiffness of tumor conditioned bone cells associated with altered f-actin cytoskeleton, could have contributed to the lower NO response to vibration.

However, while mechanical properties of both T- and W-conditioned cells were significantly less stiff than control cells (as seen in Chapter 4), only T-conditioned cells were shown here to be significantly inhibited in mechanosensing.

This implied that cell mechanical property is not sufficient as an indicator, nor is cytoskeletal organization the only factor influencing the mechanosensing process of bone cells.

In Chapter 4, it was found that there were higher levels of TGF-β1 in the T-conditioned medium compared to the W-conditioned medium. It is thus possible that the presence of growth factors in the conditioned medium could serve as negative modulators of the mechanosensing process. Moreover, it has been shown that repeated exposure to low dosage of TGF-β1 could reduce IGF-1 expression and down regulation of PI3K/Akt pathway, resulting in the inhibition of osteoblast differentiation (Ochiai et al, 2011). Since bone cells at different differentiation stages have different responses to mechanical signaling (Mikuni-Takagaki et al, 1996), inhibition of differentiation (even with 3 days exposure to tumor released factors) could give rise to differing mechanosensing properties.

Bone cells with tumor conditioning were also shown to deposit defective bone matrix i.e. amorphous collagen type I formation and reduced mineralization, which could affect its adhesion, mechanical and mechanosensing properties. Type I collagen has been demonstrated to support osteoblast differentiation and maintenance of the bone cell phenotype (Lynch et al 1995). Hence, defective bone matrix deposition arising due to tumor conditioning, could continue to serve as a reinforced negative feedback for bone cell differentiation and functionality e.g. mechanosensing.

Therefore, it appeared that tumor released factors e.g. TGF-β might have an important role in terms of influencing mechanosensing process. In an earlier

study, TGF-β, IGFII and PDGF were shown to mediate their effects on cytoskeleton through the PI3K pathway (Mercer & Mastro 2005). Here, LY294002, an inhibitor of PI3K was used at a dosage of 1μM (IC_{50} =1.40μM, 50 μM completely abolished PI3K activity (Vlahos et al 1994)). It was shown to alleviate the inhibition on mechanosensing properties of T-conditioned cells, which indicated the involvement of PI3K signaling pathway. It also appeared to help maintain cytoskeletal organization of tumor affected cells, which was corroborated by an earlier study (Mercer & Mastro 2005).

Since down regulation of PI3K/Akt pathway inhibited osteoblast differentiation (Ochiai et al 2012) and mechanosensing varies with differentiation, it was not surprising that nitric oxide levels of LY294002 treated control and W-conditioned groups decreased, as compared to respective untreated groups. However, by alleviating nitric oxide levels of treated T-conditioned groups through maintenance of cytoskeleton organization, it did highlight on the importance of cytoskeleton in mechanosensing. Furthermore, it does suggest the potential of growth factors such as TGF-β and its downstream molecules as pharmacological targets for osteoblast treatment in osteolytic metastasis.

As an interventional therapy, LMHF vibration at 0.3g and 30Hz, 20mins daily intervals did not appear to improve nitric oxide signaling in T conditioned bone cells and there was observed desensitization of the W-conditioned bone cells to vibration on the consecutive day (2^{nd} day of vibration). There was also a much higher standard deviation for control groups on the 2^{nd} day of vibration, which could be due to differential responses from heterogeneous bone cells derived from

different donors (Neidlinger-Wilke et al 1995). Similarly, a large variability even in control cultures was also observed in differences between mechanical stimulated and non-stimulated cultures (Kaspar et al 2000).

ALP activity and bone cell viability was shown to be equivalent to each respective non-vibrated group. Pre-osteoblast and osteoblast cell viability were also not affected in another two studies using LMHF vibration (Patel et al 2009, Dumas et al 2010). However, ALP activity did not improve significantly, which is in contrast to a similar study (Patel et al 2009). Hence, it indicated that there could be minimal osteogenic effect on bone cells under current study set-up.

Given that this is a first study for assessing mechanosensing changes in tumor affected bone cells, modification of rest periods between bouts of vibrations and overall vibration treatment period would help to determine the efficacy of LMHF vibrations on stimulating bone cells affected by tumor. Currently only 24 hour rest periods were used between vibrations and redesigning of experimental setup (i.e. use of larger well plates) could help to assess the vibration effects over longer duration.

The osteogenic inducement in bone cells could also be dependent on the amplitude of vibration as shown by Rubinacci et al, where 3g rather than 0.6g vibration, was shown to improve bone cortex modeling of ovariectomized rats (Rubinacci et al 2008). A variety of other factors such as duration of vibration (Patel et al 2009, Pre et al 2011), refractory periods between vibration (Sen et al 2011), frequency (Dumas et al 2010) and direction of vibration (Bacabac et al 2006) could also contribute to variation in the response of bone cells to vibration.

Thus, it is too early to make any conclusions on the efficiency of LMHF vibration on stimulating osteogenic response in tumor affected bone cells. As an *in-vitro* vibration study, it would not be readily translatable to effects *in-vivo*, which involved whole body vibration. However, it would help to establish protocols which might work in-vivo, given that those that would not work *in-vitro* would have been eliminated. In addition, it was shown here that there is the potential of growth factors such as TGF-β and its downstream molecules as pharmacological targets for osteoblast treatment in osteolytic metastasis.

5.6 Conclusions

Both W256 cell line (W) and tumor explants derived cells (T) displayed similar immunophenotypic expression and exhibited anchorage independence that indicated metastatic potential. However, size difference in colony formation suggested varying tumor subpopulations being propagated, which may explain the differences in inhibitive effects on bone cells. Correspondingly, it was demonstrated in this study that only T conditioning exerted inhibitive effects on nitric oxide release in response to LMHF vibration. It could be due to the higher levels of TGF-β1 in T-conditioned medium than that of W-conditioned medium.

Here, LY294002, an inhibitor of PI3K signaling pathway through which TGF-β, IGFII and PDGF mediate their effects on cytoskeleton, was used at a dosage of 1μM. It was shown to alleviate the inhibition on mechanosensing properties of T-conditioned cells, possibly through the maintainence of cytoskeletal organization in tumor affected cells. It suggested that growth factors

like TGF-β1 could be good pharmocological targets for osteoblast treatment in osteolytic metastasis.

Chapter 6: Conclusions

6.1 Conclusions

In this thesis, a modified method of immunocompetent model of osteolytic metastases was established, with sclerotic healing response (regression phase) and a varied osteolytic effect (progression phase).

At the bone tissue level, a novel characterization of a localized sclerotic response from microstructural, densitometric and viscoelastic parameters was carried out. Viscoelastic properties were assessed using nanoindentation and dynamic mechanical analysis, with the former technique providing information on local mechanical property changes arising due to changes in local cellular (bone formation) activity. Sclerotic response was found to be a healing flare likely in response to presence of W256 carcinoma cells. The immune system is postulated to be responsible for the evocation of sclerotic bone responses similar to the clinical scenario. Microstructural and densitometric changes showed increased bone formation and enhanced trabecular microarchitecture. Significantly reduced creep responses in both trabecular and cortical bone were found using nanoindentation, whereas elastic properties did not show a significant difference.

It was concluded that viscoelastic creep property using nanoindentation would serve as a more sensitive indicator of localized bone modelling than the elastic properties. Since significant positive correlations between elastic properties (E) and (H) with viscosity (η) were also found, it can be postulated that sclerotic response (as seen in clinical scenario) could result in lowered damping response with increased stiffening of material.

Metastatic cancer cells were found to exert inhibitive effects *in vitro* on osteoblastic cells in terms of proliferation, differentiation and morphology. However, there is no prior study on changes of mechanical properties of bone cells affected by tumor cells, which could reflect the physiological state of cells and affect bone cells in mechanosensing and bone formation activity. Bone cells mechanical property changes due to conditioning from osteolytic tumor explants (T) and W256 (W) cells were assessed using atomic force microscopy indentation.

It was shown in the course of this work that bone cell elastic moduli in W- and T-conditioned groups had decreased significantly by 61.0% and 69.6% respectively, compared to control. Hysteresis (energy dissipated) was not only shown to be negatively correlated to elastic moduli, it was also significantly increased in W- and T-conditioned groups. Changes in bone cell mechanical property could be associated with the cytoskeleton changes and possibly inhibited bone cell differentiation with tumor conditioning.

There was also significantly higher inhibition of growth rate (%) and higher inhibition of alkaline phosphatase activity (%) at 7 day exposure in T-group compared to W-conditioned group. Inhibition of bone nodule formation and mineralization was also more apparent in T group than in W group. It was thus demonstrated that there was a stronger sustained inhibitive effect on bone cells viability and differentiation by primary tumor cells than the original cell line used. This could be attributed to the higher levels of TGF-β1 in T-conditioned medium compared to W-conditioned medium.

This was also the first study to demonstrate that there was a significant changes in mechanical properties of bone cells exposed to tumor conditioned medium, which could reflect diseased state of cell and affect its mechanosensing properties.

The mechanosensing changes in primary tumor affected bone cells were further examined by assessing nitric oxide (NO) level changes to low magnitude, high frequency (LMHF) vibration. By investigating the degree of mechanosensitivity of bone cells *in vitro*, it can also serve to address another need: an understanding of how the bone formation process at the cellular level is affected by tumor conditioning.

Characterization of W256 cell line (W) and tumor explants derived cells (T) was carried out. Both displayed similar immunophenotypic expression and exhibited anchorage independence that indicated metastatic potential. However, size difference in colony formation suggested varying tumor subpopulations being propagated, which may explain the differences in inhibitive effects on bone cells.

Correspondingly, it was demonstrated that only T conditioning exerted inhibitive effects on nitric oxide release in response to LMHF vibration which indicated lowered bone cell activation. Again, it could be due to the higher levels of TGF-β1 in T-conditioned medium than that of W-conditioned medium.

Here, LY294002, an inhibitor of PI3K signaling pathway through which TGF-β, IGFII and PDGF mediate their effects on cytoskeleton, was used at a dosage of 1μM. It was shown to alleviate the inhibition on mechanosensing properties of T-conditioned cells, possibly through the maintainence of

cytoskeletal organization in tumor affected cells. It suggested that growth factors like TGF-β1 could be good pharmocological targets for osteoblast treatment in osteolytic metastasis.

On the other hand, LMHF vibration at 0.3g, 30HZ did not have an apparent improvement in stimulating osteogenic response in tumor affected cells. Changing the magnitude, frequency, intervals between vibrations and directions and type of loading could possibly assist in elucidating the usefulness of LMHF vibrations for the stimulation of osteogenesis. As an *in-vitro* system, it could help establish conditions that might work for *in-vivo* whole body vibrations.

In conclusion, sclerotic development in this immunocompetent model is shown to be reactive bone formation with reduced local creep properties. Nano-level viscoelastic property was shown to be a sensitive indicator of modelling changes in bone. In addition, the combined inhibition of bone cells viability, functionality, mechanical property and mechanosensitivity demonstrated in this thesis, could contribute to the defunct bone formation activity as observed in bone metastasis. It therefore reinforces the need to expand on osteoblast-targeted therapy for comprehensive treatment.

6.2 Original Contributions

There were three main original contributions presented in this thesis. Firstly, sclerotic healing response in bone metastasis was characterized and it was shown to constitute reactive bone formation, with significantly reduced creep responses. Nano-level creep response was indicated to be a sensitive indicator of local modelling changes.

Secondly, through the use of an osteolytic tumor culture derived from *in-vivo* model, a significant change in mechanical properties of tumor conditioned bone cells was demonstrated. It was positively associated with cytoskeletal changes and possibly inhibited bone cell differentiation. There was also a stronger sustained inhibitive effect on bone cells viability and differentiation by primary tumor cells than the original cell line used. Characterization of primary tumor cells indicated metastatic potential and similar phenotypic signature as the original W256 cell line, but with higher levels of TGF-β1 released.

Lastly, mechanosensitivity to LMHF vibration was significantly decreased in tumour affected bone cells. By inhibiting PI3K signaling pathway through which TGF-β, IGFII and PDGF mediates its effects, inhibition on mechanosensing properties of T-conditioned cells was alleviated, possibly through the maintainence of cytoskeletal organization. It suggested the potential of growth factors like TGF-β1 as pharmocological targets for osteoblast treatment in osteolytic metastasis. Overall, the combined inhibition of viability, functionality and reduced mechanosensitivity could contribute towards the defunct bone formation activity as seen in bone metastasis.

6.3 Future Work

Mechanosensing changes of bone cells to fluid-flow could be examined as part of future work, since bone cells are well known to respond to fluid flow. Here, more attention was paid to low magnitude high frequency (LMHF) vibration since it has therapeutic potential to restore bone quality. However, there were no significant mechanosensing changes resulting from the vibration intervention based on the current set-up. Further optimization of parameters such as frequency, loading magnitude, loading direction and timing of treatment intervals could be explored further to elucidate its potential for stimulating osteogenic effects in tumor affected bone cells.

Establishing an osteocyte culture would be of interest in terms of studying mechanotranduction under the influence of tumor cells. Osteocytes, rather than cells of osteoblast lineage are expected to have a bigger role to play in terms of mechanotransduction and could provide a stronger basis to determine effects of tumor on mechanotransduction and thus bone remodeling.

On further note, the isolated primary cultured tumor cells have varying metastatic potentials (Fidler 2003) and continuous in-vitro culture could have expanded one subset of cell population over another. As such, in-vivo tumor induction in SD rat using tumor explants cells could be carried out to demonstrate its potency of re-establishing an immunocompetent model of osteolytic metastases. Prior to inoculation, the primary tumor cells could be grown in 0.3% agarose (top layer) to isolate cells with metastatic potential from the

heterogeneous culture (Li et al 1989). The cells could be inoculated intra-muscular in the muscle adjacent to tibia bone of SD rat (6-8 weeks) to encourage bone metastasis (Bassani et al 1990). The choice of intramuscular inoculation was also due to the consideration that the primary tumor cells were variant cells derived from W256 carcinoma cell line which is originally susceptible to develop subcutaneously, intramuscularly or in ascite (Blouin et al 2005). Any primary tumor culture expanded from in-vivo implantation could aid in the establishment of a metastatic cell line and has been originally used to isolate B16-F10 line from B16 melanoma (Fidler 1973).

One criticism of such in-vivo selection process is that it would result in variant population of cells which could survive in the new microenvironment, not progeny cells derived from a subset of the heterogeneous parent tumor population (Fideler 2003). However, there would be a more reproducible degree of osteolysis that would facilitate for expansion of current model to drug testing applications.

Bibliography

Adachi, T., Sato, K., Higashi, N., Tomita, Y., Hojo, M., 2008. Simultaneous observation of calcium signaling response and membrane deformation due to localized mechanical stimulus in single osteoblast-like cells. J Mech. Behavior of Biomed. Mater. 1, 43-50

Alvarez, E., Westmore, M., Galvin, R.J.S., Clapp, C.L., Considine, E.L., Smith, S.J., et al,2003.Properties of bisphosphonates in the 13762 rat mammary carcinoma model of tumor-induced bone resorption. Clin Cancer Res .9, 5705-5713.

Ammann, P., 2009. Bone strength and ultrastructure. Osteoporos Int .20, 1081-1083.

Arrington, S.A., Damron, T.A., Mann, K.A., Allen, M.J.,2008. Concurrent administration of zoledronic acid and irradiation leads to improved bone density, biomechanical strength, and microarchitecture in a mouse model of tumor-induced osteolysis. J Surg Oncol .97, 284-290.

Arrington, S.A., Schoonmaker, J.E., Damron, T.A., Mann, K.A., Allen, M.J.,2006.Temporal changes in bone mass and mechanical properties in a murine model of tumor osteolysis. Bone .38, 359-367.

Bacabac, R.G., Mizuno, D., Schmidt, C.F., MacKintosh, F.C., Van Loon, J.J.W.A., Klein-Nulend, J., et al, 2008. Round versus flat: bone cell morphology, elasticity, and mechanosensing. J Biomech .41,1590-1598.

Bacabac, R.G., Smit, T.H., Van Loon, J.J.W.A., Doulabi, B.Z., Helder, M., Klein-Nulend, J., et al, 2006. Bone cell responses to high-frequency vibration stress: does the nucleus oscillate within the cytoplasm? FASEB journal: official publication of the Federation of American Societies for Experimental Biology .20,858-864.

Badraoui, R., Blouin, S., Moreau, M.F., Gallois, Y., Rebai, T., Sahnoun, Z., et al,2009. Effect of alpha tocopherol acetate in Walker 256/B cells-induced oxidative damage in a rat model of breast cancer skeletal metastases. Chem Biol Interact .182,98-105.

Barbier, A., Martel, C., de Vernejoul, M.C., Tirode, F., Nys, M., Mocaer, G., et al,1999.The visualization and evaluation of bone architecture in the rat using three-dimensional X-ray microcomputed tomography. J Bone Miner Metab .17,37-44.

Bassani, D., Sabatini, M., Scanziani, E., De Francesco, L., Coccioli, G., Guaitani, A., et al,1990. Bone invasion by Walker 256 carcinoma, line A in young and adult rats: effects of etidronate. Oncology .47, 160-165.

Bäuerle, T., Adwan, H., Kiessling, F., Hilbig, H., Armbruster, F.P., Berger, M.R., et al,2005.Characterization of a rat model with site-specific bone metastasis induced by MDA-MB-231 breast cancer cells and its application to the effects of an antibody against bone sialoprotein. Int J Cancer .115, 177-186.

Blouin, S., Baslé, M.F., Chappard, D.,2005.Rat models of bone metastases. Clin Exp Metastasis .22, 605-614.

Body, J.J.,1993. Medical treatment of tumor-induced hypercalcemia and tumor-induced osteolysis: challenges for future research. Support Care Cancer .1,26-33.

Bullough PG. Orthopaedic Pathology. Mosby; 2012.

Burdall, S., Hanby, A., Lansdown, M., Speirs, V., 2003. Breast cancer cell lines: friend or foe? Breast CancerRes. 5, 89-95.

Burger EH. Chapter 28 Experiments on cell mechanosensitivity: Bone Cells as Mechanical Engineers. In: Cowin, Stephen Corteen, editor. Bone mechanics handbook. CRC Press LLC; 2001. p. 1-15.

Bushby, A., Ferguson, V., Boyde, A., 2004. Nanoindentation of bone: Comparison of specimens tested in liquid and embedded in polymethylmethacrylate. J. Material Research. 19, 249-259.

Bussard, K.M., Mastro, A.M., 2009. Ex-vivo analysis of the bone microenvironment in bone metastatic breast cancer. J Mammary Gland Biol Neoplasia .14, 387-395.

Casimiro, S., Guise, T.A., Chirgwin, J.,2009. The critical role of the bone microenvironment in cancer metastases. Mol Cell Endocrinol .310, 71-81.

Chanda, D., Isayeva, T., Kumar, S., Siegal, G.P., Szafran, A.A., Zinn, K.R., et al,2008.Systemic osteoprotegerin gene therapy restores tumor-induced bone loss in a therapeutic model of breast cancer bone metastasis. Mol Ther .16,871-878.

Chang, Y.T., Chen, C.M., Tu, M.Y., Chen, H.L., Chang, S.Y., Tsai, T.C., et al,2011.Effects of osteoporosis and nutrition supplements on structures and nanomechanical properties of bone tissue. Journal of the mechanical behavior of biomedical materials .4, 1412-1420.

Charras, G.T., Lehenkari, P.P., Horton, M.A., 2001. Atomic force microscopy can be used to mechanically stimulate osteoblasts and evaluate cellular strain distributions. Ultramicroscopy .86,85-95.

Chappard, D., Libouban, H., Legrand, E., Ifrah, N., Masson, C., Baslé, M.F., et al,2010.Computed microtomography of bone specimens for rapid analysis of bone changes associated with malignancy. Anat Rec (Hoboken) .293,1125-1133.

Chen, N.X., Ryder, K.D., Pavalko, F.M., Turner, C.H., Burr, D.B., Qiu, J., et al, 2000. Ca(2+) regulates fluid shear-induced cytoskeletal reorganization and gene expression in osteoblasts. Am J Physiol Cell Physiol .278,C989-C997.

Chen, X., Goh, J.C.H., Teoh, S.H., De, S.D., Soong, R., Lee, T., et al, 2013a. Localized sclerotic bone response demonstrated reduced nanomechanical creep properties. Journal of the Mechanical Behavior of Biomedical Materials. 17, 198-208.

Chen, X., Lim, C.T., Lee, T., Mechanical and mechanosensing properties of tumor affected bone cells were inhibited via PI3K/Akt pathway. 2013b J Mech Behav. Biomed. Mat. [For submission]

Chen, X., Nadiarynkh, O., Plotnikov, S., Campagnola, P.J., 2012. Second harmonic generation microscopy for quantitative analysis of collagen fibrillar structure. Nature Protocols. 7(4), 654-669.

Clines, G.A., Guise, T.A.,2008. Molecular mechanisms and treatment of bone metastasis. Expert Rev Mol Med.10, e7.

Coleman, R.E., Guise, T.A., Lipton, A., Roodman, G.D., Berenson, J.R., Body, J.J., et al,2008. Advancing treatment for metastatic bone cancer: consensus recommendations from the Second Cambridge Conference. Clin Cancer Res .14, 6387-6395.

Costa, L., Major, P.P.,2009. Effect of bisphosphonates on pain and quality of life in patients with bone metastases. Nat Clin Pract Oncol .6,163-174.

Cowey, S., Szafran, A.A., Kappes, J., Zinn, K.R., Siegal, G.P., Desmond, R.A., et al,2007. Breast cancer metastasis to bone: evaluation of bioluminescent imaging and microSPECT/CT for detecting bone metastasis in immunodeficient mice. Clin Exp Metastasis .24,389-401.

Cox, L., van Donkelaar, C., van Rietbergen, B., Emans, P., Ito, K., 2012. Decreased bone tissue mineralization can partly explain subchondral sclerosis observed in osteoarthritis. Bone. 50, 1152-1161.

Currey, J.D., 1975. The effects of strain rate, reconstruction and mineral content on some mechanical properties of bovine bone. J Biomech. 8, 81-86.

Dallas, S.L., Snyder, S.O., Miyazono, K., Twardzik, D., Mundy, G.R., Bonewald, L.F., 1994. Characterization and Autoregulation of latent transforming growth factor β (TGF β) complexes in osteoblast-like cell lines. J Biological Chem. 269(4), 6815-6822

Darling, E.M., Topel, M., Zauscher, S., Vail, T.P., Guilak, F.,2008. Viscoelastic properties of human mesenchymally-derived stem cells and primary osteoblasts, chondrocytes, and adipocytes. J Biomech .41,454-464.

Dhurjati, R., Krishnan, V., Shuman, L.A., Mastro, A.M., Vogler, E.A.,2008. Metastatic breast cancer cells colonize and degrade three-dimensional osteoblastic tissue in vitro. Clin Exp Metastasis .25,741-752.

Dong, X.N., Yeni, Y.N., Les, C.M., Fyhrie, D.P.,2004.Effects of end boundary conditions and specimen geometry on the viscoelastic properties of cancellous bone measured by dynamic mechanical analysis. J Biomed Mater Res A .68, 573-583.

Dufour, C., Holy, X., Marie, P.J., 2008. Transforming growth factor-β prevents osteoblast apoptosis induced by skeletal unloading via PI3K/Akt, Bcl-2 and phosphor-Bad signaling Am J Physiol Endocrinol Metab 294, 794-801.

Dumas, V., Ducharne, B., Perrier, A., Fournier, C., Guignandon, A., Thomas, M., et al,2010.Extracellular matrix produced by osteoblasts cultured under low-magnitude, high-frequency stimulation is favourable to osteogenic differentiation of mesenchymal stem cells. Calcif Tissue Int .87, 351-364.

Fan, X., Roy, E., Zhu, L., Murphy, T., Ackert-Bicknell, C., Hart, C., et al,2004. Nitric oxide regulates receptor activator of nuclear factor-kappaB ligand and osteoprotegerin expression in bone marrow stromal cells. Endocrinology. 145,751-759.

Ferguson, V.L., 2009. Deformation partitioning provides insight into elastic, plastic, and viscous contributions to bone material behavior. J. Mech. Behavior of Biomed Mater. 2, 364-374.

Ferretti, J.L., Capozza, R.F., Zanchetta, J.R.,1996.Mechanical validation of a tomographic (pQCT) index for noninvasive estimation of rat femur bending strength. Bone .18, 97-102.

Fidler, I.J.,1973. Selection of successive tumour lines for metastasis. Nat New Biol .242, 148-149.

Fidler, I.,2003. The pathogenesis of cancer metastasis: the 'seed and soil' hypothesis revisited. Nat RevCancer. .3,453-458.

Fortis, A.P., Kostopoulos, V., Panagiotopoulos, E., Tsantzalis, S., Kokkinos, A.,2004. Viscoelastic properties of cartilage-subchondral bone complex in osteoarthritis. J Med Eng Technol .28,223-226.

Fritz, V., Louis-Plence, P., Apparailly, F., Noël, D., Voide, R., Pillon, A., et al,2007. Micro-CT combined with bioluminescence imaging: a dynamic approach to detect early tumor-bone interaction in a tumor osteolysis murine model. Bone .40, 1032-1040.

Gasser, J.A.,1995. Assessing bone quantity by pQCT. Bone .17,145-154S.

Guaitani, A., Sabatini, M., Coccioli, G., Cristina, S., Garattini, S., Bartosek, I., et al,1985.An experimental rat model of local bone cancer invasion and its responsiveness to ethane-1-hydroxy-1,1-bis(phosphonate). Cancer Res .45,2206-2209.

Halvorson, K.G., Sevcik, M.A., Ghilardi, J.R., Sullivan, L.J., Koewler, N.J., Bauss, F., et al, 2008.Intravenous ibandronate rapidly reduces pain, neurochemical indices of central sensitization, tumor burden, and skeletal destruction in a mouse model of bone cancer. J Pain Symptom Manage .36,289-303.

Herbert, E.G., Oliver, W.C., Pharr, G.M., 2008. Nanoindentation and the dynamic characterization of viscoelastic solids. J Phys.D: Appl Phys. 41, 1-9.

Hiraga, E., Williams, P.J., Mundy, G.R., Yoneda, T., 2001.The Bisphosphonate Ibandronate Promotes Apoptosis in MDA-MB-231 Human Breast Cancer Cells in Bone Metastases. Cancer Res. 61, 4418-4424.

Hofmann, T., Heyroth, F., Meinhard, H., Franzel, W., Raum, K., 2006. Assessment of composition and anistropic elastic properties of secondary osteon lamellae. J Biomech 39, 2282-2294.

Hou, W.W., Zhu, Z.L., Zhou, Y., Zhang, C.X., Yu, H.Y., 2011. Involvement of Wnt activation in the micromechanical vibration-enhanced osteogenic response of osteoblasts. J Orthop Sci .16, 598-605.

Huber, S., Ulsperger, E., Gomar, C., Koderhold, G., Czembirek, H.,2002.Osseous metastases in breast cancer: radiographic monitoring of therapeutic response. Anticancer Res .22,1279-1288.

Huja, S., Hay, J., Rummel, A., Beck, F.,2010. Quasi-static and harmonic indentation of osteonal bone. journal of Dental Biomechanics .1-3.

Isaksson, H., Malkiewicz, M., Nowak, R., Helminen, H.J., Jurvelin, J.S.,2010a. Rabbit cortical bone tissue increases its elastic stiffness but becomes less viscoelastic with age. Bone .47,1030-1038.

Isaksson, H., Nagao, S., Małkiewicz, M., Julkunen, P., Nowak, R., Jurvelin, J.S., et al,2010b. Precision of nanoindentation protocols for measurement of viscoelasticity in cortical and trabecular bone. J Biomech .43,2410-2417.

Ishimoto, T., Nakano, T., Yamamoto, M., Tabata, Y.,2011.Biomechanical evaluation of regenerating long bone by nanoindentation. J Mater Sci Mater Med .22, 969-976.

Jaasma, M.J., Jackson, W.M., Keaveny, T.M.,2006.Measurement and characterization of whole-cell mechanical behavior. Ann Biomed Eng .34,748-

758.

Jaganjac, M., Poljak-Blazi, M., Zarkovic, K., Schaur, R.J., Zarkovic, N.,2008.The involvement of granulocytes in spontaneous regression of Walker 256 carcinoma. Cancer Lett .260, 180-186.

Jamsa, T., Jalovaara, P., Peng, Z., Väänänen, H.K., Tuukkanen, J.,1998.Comparison of three-point bending test and peripheral quantitative computed tomography analysis in the evaluation of the strength of mouse femur and tibia. Bone .23, 155-161.

Jamsa, T., Koivukangas, A., Kippo, K., Hannuniemi, R., Jalovaara, P., Tuukkanen, J., et al,2000. Comparison of radiographic and pQCT analyses of healing rat tibial fractures. Calcif Tissue Int .66,288-291.

Jiang, G.Z., Matsumoto, H., Hori, M., Gunji, A., Hakozaki, K., Akimoto, Y., et al,2008. Correlation among geometric, densitometric, and mechanical properties in mandible and femur of osteoporotic rats. J Bone Miner Metab .26,130-137.

Jiang, Y., Zhao, J., White, D.L., Genant, H.K.,2000.Micro CT and Micro MR imaging of 3D architecture of animal skeleton. J Musculoskelet Neuronal Interact .1, 45-51.

Jones, D.S.,1999. Dynamic mechanical analysis of polymeric systems of pharmaceutical and biomedical significance. Int J Pharm .179,167-178.

Jung, A., Bornand, J., Mermillod, B., Edouard, C., Meunier, P.J.,1984.Inhibition by diphosphonates of bone resorption induced by the Walker tumor of the rat. Cancer Res .44, 3007-3011.

Kakonen, S.M., Mundy, G.R.,2003. Mechanisms of osteolytic bone metastases in breast carcinoma. Cancer .97,834-839.

Kasper, D., Seidl, W., Neidlinger-Wilke, C., Ignatius, A., Claes, L., 2000. Dynamic cell stretching increases human osteoblast proliferation and CICP synthesis but decreases osteoclacin synthesis and alkaline phosphatase activity. J Biomech. 33, 45-51.

Kelly, G.M., Kilpatrick, J.I., van Es, M.H., Weafer, P.P., Prendergast, P.J., Jarvis, S.P., et al,2011.Bone cell elasticity and morphology changes during the cell cycle. J Biomech .44,1484-1490.

Kim, D.G., Huja, S.S., Lee, H.R., Tee, B.C., Hueni, S.,2010. Relationships of viscosity with contact hardness and modulus of bone matrix measured by nanoindentation. J Biomech Eng .132, 024502.

Kim, D.G., Huja, S.S., Navalgund, A., D'Atri, A., Tee, B.C., Reeder, S., Lee, H.R., 2013. Effect of estrogen deficiency on regional variation of a viscoelastic tissue property of bone. J Biomech. 46, 110-115.

Kinder, M., Chislock, E., Bussard, K.M., Shuman, L., Mastro, A.M.,2008. Metastatic breast cancer induces an osteoblast inflammatory response. Exp Cell Res .314, 173-183.

Knott, L., Whitehead, C.C., Fleming, R.H., Bailey, A.J.,1995. Biochemical changes in the collagenous matrix of osteoporotic avian bone. Biochem J .310 (Pt 3),1045-1051.

Kokoroghiannis, C., Charopoulos, I., Lyritis, G., Raptou, P., Karachalios, T., Papaioannou, N., et al, 2009. Correlation of pQCT bone strength index with mechanical testing in distraction osteogenesis. Bone .45,512-516.

Kostenuik, P., Orr, F., Suyama, K., Singh, G.,1993. Increased Growth Rate and Tumor Burden of Spontaneously Metastatic Walker 256 Cancer Cells in the skeleton of Bisphosphonate-treated Rats. Cancer Res .5, 5452-5457.

Kozlow, W., Guise, T.A., 2005. Breast cancer metastasis to bone: mechanisms of osteolysis and implications for therapy. J Mammary Gland Biol Neoplasia .10,169-180.

Kreja, L., Liedert, A., Hasni, S., Claes, L., Ignatius, A.,2008. Mechanical regulation of osteoclastic genes in human osteoblasts. Biochem Biophys Res Commun .368,582-587.

Krempien, R., Huber, P.E., Harms, W., Treiber, M., Wannenmacher, M., Krempien, B., et al,2003. Combination of early bisphosphonate administration and irradiation leads to improved remineralization and restabilization of osteolytic bone metastases in an animal tumor model. Cancer .98,1318-1324.

Kurth, A.A., Kim, S.Z., Sedlmeyer, I., Bauss, F., Shea, M.,2002. Ibandronate treatment decreases the effects of tumor-associated lesions on bone density and strength in the rat. Bone .30,300-306.

Kurth, A.A., Müller, R.,2001. The effect of an osteolytic tumor on the three-dimensional trabecular bone morphology in an animal model. Skeletal Radiol .30,94-98.

Kurth, A.H., Kim, S.Z., Sedlmeyer, I., Hovy, L., Bauss, F.,2000.Treatment with ibandronate preserves bone in experimental tumour-induced bone loss. J Bone Joint Surg Br .82, 126-130.

Kurth, A.H., Wang, C., Hayes, W.C., Shea, M., 2001. The evaluation of a rat model for the analysis of densitometric and biomechanical properties of tumor-

induced osteolysis. J Orthop Res .19,200-205.

Kurth, A.A., Kim, S.Z., Shea, M., Bauss, F., Hayes, W.C., Müller, R., et al,2007. Preventative ibandronate treatment has the most beneficial effect on the microstructure of bone in experimental tumor osteolysis. J Bone Miner Metab .25,86-92.

Kuznetsova, T.G., Starodubtseva, M.N., Yegorenkov, N.I., Chizhik, S.A., Zhdanov, R.I.,2007.Atomic force microscopy probing of cell elasticity. Micron .38,824-833.

Lekka, M., Lekki, J., Marszalek, M.,1999. Local elastic properties of cells studied by SFM. Arztl Forsch .141,345-349.

Les, C.M., Spence, C.A., Vance, J.L., Christopherson, G.T., Patel, B., Turner, A.S., et al,2004. Determinants of ovine compact bone viscoelastic properties: effects of architecture, mineralization, and remodeling. Bone .35,729-738.

Les, C.M., Vance, J.L., Christopherson, G.T., Turner, A.S., Divine, G.W., Fyhrie, D.P., et al,2005. Long-term ovariectomy decreases ovine compact bone viscoelasticity. J Orthop Res .23,869-876.

Lespessailles, E., Jaffré, C., Beaupied, H., Nanyan, P., Dolléans, E., Benhamou, C.L., et al,2009.Does exercise modify the effects of zoledronic acid on bone mass, microarchitecture, biomechanics, and turnover in ovariectomized rats? Calcif Tissue Int .85,146-157.

Lespessailles, E., Chappard, C., Bonnet, N., Benhamou, C.L.,2006.Imaging techniques for evaluating bone microarchitecture. Joint Bone Spine .73,254-261.

Li, J., Chen, G., Zheng, L., Luo, S., Zhao, Z.,2007.Osteoblast cytoskeletal modulation in response to compressive stress at physiological levels. Mol Cell Biochem .304,45-52.

Li, L., Price, J.E., Fan, D., Zhang, R.D., Bucana, C.D., Fidler, I.J., et al,1989.Correlation of growth capacity of human tumor cells in hard agarose with their in vivo proliferative capacity at specific metastatic sites. J Natl Cancer Inst .81, 1406-1412.

Li, R.D., Deng, Z.L., Hu, N., Liang, X., Liu, B., Luo, J et al. 2012a, Biphasic effects of TGFβ1 on BMP9-induced osteogenic differentiation of mesenchymal stem cells. BMB Reports. 45(9), 509-514

Li, Z., Peng, S., Pan, H., Tang, B., Lam, R.W.M., Lu, W.W., et al,2012b.Microarchitecture and Nanomechanical Properties of Trabecular Bone

After Strontium Administration in Osteoporotic Goats. Biol Trace Elem Res .145,39-46.

Li, Z., Schem, C., Shi, Y.H., Medina, D., Zhang, M.,2008. Increased COX2 expression enhances tumor-induced osteoclastic lesions in breast cancer bone metastasis. Clin Exp Metastasis .25,389-400.

Lieber, S.C., Aubry, N., Pain, J., Diaz, G., Kim, S.J., Vatner, S.F., 2003. Aging increases stiffness of cardiac myocytes measured by atomic foce microscopy nanoindentation. Am J Physiol Heart Circ. Physiol. 287, H645-H651.

Lim, C., Zhou, E., Li, A., Vedula, S., Fu, H.,2006. Experimental techniques for single cell and single molecule biomechanics. Materials Science and Engineering: C .26, 1278-1288.

Lynch, M., Stein, J., Stein, G., Lian, J.,1995. The influence of type I collagen on the development and maintenance of the osteoblast phenotype in primary and passaged rat calvarial osteoblasts: modification of expression of genes supporting cell growth, adhesion, and extracellular matrix mineralization. Exp Cell Res. 216, 35-45.

Mann, K.A., Lee, J., Arrington, S.A., Damron, T.A., Allen, M.J.,2008.Predicting distal femur bone strength in a murine model of tumor osteolysis. Clin Orthop Relat Res .466,1271-1278.

Mao-Ying, Q.L., Zhao, J., Dong, Z.Q., Wang, J., Yu, J., Yan, M.F., et al,2006.A rat model of bone cancer pain induced by intra-tibia inoculation of Walker 256 mammary gland carcinoma cells. Biochem Biophys Res Commun .345,1292-1298.

Martiniakov á, M., Grosskopf, B., Omelka, R., Vondr ákov á, M., Bauerov á, M.,2006. Differences among species in compact bone tissue microstructure of mammalian skeleton: use of a discriminant function analysis for species identification. J Forensic Sci.51,1235-1239.

Masters, J.R.W. , 2010. Human cancer in primary culture, Kluwer Academics Publishers, Hingham.

Mastro, A.M., Gay, C.V., Welch, D.R., Donahue, H.J., Jewell, J., Mercer, R., et al,2004.Breast cancer cells induce osteoblast apoptosis: a possible contributor to bone degradation. J Cell Biochem .91,265-276.

McGarry, J.G., Maguire, P., Campbell, V.A., O'Connell, B.C., Prendergast, P.J., Jarvis, S.P., et al,2008.Stimulation of nitric oxide mechanotransduction in single osteoblasts using atomic force microscopy. J Orthop Res .26,513-521.

Medhurst, S.J., Walker, K., Bowes, M., Kidd, B.L., Glatt, M., Muller, M., et al,2002.A rat model of bone cancer pain. Pain .96,129-140.

Mercer, R., Miyasaka, C., Mastro, A.M.,2004.Metastatic breast cancer cells suppress osteoblast adhesion and differentiation. Clin Exp Metastasis .21,427-435.

Mercer, R.R., Mastro, A.M.,2005. Cytokines secreted by bone-metastatic breast cancer cells alter the expression pattern of f-actin and reduce focal adhesion plaques in osteoblasts through PI3K. Exp Cell Res .310,270-281.

Mikuni-Takagaki, Y., Suzuki, Y., Kawase, T., 1996. Distinct responses of different populations of bone cells to mechanical stress. Endocrinology. 137, 2028-35.

Mittra, E., Akella, S., Qin, Y.X., 2006. The effects of embedding material, loading rate and magnitude, and penetration depth in nanoindentation of trabecular bone. J Biomed Mater Res A. 79, 86-93.

Muthukumaran, P., Lim, C.T., Lee, T.,2012. Estradiol influences the mechanical properties of human fetal osteoblasts through cytoskeletal changes. Biochem Biophys Res Commun.

Myers, K.A., Rattner, J.B., Shrive, N.G., Hart, D.A.,2007. Osteoblast-like cells and fluid flow Cytoskeleton-dependent shear sensitivity. Biochem Biophys Res Commun .364,214-219.

Nazarian, A., von Stechow, D., Zurakowski, D., Müller, R., Snyder, B.D.,2008.Bone volume fraction explains the variation in strength and stiffness of cancellous bone affected by metastatic cancer and osteoporosis. Calcif Tissue Int .83,368-379.

Neidlinger-Wilke, C., Stalla, I., Hoellen, I., Kinzl, L., Claes, L., 1995. Osteoblasts from osteoporotic bone fail to increase proliferation and TGFbeta release in response to cyclic strain. Cal. Tiss. Int. 56,495

Neudert, M., Fischer, C., Krempien, B., Bauss, F., Seibel, M.J.,2003.Site-specific human breast cancer (MDA-MB-231) metastases in nude rats: model characterisation and in vivo effects of ibandronate on tumour growth. Int J Cancer .107 ,468-477.

Nicolson, G., Poste, G.,1983. Tumor cell diversity and host responses in cancer metastasis--part II--host immune responses and therapy of metastases. Curr Probl Cancer. 7,1-42.

Ochiai, H., Okada, S., Saito, A., Hoshi, K., Yamshita, H et al. 2012. Inhibition of Insulin-like growth factor-1 (IGF-1) Expression by Prolonged Transforming Growth Factor-β1 (TGF- β1) Administration Supresses Osteoblast differentiation. J Biological Chem. 27, 22654-22661.

Olesiak, S.E., Oyen, M.L., Ferguson, V.L., 2010. Viscous-elastic-plastic behavior of bone using Berkovich nanoindentation. Mech Time-Depend Mater. 14, 111-124.

Ottewell, P.D., Deux, B., Mönkkönen, H., Cross, S., Coleman, R.E., Clezardin, P., et al,2008. Differential effect of doxorubicin and zoledronic acid on intraosseous versus extraosseous breast tumor growth in vivo. Clin Cancer Res .14,4658-4666.

Ottewell, P.D., Monkkonen, H., Jones, M., Lefley, D.V., Coleman, R.E., Holen, I., et al,2008.Antitumor effects of doxorubicin followed by zoledronic acid in a mouse model of breast cancer. J Natl Cancer Inst .100,1167-1178.

Ozcivici, E., Garman, R., Judex, S.,2007.High-frequency oscillatory motions enhance the simulated mechanical properties of non-weight bearing trabecular bone. J Biomech .40,3404-3411.

Ozcivici, E., Luu, Y.K., Rubin, C.T., Judex, S., Agarwal, S.,2010.Low-level vibrations retain bone marrow's osteogenic potential and augment recovery of trabecular bone during reambulation. PloS one .5,e11178.

Papachroni, K.K., Karatzas, D.N., Papavassiliou, K.A., Basdra, E.K., Papavassiliou, A.G.,2009.Mechanotransduction in osteoblast regulation and bone disease. Trends Mol Med .15,208-216.

Patel, M.J., Chang, K.H., Sykes, M.C., Talish, R., Rubin, C., Jo, H., et al,2009.Low magnitude and high frequency mechanical loading prevents decreased bone formation responses of 2T3 preosteoblasts. J Cell Biochem .106,306-316.

Pathak, S., Gregory Swadener, J., Kalidindi, S.R., Courtland, H.W., Jepsen, K.J., Goldman, H.M., et al,2011.Measuring the dynamic mechanical response of hydrated mouse bone by nanoindentation. Journal of the mechanical behavior of biomedical materials .4,34-43.

Phadke, P.A., Mercer, R.R., Harms, J.F., Jia, Y., Frost, A.R., Jewell, J.L., et al,2006.Kinetics of metastatic breast cancer cell trafficking in bone. Clin Cancer Res .12,1431-1440.

Ponik, S.M., Triplett, J.W., Pavalko, F.M.,2007.Osteoblasts and osteocytes respond differently to oscillatory and unidirectional fluid flow profiles. J Cell Biochem .100,794-807.

Pre, D., Ceccarelli, G., Gastaldi, G., Asti, A., Saino, E., Visai, L., et al,2011.The differentiation of human adipose-derived stem cells (hASCs) into osteoblasts is promoted by low amplitude, high frequency vibration treatment. Bone .49,295-303.

Priolo, F., Cerase, A.,1998. The current role of radiography in the assessment of

skeletal tumors. Eur J Radiol .27,S77-S85.

Rebelo, L.M., De Sousa, J.S., Filho, J.M., Radmacher, M., 2013. Nanotechnology. 24, 1-12.

Rho, J.Y., Tsui, T.Y., Pharr, G.M.,1997.Elastic properties of human cortical and trabecular lamellar bone measured by nanoindentation. Biomaterials .18,1325-1330.

Ritchie, R., Buehler, M., Hansma, P.,2009. Plasticity and toughness in bone. American Institute of Physics .41-46.

Ritchie, R.O.,2011.The conflicts between strength and toughness. Nat Mater .10,817-822.

Rizzoli, R., Fleisch, H.,1987.The Walker 256/B carcinosarcoma in thyroparathyroidectomized rats: a model to evaluate inhibitors of bone resorption. Calcif Tissue Int .41,202-207.

Rotsch, C., Radmacher, M.,2000.Drug-Induced Changes of Cytoskeletal Structure and Mechanics in Fibroblasts: an Atomic Microscopy study. Biophys J .78,520-535.

Rubin, C., Turner, A.S., Mallinckrodt, C., Jerome, C., McLeod, K., Bain, S., et al,2002.Mechanical strain, induced noninvasively in the high-frequency domain, is anabolic to cancellous bone, but not cortical bone. Bone .30,445-452.

Rubin, C., Recker, R., Cullen, D., Ryaby, J., McCabe, J., McLeod, K., et al,2004.Prevention of postmenopausal bone loss by a low-magnitude, high-frequency mechanical stimuli: a clinical trial assessing compliance, efficacy, and safety. J Bone Miner Res .19,343-351.

Rubinacci, A., Marenzana, M., Cavani, F., Colasante, F., Villa, I., Willnecker, J., et al,2008. Ovariectomy sensitizes rat cortical bone to whole-body vibration. Calcif Tissue Int .82,316-326.

Salvo, N., Christakis, M., Rubenstein, J., de Sa, E., Napolskikh, J., Sinclair, E., et al,2009.The role of plain radiographs in management of bone metastases. J Palliat Med .12,195-198.

Sasaki, A., Boyce, B.F., Story, B., Wright, K.R., Chapman, M., Boyce, R., et al,1995. Bisphosphonate risedronate reduces metastatic human breast cancer burden in bone in nude mice. Cancer Res .55,3551-3557.

Sen, B., Xie, Z., Case, N., Styner, M., Rubin, C.T., Rubin, J., et al,2011. Mechanical signal influence on mesenchymal stem cell fate is enhanced by incorporation of refractory periods into the loading regimen. J Biomech .44,593-599.

Shahnazari, M., Yao, W., Dai, W., Wang, B., Ionova-Martin, S.S., Ritchie, R.O et al., 2010. Higher doses of bisphosphonates further improve bone mass, architecture, and strength but not the tissue material properties in aged rats. Bone. 46, 1267-1274.

Sheng, Z.F., Dai, R.C., Wu, X.P., Ma, Y.L., Xu, K., Zhang, Y.H., et al,2008.The influence of center of rotation on the assessment of trabecular bone densitometric and structural properties. Ann Biomed Eng .36,1934-1941.

Shepherd, T.N., Zhang, J., Ovaert, T.C., Roeder, R.K., Niebur, G.L.,2011.Direct comparison of nanoindentation and macroscopic measurements of bone viscoelasticity. Journal of the mechanical behavior of biomedical materials .4,2055-2062.

Shi, H.F., Cheung, W.H., Qin, L., Leung, A.H.C., Leung, K.S.,2010.Low-magnitude high-frequency vibration treatment augments fracture healing in ovariectomy-induced osteoporotic bone. Bone. 46,1299-1305.

Simpkins, H., Lehman, J.M., Mazurkiewicz, J.E., Davis, B.H.,1991.A morphological and phenotypic analysis of Walker 256 cells. Cancer Res .51,1334-1338.

Siu, W., Qin, L., Leung, K.,2003.pQCT bone strength index may serve as a better predictor than bone mineral density for long bone breaking strength. J Bone Miner Metab .21,316-322.

Slavo, N., Christakis, M., Rubenstein, J.,2009.The role of plain radiographs in management of bone metastases. J Palliat Med .12,195-198.

Sokolov, I.,2007.Atomic Force Microscopy in Cancer Cell Research. Cancer Nanotechnology .1-17.

Song, H., Shahverdi, K., Huso, D.L., Wang, Y., Fox, J.J., Hobbs, R.F., et al,2008.An immunotolerant HER-2/neu transgenic mouse model of metastatic breast cancer. Clin Cancer Res .14,6116-6124.

Tai, K., Dao, M., Suresh, S., Palazoglu, A., Ortiz, C.,2007.Nanoscale heterogeneity promotes energy dissipation in bone. Nat Mater .6,454-462.

Takai, E., Costa, K.D., Shaheen, A.T.,2005.Osteoblast Elastic Modulus Measured by Atomic Force Microscopy Is Substrate Dependent. Ann Biomed Eng .33,963-971.

Tanaka, S.M., Sun, H.B., Roeder, R.K., Burr, D.B., Turner, C.H., Yokota, H., et al,2005.Osteoblast responses one hour after load-induced fluid flow in a three-dimensional porous matrix. Calcif Tissue Int .76,261-271.

Teo, J.C.M., Si-Hoe, K.M., Keh, J.E.L., Teoh, S.H.,2006.Relationship between

CT intensity, micro-architecture and mechanical properties of porcine vertebral cancellous bone. "Clin Biomech (Bristol .21,235-244.

Tudor, G.R., Finlay, D., Taub, N.,1997.An assessment of inter-observer agreement and accuracy when reporting plain radiographs. Clin Radiol .52,235-238.

Turner, C., Takano, Y., Owan, I., Murrell, G.,1996.Nitric oxide inhibitor L-NAME suppresses mechanically induced bone formation in rats. Am J Physiol. .270,E634-E639.

Vatsa, A., Mizuno, D., Smit, T.H., Schmidt, C.F., MacKintosh, F.C., Klein-Nulend, J., et al,2006.Bio imaging of intracellular NO production in single bone cells after mechanical stimulation. J Bone Miner Res .21,1722-1728.

Vlahos, C.J., Matter, W.F., Hui, K.Y., Brown, R.F., 1994. A Specific Inhibitor of Phosphatidylinositol 3-Kinase, 2-(4-Morpholinyl)-8-phenyl-4H-1-benzopyran-4-one (LY294002). J Biological Chem. 269(7), 5241-5248.

Wenger, K.H., Freeman, J.D., Fulzele, S., Immel, D.M., Powell, B.D., Molitor, P., Chao, Y.J., Gao, H.S., Elsalanty, M., Hamrick, M.W., Isales. C.M., Yu, J.C., 2010. Effect of whole body vibration on bone properties in aging mice. Bone. 47, 746-755.

Whitehouse, WJ., 1974. The quantitative morphology of anisotropic trabecular bone. J Microsc.1, 153–8.

Willems, H.M.E., Heuvel, E.G.H.M., Castelein, S., Buisman, J.K., Bronckers, A.L.J.J., Bakker, A.D., et al,2011. Fluoride inhibits the response of bone cells to mechanical loading. Odontology .99,112-118.

Wolfram, U., Wilke, H.J., Zysset, P.K., 2010. Rehydration of vertebral trabecular bone: influences on its anisotropy, its stiffness and the indentation work with a view to age, gender and vertebral level. Bone. 46, 348-354.

Xie, L., Rubin, C., Judex, S.,2008.Enhancement of the adolescent murine musculoskeletal system using low-level mechanical vibrations. J Appl Physiol .104,1056-1062.

Yamashita, J., Furman, B.R., Rawls, H.R., Wang, X., Agrawal, C.M.,2001.The use of dynamic mechanical analysis to assess the viscoelastic properties of human cortical bone. J Biomed Mater Res .58,47-53.

Yang, X., Chan, Y., Muthukumaran, P., Dasde, S., Teoh, S., Lee, T., et al,2011.Ibandronate does not reduce the anabolic effects of PTH in ovariectomized rat tibiae: a microarchitectural and mechanical study. Bone. .48,1154-1163.

Yang, X., Muthukumaran, P., Dasde, S., Teoh, S., Choi, H., Lim, S.K., 2013. Positive alterations of viscoelastic and geometric properties in ovariectomized rat femurs with concurrent administration of ibandronate and PTH. Bone 52, 308-317

Yeni, Y.N., Christopherson, G.T., Turner, A.S., Les, C.M., Fyhrie, D.P.,2004.Apparent viscoelastic anisotropy as measured from nondestructive oscillatory tests can reflect the presence of a flaw in cortical bone. J Biomed Mater Res A .69,124-130.

Yeni, Y.N., Shaffer, R.R., Baker, K.C., Dong, X.N., Grimm, M.J., Les, C.M., et al,2007.The effect of yield damage on the viscoelastic properties of cortical bone tissue as measured by dynamic mechanical analysis. J Biomed Mater Res A .82,530-537.

Zheng, Y., Zhou, H., Brennan, K., Blair, J.M., Modzelewski, J.R.K., Seibel, M.J., Dunstan, C.R., 2007. Inhibition of bone resorption, rather than direct cytotoxicity, mediates the anti-tumour actions of ibandronate and osteoprotegrin in a murine model of breast cancer bone metastasis. Bone 40, 471-478.

Zhao L., Jiang, S., Hantash, B., 2010. Transforming Growth Factor β1 induces osteogenic differentiation of Murine Bone Marrow Stromal Cells. Tissue Eng. Part A. 16 (2), 725-733.

Zhou, S. 2011. TGF-β Regulates β-Catenin Signaling and Osteoblast Differentiation in Human Mesenchymal Stem Cells. J Cellular Biochem. 112, 1651-1660.

Zhu, G.Y., Zhang, Y.Y., Gu, S.Z., Chen, X.,2009.Inhibitory effects of breast cancer cells on proliferation and differentiation of osteoblasts. Chinese journal of Cancer.28,449-455.

Zysset, P.K., Guo, X.E., Hoffler, C.E., Moore, K.E., Goldstein, S.A., 1999. Elastic modulus and hardness of cortical and trabecular bone lamellae measured by nanoindentation in the human femur. J Biomech 32, 1005-1012

Appendix

Vita

CHEN Xiuli received her Bachelor of Engineering (Honours) degree in Bioengineering from National University of Singapore in 2008. Her bachelor thesis title is “Bead based bioassays on microarrays”. During her PhD candidature, her research work has mainly focused on bone metastasis, bone and cellular property changes in the development of bone metastasis.

Publications arising from the thesis

Chen, X., Teoh, SH., Goh, J., Dasde, S., and Lee, T., 2013. Localized sclerotic bone response demonstrated reduced nanomechanical creep properties. Journal of the Mechanical Behavior of Biomedical Materials. 17,198-208

Chen, X., Lim, C.T., Lee, T., Mechanical and mechanosensing properties of tumor affected bone cells were inhibited via PI3K/Akt pathway. J Mech Behav. Biomed. Mat. [For submission]